UNIVERSITEIT VAN PRETORIA
UNIVERSITY OF PRETORIA
YUNIBESITHI YA PRETORIA

NATURAL CONVECTION OF MULTI-WALLED CARBON NANOTUBES WITH WATER IN A SQUARE ENCLOSURE

by

IBRAHIM GARBADEEN

Submitted in partial fulfilment of the requirements for the degree of

MASTER OF ENGINEERING
In the Department of Mechanical and Aeronautical Engineering
University of Pretoria
December 2015

Supervisor: Dr M Sharifpur
Co-supervisor: Prof J Slabber
Co-supervisor: Prof JP Meyer

ABSTRACT

Title: : Natural convection of multi-walled carbon nanotubes with water mixtures in a square enclosure
Author : Ibrahim Garbadeen
Supervisors : Dr Mohsen Sharifpur; Prof Johan Slabber; Prof Josua Meyer
Department : Mechanical and Aeronautical Engineering
University : University of Pretoria
Degree : Master of Engineering (Mechanical Engineering)

The use of nanofluids in buoyancy-driven heat transfer can be very useful in enhancing the performance of various heat transfer applications. In this thesis, natural convection by multi-walled-carbon nanotubes (MWCNT) was studied in a square enclosure with differential heating by two opposite walls. Low particle concentrations of 0 – 1% based on volume were considered at Rayleigh numbers of 10^4 – 10^8. Thermal conductivities and viscosities of the nanofluids were experimentally determined. It was found that thermal conductivity and viscosity increased with increasing concentration by 6% and 58%, respectively. Models based on these experimental results were obtained and subsequently used in a numerical study of a two-dimensional simulation of natural convection in a square cavity using a commercial code. Results revealed an initial enhancement in the Nusselt numbers to a maximum of 22% which occurs at 0.14 % particle concentration and a Rayleigh number of 10^8. Beyond the maximum, the Nusselt number deteriorated. This was true for the different Rayleigh numbers studied with percentage enhancement in the Nusselt number increasing with increasing Rayleigh numbers. Further analysis was done to predict heat transfer performance of higher particle concentrations up to 8% which showed a general decline in the Nusselt numbers by increasing particle concentration. An experimental setup was subsequently used to study natural convection in an insulated square cavity with different temperature differences between the two opposite sides for particle concentrations of 0–1% at Rayleigh numbers between 2.1×10^8 and 6×10^8. Results from the experimental and numerical studies were subsequently compared and the validity of projected results for higher particle concentration was therefore assessed. The experimental results supported the overall behaviours of the nanofluids obtained from the numerical analysis. However, the experimental results of maximum enhancement in the Nusselt number was 42% at particle concentration 0.1% and a Rayleigh number of 6×10^8. Nevertheless, both results indicated the existence of an optimum

particle concentration at which heat transfer in MWCNT nanofluids is maximised. The variation in the performance nanofluid was attributed to the counteracting, non-linear effects of thermal conductivity and viscosity both of which increases by increasing particle concentration. The thermal conductivity effect which improves heat transfer performance was observed to be more dominant for a very narrow range of low particle concentration up to 0.1 % while the viscous effect which diminishes heat transfer performance was found to be more dominant at higher particle concentration.

Keywords: *Nanofluids, MWCNT, natural convection, cavity flow, volume fraction, viscosity.*

ACKNOWLEDGEMENTS

My gratitude goes to supervisors Dr Mohsen Sharifpur and Prof Johan Slabber for their technical guidance and support and to Prof Josua Meyer for his technical and financial support which greatly facilitated the research work.

I am also grateful to all the staff and colleagues at the Thermoflow Research Group, especially Hadi Ghodsinezhad to whom I am greatly indebted for his support and lab expertise.

TABLE OF CONTENT

LIST OF FIGURES

LIST OF TABLES

NOMENCLATURE

A	Area, y-intercept
a	Wire radius
c_p	Specific heat
D	Tube diameter
d	Particle diameter
DI	De-ionised Water
F_s	Spring force
g	Acceleration due to gravity
h	Heat transfer coefficient
k_B	Boltzmann constant
k	Thermal conductivity
L	Length
δL	Change in length
m	Mass, gradient
$\dot{m}$	Mass flow rate
n	Empirical shape factor given by $n = 3/\psi$
Nu	Nusselt number
Pr	Prandtl number
q	Rate of heat transfer
r	Radius
r_c	Apparent radius of particle clusters
R	Resistance
Re	Reynolds number
T	Temperature
δT	Error in temperature
t	Time
v	Dynamic viscosity
v_s	Sedimentation velocity
x	Distance

Greek symbols

α	Diffusivity; temperature coefficient of resistance
β	Ratio of the nano-layer thickness to the original particle radius; thermal coefficient
γ	Ratio of nano-layer thermal conductivity to particle thermal conductivity; Euler constant
Δ	Difference
Λ	Mean free path of fluid molecules
λ	Thermal conductivity ratio, k_w/k_f
μ	Dynamic viscosity
ρ	Base fluid density; resistivity coefficient
σ	Thermal coefficient of expansion
$\sigma_{n,\gamma}$	Thermal neutron cross-sections for n, γ reaction
ϕ	Volume concentration of particles
ψ	Particle sphericity
ω	Specific heat ratio, c_{pw}/c_{pf}

Subscripts

c	Cross section; cold
eff	Effective
f	Base fluid
g	Glass spacer
id	Ideal
h	Hot
K	Knudsen effect
n	Nanofluid
o	Ambient, initial
p	Particle
pe	Modified particle property
r	Reference
rad	Radiation
ref	Reflection
var	Variable

PUBLICATIONS IN JOURNALS AND CONFERENCE PROCEEDINGS

The following articles and conference papers were produced during this research.

Journal articles

I.D Garbadeen, M. Sharifpur, J.M. Slabber, J.P. Meyer, Experimental study on natural convection of MWCNT-water nanofluids in a square enclosure, *International Journal of Heat and Mass Transfer,* Submitted 14 August 2015. (Under review)

Conference papers

I.D Garbadeen, M. Sharifpur, J.M. Slabber, J.P. Meyer, Numerical study on natural convection of MWCNT nanofluids in an enclosure based on experimental conductivity and viscosity, *Proceedings of the 11th International Conference on Heat Transfer, Fluid Mechanics and Thermodynamics,* Kruger National Park, 20–23July 2015.

CHAPTER 1. INTRODUCTION

1.1 Background

A general trend in technological development is the need for ever smaller, but bigger efficiency heat exchangers. This has placed an increasing demand for coolant fluids with improved thermal properties. As a result, plenty of research has emerged into the different techniques of passively improving heat transfer characteristics with minimal power cost. Among many techniques investigated, the application of nanofluids which are colloidal dispersions of nanometre-sized particles in a heat transfer fluid (base fluid) has received particular attention. This is because it has been demonstrated that they have enhanced thermal properties compared to conventional heat transfer fluids. Enhancement factors as high as 38% were measured by Assael *et al.* for just 0.6% particle concentration of multi-walled carbon nanotubes [1]. Such levels of enhancement render nanofluids with a high potential of replacing current coolant fluids in various engineering applications. This section explores the present state of heat transfer and the motivation for improvement. Furthermore, the choice for carbon nanofluids to achieve the desired enhanced heat transfer is explained.

1.2 Motivation

Convective heat transfer is an essential area of research because of its involvement in many heat transfer applications in the industry. Natural convection in particular is a passive mode of heat transfer and therefore can be exploited to improve the performance of heat transfer applications without increased power input. The use of nanofluids as heat transfer fluid through natural convection has the potential of further enhancing the performance and compactness of heat transfer applications. This enhancement can be very significant, for example in the operation and safety of nuclear reactors, cooling in electronics, heating in concentrated solar power plants and HVAC systems in buildings.

A large number of studies have been undertaken in improving the thermal conductivity of the coolant itself. An intuitive method of doing so would be to disperse solids, known to have far superior thermal conductivity, into the proposed liquid coolant with the expectation that the effective thermal conductivity of the solution will be better than the base fluid. Maxwell [2] as early as 1881 had started studying the thermal conductivities of micrometre-sized liquid suspensions or slurries. Maxwell's slurries have performed

poor as heat transfer fluids. This is because the particles did not easily form a homogeneous solution and would settle to the bottom where they have no effect on heat transfer of the base fluid. Another problem with such slurries is the large particle inertia and the subsequent increase in pump power requirements. Lastly, the particles tend to erode and clog up heat transfer channels therefore increasing need for maintenance.

The idea of heat transfer enhancement by particle dispersion was resuscitated in the 1990s when Choi [3], with the help of modern technology, was able to disperse nanoscale particles in base fluids to improve their thermal conductivity. His result would spur one of the most prolific areas of research in the field of heat transfer. The fluid developed by Choi is commonly referred to as nanofluids and several subsequent studies have demonstrated their enhancement capabilities.

However, while much attention has focused on thermal conductivity and forced convection in nanofluids, very limited research involving natural convection and nanofluids is available. Das *et al*. [4] also commented that it is improved heat transfer in convective conditions that gives a sufficient motivation for the use of nanofluids as potential heat transfer fluids and not simply the enhancement in thermal conductivity. Unlike metal oxides, work on carbon-water nanoparticles is also limited. To the author's best knowledge with the writing of this thesis, no experimental study of natural convection in carbon nanofluids is available. Therefore, the current study attempts to fill this space and focuses on natural convection of MWCNT in a square enclosure.

1.3 Objective of research

Given the high enhancement of thermal conductivity in MWCNT nanofluids and the importance of carbon in various industries, the present study will investigate the heat transfer performance of aqueous MWCNT nanofluids as characterised by the Nusselt number, at varying particle concentrations, in natural convection conditions using both CFD and experimental analysis, to determine the efficacy of using such nanofluids as a heat transfer fluid.

1.4 Scope, method and limitations

In present study aqueous MWCNT nanofluids are prepared using the two-step method outlined in Chapter 2 and MWCNT particles provided by the company MK Nano in the particle concentration range 0.01–1%. The MWCNT particles had inner diameter 3–5

nm, outer diameter 10–20 nm and lengths of 10–30 μm as characterised by using the Transmission Electron Microscope (TEM) micrograph. Thermal conductivity measurements of the prepared samples were conducted using the KD2 Pro from Decagon devices and a stated accuracy of $\pm$ 5%. Viscosity measurements of the different samples were also taken using the Sine-wave Vibro Viscometer SV-10 with the manufacturer-stated error of $\pm$ 1 %.

CFD analysis using CD Adapco's Star-CCM+ Code (v 8.06) to model natural convection in a 2D square domain and differentially heated sides at Rayleigh numbers $10^4 - 10^8$ using experimental results of thermal conductivity and viscosity obtained at bulk temperature 27 °C.

Finally, experimental study was performed on MWCNT nanofluids in a square cavity for Rayleigh numbers between 2.1×10^8 and 6×10^8 with base fluid at Prandtl number 5.83 and particle concentrations range $0 \leq \phi \leq 1.0$ %.

1.5 Organisation of the dissertation

The dissertation consists of six chapters which are further divided into appropriate sub-chapters to highlight individual aspects of research and easy referencing.

Chapter 1 provides the necessary background and motivation for the present study, which leads to the formulation of the objective and scope.

Chapter 2 presents a review done on available literature on important aspects of the study, which include nanofluid preparation method and stability, theory and measurement of thermal conductivity, measurement of viscosity and natural convection in aqueous nanofluids.

Chapter 3 discusses the apparatus and procedure used in the preparation of aqueous MWCNT nanofluid samples and the experimental determination of thermal conductivity and viscosity of the nanofluids. Results of measurements taken are also presented and analysed.

In chapter 4 the mathematical model used in the CFD analysis is developed and a mesh independence study is carried out by checking for convergence, compared with benchmark results. The results of temperature and velocity profiles obtained for different

volume concentration and Rayleigh numbers from the CFD analysis are presented and discussed.

Chapter 5 deals with the determination of the heat transfer performance of the different particle concentrations of aqueous MWCNT nanofluids in a full scale experimental setup. The experimental procedure is discussed and results obtained are analysed and discussed.

Chapter 6 presents an overall summary of all results obtained in the study and offers conclusions and recommendations.

CHAPTER 2. LITERATURE REVIEW

2.1 Introduction

The need for higher efficiency heat transfer fluids, together with the potential of nanofluids to fulfil such demands, has caused a large body of work to develop around nanofluids. The two main parameters often studied are primarily thermal conductivity followed by viscosity changes in different nanofluids. An overview of the work done on nanofluids so far reveals overwhelming support for thermal conductivity as well as viscosity enhancement in nanofluids with an increase in particle concentration. However, many inconsistencies exist in published results on natural convection in nanofluids. Due to very little standardisation practices in this field, this chapter starts with the different methods of preparation and stability of nanofluids, followed by discussing the theory and measurement of the thermal conductivity, approximations and errors involved in the different experimental methods. This is followed by a review of viscosity measurements and natural convection in nanofluids.

2.2 Preparation of nanofluids

The suspension of solids in a base fluid to improve its thermal properties is borne from the fact that in general, solids have much higher thermal conductivity and heat capacity than liquids. As such, a large number of solid-liquid combinations can be conceived depending on the application. The preparation of nanofluid is of crucial importance as it ultimately determines the performance of the nanofluid. Examples of common nanoparticles used in various research works are metals, metal oxides, metal carbides and carbon nanotubes (CNTs), while examples of common base fluid used include: water, ethylene glycol (EG), glycerol and oils. For long term application, it is necessary that the resultant nanofluid is very stable with negligible agglomeration of particles and chemically stable with the base fluid. There are two distinct methods of preparing nanofluids, namely single-step method and two-step method which are described as:

a. Single-step method:

As the name suggests, the manufacture and the subsequent dispersal of the nanofluid are done in a single step. The original technique, as developed by Akoh *et.al* [5] and subsequent modification most notably by Eastman *et al*. [6], involves the evaporation of the solid (the source material) in a vacuum and allowed to condense onto a flowing low

vapour pressure thin film of the base fluid as nanoparticles. The base fluid is maintained at a low temperature to prevent it from heating up. This particular variation of the single-step method is also called the Vacuum Evaporation onto a Running Oil Substrate (VEROS). Other variations of the single-step process mainly differ by the means by which the source material is vaporised. This include laser ablation [7], microwave irradiation [8] or submerged arc nano-synthesis [9]. This method is limited to a base fluid with low vapour pressure otherwise the agglomeration of nanoparticles occurs.

b. Two-step method

This method of nanofluid preparation is widely used as an alternative to the often expensive and advanced single-step method. The first step of the two-step method involves the preparation of nanoparticles often in powder form. This can be achieved by chemical reactions or by vapour condensation. The resultant nanoparticles are then dispersed in a base fluid in a separate step. Methods used to thoroughly disperse nanoparticles in nanofluids include electro-magnetic force or mechanical agitation, high shear mixing or more commonly, by means of ultrasound [6]. Nanoparticles are widely available commercially, which further simplifies the preparation of nanofluids using this method. A major limitation of this method is the tendency of nanoparticles to agglomerate as well as settling down, thereby requiring repeated ultrasonication or the use of surfactants to maintain a homogenous solution. A comparison of the two methods of nanofluid preparation is given in Table 2-1 below.

Table 2-1: Comparison of methods of nanofluid preparation

	Single-step method	**Two-step method**
Advantages	▪ Agglomeration of nanoparticles' minimisation ▪ There's control over particle size	▪ Easily prepared on large scale ▪ Suitable for oxide nanoparticles
Disadvantages	▪ Not suitable for high vapour pressure fluids ▪ Oxidation of pure metal may occur ▪ Presence of residual reactants in nanofluids	▪ Tends to agglomerate ▪ Less suitable for metallic particles

2.3 Stability of nanofluids

It's important to be able to quantifiably measure the stability of nanofluids in order to understand and compare the stability of different nanofluids. The easiest method of deducing the stability of nanofluids is the sedimentation method [10]. This simply measures the amount of sediment formed over a given time. To avoid long test times for the more stable nanofluids, a sample can be centrifuged at known RPM and the time taken for sedimentation to begin is measured. An example of a stability measurement is silver nanofluids prepared using the single method and the use of stabilizing agents [11]. This showed a one month stability in a quiescent state and ten hours when centrifuged at 3000 RPM [12].

Three methods of assessing the stability of nanofluids are widely used in research, which includes visual observation of the amount of sedimentation that has taken place after a given time, Zeta potential and spectrophotometry. The latter two are more quantitative. Zeta potential refers to the potential difference across the stationary double layer of fluid bound to the particle and separating it from the rest of the fluid. However, high viscosity or low concentration nanofluids may restrict the applicability of the zeta potential method and spectrophotometry may, therefore, be better suited. It works on the basis of measuring the difference in intensity between incident and emergent light passing through a sample. The difference arises from absorption and/or scattering of light by nanoparticles in the fluid. This difference in intensities can be measured accurately using a spectrophotometer which can then be used to quantitatively characterise the stability of the nanofluid. An example of a commonly used spectrophotometry is the UV-Vis spectrophotometry, which uses light in the UV and Visible region (hence the name). Unlike zeta potential method, UV-Vis spectrophotometry is applicable to virtually all base fluids. However, its application is not suitable to carbon nanotubes (CNT) nanofluids or more generally to nanofluids with very high particle concentration [12]. This is because the solution is often too dark to reliably measure difference in incident and emergent light intensities.

The sedimentation velocity, v_s for a quiescent nanofluid can be obtained using Stokes' Law:

$$v_s = \frac{2}{9}\frac{\rho_p - \rho_f}{\mu} g\, R^2$$

where the densities of particle and fluid are ρ_p and ρ_f respectively, μ is the viscosity, R is the radius of particle and g the gravitational acceleration. The smaller the radius of the nanoparticles, the lower the sedimentation velocity; therefore the nanofluid stability is higher. However, a smaller radius also results in increased surface energy which causes an increased tendency for particles to aggregate by means of strong Van der Waal forces between them. There are several techniques developed to counter these effects and these are broadly categorised into chemical and physical treatments.

Widely-used chemical treatments of nanofluids to improve stability include the use of surfactants and the pH adjustment of the nanofluid. Surfactants function by binding onto and altering the surface characteristics of nanoparticles and results in increased wettability at the particle-fluid interface and the nanoparticle, therefore, displaying hydrophilic behaviour in relation to the base fluid. These increases stability as nanoparticles remain dispersed in the base fluid. Surfactants can also act by increasing the surface charge of nanoparticles and as a result, the zeta potential is increased. As discussed above, increased zeta potential is indication of increased nanofluid stability.

Surfactants are widely used because of their easy and low cost application. However, they may limit the thermal conductivity of the nanofluid by increasing the thermal resistance between nanoparticles and base fluids [12]. Therefore, care must be taken when selecting the appropriate surfactant. Another drawback of using surfactant is the temperature variability encountered in most heat transfer applications. Subjecting surfactants to such conditions could lead to breakdown of surface bonds between surfactant and particle which decreases overall stability of the nanofluid.

The pH adjustment of nanofluid is done by acid treatment which increases the hydrophilic properties of the nanoparticles [13]. The zeta potential is increased by formation of hydroxyl groups on particle surfaces, resulting in a stronger repulsive force enough to overcome Van der Waal (VDW) forces of attraction according to the DVLO theory [14]. The DVLO model explains the aggregation of aqueous dispersion by combining VDW attraction and the electrostatic repulsion effects. The optimum pH level will vary with different nanoparticles. Examples of suitable pH level for alumina, copper and graphite nanoparticles are 8.0, 9.5 and 2.0 respectively [15]. However, like using surfactants, temperature variation can have limiting effects on nanofluids.

Nanofluid stability can also be improved by physical means. Unlike the chemical approach which seeks to modify the surface properties of nanoparticles, the physical approach acts by breaking down particle agglomeration using for example ultrasound, magnetic forces or a high shear stirrer [16]. Treatment times may range from a few minutes to several hours depending on the nanoparticle and base fluid in use, the concentration and the volume of nanofluid. Table 2-2 shows examples of ultrasound treatment times and stability of different nanofluids in aqueous solutions [15]. Physical means can be used in conjunction with the chemical approaches to achieve better stability.

Table 2-2: Examples of ultrasound treatment and stability*

Nanoparticle	Size	Concentration, Vol. %	Treatment time (Hours)	Stability, (Hours)	Reference
Al_2O_3	11.4 nm	0.8	6	N/A	[17]
Al_2O_3	38.4 nm	1–4	11	> 12	[18]
Al_2O_3	43.4 nm	0.33–5	6	N/A	
CuO	28.6 nm	1–4	11	> 12	[18]
Cu	25 nm	–	1	N/A	[19]
TiO_2	21 nm	0–1.2	2	N/A	[20]

* Stability times too long for measurement indicated by N/A.

2.4 Theory of thermal conductivity of nanofluids

Although nanofluids have been the interest of much research over the past two decades, there's yet to be a comprehensive theory that accurately describes their behaviour. As a result, values of thermal conductivity of a nanofluid are largely (semi) empirical. There are three modes of heat transfer namely: conduction, convection and radiation, however, studies in nanofluids mainly focus on conductivity. This relates to the basis of preparing nanofluids in the first place, i.e. to enhance the thermal conductivity of fluids using solids because of their generally superior thermal conductivity as shown in Table 2-3.

Table 2-3: Thermal conductivities of select materials at room temperature

Material	k, W/m. °C
Water	0.613
Ethylene glycol	0.258
Engine oil	0.145
Cu	401
Al	205
C (Diamond)	2 300

Several researchers in nanofluids for example [6] and [21] have demonstrated that minute concentrations of metals (or metal oxides as they offer better stability) in a base fluid resulted in a marked increase in thermal conductivity. The starting point in trying to analyse nanofluids is to adapt Maxwell's Effective Medium Theory (EMT), originally applied to any heterogeneous dual-phase mixture, to nanofluids. The theory is static in nature and based on the effect of thermal conductivity of the respective thermal conductivity of the two materials, their composition and manner of distribution in the mixture [2]. Later improvements on this theory include the effects of particle shape and thermal resistance at interface, [22], [23], [24],[25]. Therefore, the effective thermal conductivity, k_{eff} of a nanofluid from a simplified EMT equation is given by [4]:

$$\frac{k_{eff}}{k_f} = \frac{k_p + \left(\frac{3}{\psi} - 1\right) k_f + \left(\frac{3}{\psi} - 1\right)(k_p - k_f)\phi}{k_p + \left(\frac{3}{\psi} - 1\right) k_f - (k_p - k_f)\phi}$$

where $k_p \; and \; k_f$ are the conductivities of the particle and base fluid respectively and ϕ, the volume concentration of particles with ψ is defined as the particle sphericity which is equivalent to the ratio of the surface area of a sphere (with a volume equal to the particle's volume) to the actual surface area of the particle. From this definition, long thin nanotubes, as is used in carbon nanofluids, would give rise to very high effective thermal conductivities. This, in conjunction with the already high conductivity of carbon, may explain the tremendous enhancement of up to 150 % as observed in carbon nanofluids as observed by Choi *et al*. [26], [27]. Although this model can be used to estimate and compare conductivities of different nanofluids, it still falls short of accuracy. For example, the assumption of a well dispersed, uniform and stationary nanofluid, which is

inherent in the model, means the effects of agglomeration of nanoparticles on thermal conductivity are ignored.

In trying to improve the static model above and explain the underlying chemistry for such enhancement a more dynamic (as opposed to the static model) approach was considered. Four mechanisms have often been suggested and investigated widely, namely [28]:

- Brownian motion;
- the presence of an interfacial solid-liquid layer;
- agglomeration of nanoparticles; and
- the nature of heat transport in the nanoparticle [29], [30].

A quick survey of the literature will, however, immediately show that there is such a wide variation in published results and none of the proposed mechanisms can satisfactorily explain the phenomenon on their own, indicating several mechanisms are involved. To illustrate the difficulty in arriving at a unified theory, consider the following: due to the small sizes of particles, Brownian motion is thought to be a significant factor in the form of increased micro-mixing, but as the particles agglomerate and form clusters, they contribute more to the effective thermal conductivity than individual particles, even though Brownian motion is reduced. However, since the sedimentation rate will increase as particles agglomerate, more particles settle out of solution and it therefore reduces their contribution to the enhancement. The interfacial layer (between particle surface and the rest of the liquid which has an increased thermal conductivity value compared to the bulk fluid) will also affect the effective thermal conductivity of the nanofluid.

However, it's been shown that the EMT corrected for the different mechanisms discussed above correspond better with measured results [31], [32]. A summary of the Maxwell model and subsequent modifications are presented in Table 2-4 along with the corrections made. Only models that apply to non-spherical nanoparticles are considered here.

Table 2-4: Models of thermal conductivity in nanofluids based on EMT and modifications

Equation	Considerations	Ref
$\frac{k_{eff}}{k_f} = \frac{k_p + (\frac{3}{\psi} - 1)k_f + (\frac{3}{\psi} - 1)(k_p - k_f)\phi}{k_p + (\frac{3}{\psi} - 1)k_f - (k_p - k_f)\phi}$	The original Maxwell EMT considers only the conductivities of the spherical particle, base fluid and volume fractions. In Hamilton and Crosser's modification, the shape factor $n = 3/\psi$ is used.	[2]
$\frac{k_{eff}}{k_f} = \left[1 + \frac{\eta\phi/3}{\frac{k_f}{\eta k_{33}} + H\left(\frac{\eta L}{d}\right)}\right]$ $\eta = L^{ce}/L$ $k_{33} = k_{33}^c/(1 + 2R_K k_{33}^c/L)$ $H(p) = \frac{1}{p^2-1}\left[\frac{p}{\sqrt{(p^2-1)}}\ln\left(p + \sqrt{p^2-1}\right) - 1\right]$ where $p = L/d$	This is one of the most comprehensive models proposed by Deng and Zheng. The following factors are accounted for: the non-straightness of nanotubes (η), the length of the nanotube L, the average length between two ends of a non-straight nanotube L^{ce}, and the diameter of the nanotube d. The thermal conductivity along the longitudinal axis is k_{33}^c and the factor R_k denotes the Kapitza resistance – the interfacial thermal resistance at the solid-medium boundary measured in m^2K/W. A high thermal anisotropy $k_{11}^c/k_{33}^c \ll 1$ is required for this model.	[33]
$\frac{k_{eff}}{k_f} = \frac{3 + \phi(\beta_x + \beta_z)}{3 - \phi(\beta_x)}$ $\beta_x = \frac{2(k_{11}^c - k_b)}{k_{11}^c + k_f}; \quad \beta_z = \frac{k_{33}^c}{k_f} - 1$ $k_{11}^c = \frac{k_p}{1 + \frac{2a_k k_p}{d\, k_f}}; \quad k_{33}^c = \frac{k_p}{1 + \frac{2a_k k_p}{L\, k_f}}$ $a_k = R_k k_f = 8(10^{-8})\frac{m^2K}{W}k_f$	This is a comprehensive revision by Nan *et al*. of the Maxwell's EMT which takes into account the effect of interfacial resistance R_k factored into the term a_k referred to as the Kapitza radius. The coefficients β_x and β_z are calculated from the anisotropic thermal conductivity of the nanotubes along the transverse (k_{11}^c) and longitudinal (k_{33}^c) directions respectively.	[34]

Not included in Table 2-4 are computer-based models. These have enjoyed a fair amount of success, for example, Yu & Choi's [35] model based on fractal theory. Fractal theory deals with the stochastic process of agglomeration and polarization of nanoparticles on a small scale. This model has been shown to fit well with experiments on aqueous CuO nanofluids of particle size up to 50 nm and <0.5 vol. concentration. Another fairly successful model is the Bhattacharya *et al* [36] model based on computer simulation of particles in the Brownian motion.

2.5 Measurement of thermal conductivity

Measurement of thermal conductivity has always proven to be a challenge; and with the physiochemical complexities of nanofluids, it has become an important research area all on its own. All classical measurement techniques are based on Fourier's law of heat conduction. The thermal conductivity, k is obtained from the steady state one dimensional temperature difference ΔT between two points in a sample with known separation distance Δx, cross section area A and rate of heat transfer q.

$$k = \frac{q/A}{\Delta T/\Delta x}$$

Although the basis is quite simple, experimentally, it is difficult to achieve the one-dimensional heat transfer across Δx necessary for equation 2.3 to be applicable. In fluids the additional challenge of eliminating the contribution from convection heat transfer is faced. This will occur immediately if there is a temperature gradient parallel to the gravitational field. Since the development of a temperature gradient is almost unavoidable, it means the window to take useful readings becomes small. A determination of the correct time frame is presented later. In the case of nanofluids, it becomes also necessary to maintain original homogeneity in order to measure true thermal conductivity.

The use of different techniques by different research groups to measure thermal conductivity has contributed to the inconsistencies in published results. Therefore, the problem of selecting the most accurate (and precise) technique for measuring thermal conductivity presents itself. All experimental approaches can broadly be categorised into steady-state methods and transient methods with the preferred method of measurement being the transient method and, particularly, the Transient Hot Wire (THW) method. The

THW method is considered to be the most accurate [37] and also the most widely used in research. More attention is therefore paid to this method.

Table 2-5 shows a summary of some of the research done on water-based nanofluids and the maximum enhancement measured relative to water.

Table 2-5: Examples of previous studies on maximum thermal conductivity increase in aqueous nanofluids

Nanoparticle	Base fluid	Particle size (nm)[1]	Vol. %	% increase	Temperature °C	Reference
Al_2O_3	Water	33	5.0	30		Eastman *et al*. [6]
		24.4	4.3	10	21–52	Lee *et al*. [13]
		38	4.0	25	24	Das *et al*. [17]
		28	3.0	12		Wang *et al*. [16]
CuO	Water	36	5.0	60		Eastman *et al*. [6]
		23	10	35	24	Wang *et al*. [13]
		18.6	4.3	10	21–52	Lee *et al*. [13]
		28.6	4.0	36		Das *et al*. [17]
MWCNT[2]	Water	ϕ15 nm x 30 μm	1.0	7.0	"room"	Xie *et al*. [13]
		ϕ20 nm x 10 μm	0.84	31	20–45	Wen & Ding [38]
		ϕ130 nm x 10 μm	0.6	38	25	Assael *et al*. [39]
ND-Ni [3]	Water	25	3	21	20–60	Sundar *et al.*[40]

[1] Average particle diameter; for nanotubes – average diameter by length
[2] MWCNT – Multi-walled carbon nanotubes
[3] ND-Ni – Nanodiamond-nickel nano-composite nanofluids

Aybar *et al*. [28] identified the important factors affecting thermal conductivity of nanofluids as particle size and volume fraction, temperature, pH and the nano-layer properties. Having such large numbers of variables makes standardisation and comparison of results across the various research groups difficult. Furthermore, there are four major mechanisms of thermal conductivity enhancement in nanofluids, namely Brownian motion, nano-layer, clustering, and the nature of heat transport in the nanoparticles [28]. These mechanisms occur in nanofluids simultaneously but in varying degrees of significance. As a result, mathematical models predicting nanofluid behaviour have been limited to a very narrow range of the factors affecting thermal conductivity. Nevertheless, Table 2-5 attempts to compare the various results from different researchers working with aqueous-based nanofluids. Lee *et al*. [13] using 24.4 nm Al_2O_3 nanoparticles reports a lower percentage enhancement than Das *et al*. [41] using 38.4 nm

Al_2O_3 nanoparticles while working at the same volume concentration of ≈ 4.0 %. A similar observation can be made for carbon nanotubes when comparing Wen & Ding's [38] results using 20 nm diameter tubes with Assael *et al*. [39] using 130nm. This would suggest that the heat transfer performance of nanofluids increase with size of nanoparticles. However, larger sized nanoparticles have the disadvantage of increasing the pump power required to circulate nanofluids in engineering applications. Sedimentation is also reduced due to their increased weight and this reduces overall nanofluid stability.

Lee and Wang's results for CuO nanofluids in Table 2-5 also show a higher thermal conductivity enhancement is measured for increased volume concentration. Using similar nanoparticle sizes, Lee *et al*. obtained 10% enhancement for 4.3% volume concentration while Wang obtained 35% enhancement for 10% concentration – i.e. doubling the nanoparticle concentration tripled the enhancement. Comparison is more challenging when nanotubes are included since they have two principle dimensions to consider namely diameter and length. Nevertheless, carbon can have much higher thermal conductivity when compared to metals and metal oxides by two orders of magnitude [4], [42]. This explains why small concentrations of MWCNT in Table 2-5 give rise to significant enhancement in thermal conductivity, for example Assael *et al*. [39] measured 38% enhancement for just 0.6% concentration of MWCNT. Therefore, carbon nanofluids are expected to have a higher percent enhancement for equivalent size and concentration. However, further research will be required to confirm such levels of enhancement.

Although examples of results presented in Table 2-5 do not include several of the inconsistencies found in literature, the amount of published results corroborating the heat transfer enhancement capabilities of nanoparticles is sufficient to confirm the effect and is now widely accepted. The main reason to want to use carbon nanofluids as a replacement reactor coolant is due to its significant enhancement thermal conductivity. This enhancement is achieved without the disadvantage of low stability as seen for the original Maxwell slurries since the small size of nanoparticles greatly reduces rate of sedimentation. Finally, reduction in pump requirement is brought about by the enhancement in thermal conductivity. Das *et al*. [4] estimates that to double the heat transfer of an ordinary coolant, pumping power will have to be increased at least tenfold. However, the same heat transfer can be achieved by simply trebling the thermal

conductivity of the coolant [3] with negligible increase in pump power requirement provided viscosity is maintained fairly constant. The small volume fraction of nanoparticles used in preparing nanofluids makes this feasible.

2.6 Measurement of viscosity

Viscosity is a measure of a fluid's resistance to flow; the higher the viscosity, the higher the resistance to flow. Introducing nanoparticles into a base fluid alters its rheology and in turn will have implications on pumping requirements and convective heat transfer of the engineering systems utilizing the nanofluid. It is a very important property, because the advantage of thermal conductivity enhancement in nanofluids as a heat transfer fluid can be offset by an increase in the fluid viscosity. An overview of literature reveals viscosity measurement has generated less interest than thermal conductivity, but factoring all these parameters into a single consistent theoretical model has proven difficult. The starting point of most theoretical models is with Einstein's equation which gives the viscosity for infinitely dilute suspensions of hard spheres.

$$\mu = \mu_o(1 + 2.5\phi)$$

Einstein's equation is only useful for $\phi < 0.01$, because as volume concentration increases, interactions between the disturbances around individual particles become increasingly significant to the viscosity. Brinkman [43] proposed a model which allows for higher volume concentration and has wide usage in numerical research into convection.

$$\mu = \frac{\mu_o}{(1-\phi)^{2.5}}$$

The effects of such hydrodynamic interactions along with other developments in the theory are given in Table 2-6. There are far less models that take into account the non-spherical shape of nanotubes. Brenner and Condiff [44] were the first to propose a viscosity model that accounts for aspect ratio (r) in nanoparticles.

$$\mu = \mu_o(1 + \eta\phi)$$

$$\eta = \frac{0.312r}{ln\,(2r) - 1.5} + 2 - \frac{0.5}{ln\,(2r) - 1.5} - \frac{1.872}{r}$$

Table 2-6: Viscosity models

Model	Equation	Description
Batchelor (1977) [45]	$\frac{\mu(0)}{\mu_o} = 1 + [\mu]\phi + k_H(([\mu]\phi)^2 + O(\phi^3))$	Hydrodynamic interactions around individual particles considered and represented in the Huggins Coefficient k_H.Valid for $\phi < 0.1$ The intrinsic viscosity $[\mu]$ is given by $[\mu] = \frac{\mu - \mu_0}{\mu_0 \phi}$
Krieger & Doherty [46]	$\frac{\mu}{\mu_o} = \left(1 - \frac{\phi}{\phi_m}\right)^{-[\mu]\phi_m}$	Includes the effect of multi-particle collisions and using the coefficient ϕ_m - the maximum particle packing fraction with values [0.495 – 0.54] for quiescent low shear rates and 0.605 for high shear rates
Modified Krieger & Doherty (1959) [47]	$\frac{\mu}{\mu_o} = \left(1 - \frac{\phi_a}{\phi_m}\right)^{-[\mu]\phi_m}$ $\phi_a = \phi(\frac{a_a}{a})^{3-D}$	Takes into account aggregation of particles where aggregates are characterised by: a – radii of particle a_a – radii of aggregate D –fractural index

The various viscosity measurement techniques can be categorised into two groups, namely viscometers and rheometers. Viscometers, the more common of the two, are used for Newtonian fluids whose viscosity values remain constant over a range of shear stress. The instruments are of relatively simpler design and cheaper. Rheometers function over a wider range of shear rates and offer more measurement parameters. They are used for Non-Newtonian fluids whose viscosities vary over a range of shear rates, i.e. the viscosity changes with different flow conditions.

The basis of operation of most viscometers is to measure the drag force created in the fluid in response to movement generated by the measuring device. This movement can be

in the form of a falling sphere, a rotating spindle or a vibrating disk. For viscometers to be valid it's necessary to determine whether the viscosity of nanofluids is shear-independent, i.e. whether the fluid is Newtonian. For example Chen, 2007 [47] reported a Newtonian behaviour while Kole, 2013 [48] reported a non-Newtonian behaviour. It has also been demonstrated by detailed rheological analyses that indeed both behaviours can be exhibited and it depends on the usual nanofluid variables like particle size, shape, concentration and base fluid viscosity.

There are fewer studies into the viscosity of nanofluids compared to thermal conductivity [49]. This is probably due to the assumption that since small volume concentrations of nanoparticles are involved the thermal conductivity enhancement is more dominant in characterising the overall heat transfer capability of the nanofluid. Table 2-7 shows a summary of studies done on nanofluid viscosity.

Table 2-7: Summary of approximate % increase in viscosity relative to base fluid found in literature

Nanoparticle	Base fluid	Vol. %	%	Temperature K	Reference
Al_2O_3	Water	30	20-30	24	Wang *et al*. [14]
	Water	0.01 – 3	30	21 – 39	Lee *et al*. [50]
	Water	0.15 – 9	60	20 – 70	Nguyen *et al*. [51]
	Water	5.0	82	–24	Murshed *et al*. [52]
	EG	30	20-30	20 – 50	Wang *et al*. [14]
	EG	0.5 – 6	60		Anoop *et al*. [53]
CuO	EG	5	83.4	–10–50	Liu *et al*. [54]
	Water	1–10	90	-30–50	Pastoriza-Gallego *et al*. [55]
	Water: EG 40:60	0 –6	98		Namburu *et al*. [56]
MWCNT	Water	0.2	70	5–65	Chen *et al*. [57]
	Water	0.5–3 wt.%	20	-20–150	Phuoc *et al*. [58]
	Water: EG 30:70	0.041–0.395	–	10–50	Kole & Dey [48]
Graphite	BF#1 [1]	2 wt.%	67.6	35–70	Yang *et al*. [59]
	BF#2 [2]		65.6		
SWCNH [3]	Water	0.01–1 wt.%	71	10 – 80	Bobbo *et al*. [60]

[1]BF#1 – automatic transmission fluid
[2]BF#1 – synthetic base-oils with commercial additive packages
[3]SWCNH – single-walled carbon nanohorn

The results by Wang[14], Murshed[52] and Liu *et al*. [54] in Table 2-7 were obtained at a single temperature and they show an increase in viscosity when compared to the base fluid. All the other results, however, show a decrease in viscosity over the temperature range indicated. The use of very low volume concentrations in the study of Lee *et al.* [50] reveals a nonlinear relation between viscosity and particle concentration indicating the presence of particle-particle interactions. That's why Lee's result varied from Einstein's prediction. In Chen *et al*. [57], he further noted the increase was substantial for temperatures after 328K. The effect of base fluid on viscosity as studied by Xie *et al*. [61] showed the enhancement ratios of viscosity of ethylene glycol-based nanofluids are smaller than those of water-based nanofluids, according to Sridhara [62]. The study by Pastoriza-Gallego *et al*. [55] shows the effect of particle size on viscosity with results indicating smaller particles (11 nm in Table 2-7) demonstrating larger percentage change

in viscosity over the temperature range; as high as 100% for 10 wt.%. One of the few studies on Water/EG mixture-based nanofluids by Namburu *et al* [56] show an exponential decrease in viscosity with temperature. He also observed Newtonian behaviour in his nanofluid. The only probable exceptions to the trends discussed so far are studies by Prasher *et al*. [63] and Chen *et al*. [47] who both measured negligible correlation between viscosity and temperature for the range 293–333 K. This was attributed to the negligible Brownian diffusion in the temperature range considered.

All models predict an increase in viscosity with increasing particle concentration and this has been confirmed experimentally with results in varying degrees of agreement [64], [65], [66]. Although none of the models in Table 2-7 include temperature effects, strong temperature dependence have been measured with Indhuja *et al*. [66] measuring 15% decrease in viscosity over temperature change of 27–60°C for water-based MWCNT nanofluids. This is contradicted by Chen *et al*. [57] who observed significant increase in viscosity for temperatures > 55 °C for water-based MWCNT nanofluids. Both results are further contradicted by Prasher *et al*. [88] who observed no significant variation with temperature for propylene glycol-based alumina nanofluids. Another source of discrepancy is with particle size where He *et al*. [67] observed increase in viscosity with increasing particle size of TiO2 in water. This differs with results from Lu & Fan [68] and Anoop *et al*. [69] who observed a decrease in viscosity with increasing particle size. Both sets of results were further contradicted by Prasher *et al*. [63] who observed no significant correlation of viscosity with nanoparticle diameter of alumina particles in propylene glycol. Other factors like different experimental procedure used by the researchers and the nanofluid manufacture/preparation process contribute to discrepancies found in the literature.

2.7 Natural convection

Numerous researches into nanofluids has focused on thermal conductivity with fewer studies into the convective behaviour of nanofluids as noted by Das *et al.*[4] and even fewer in natural convection according to Wang *et al.*[16]. This could imply an underestimation of the importance of natural convection in heat transfer applications. However, natural convection is a cheaper form of heat transfer as there is no need for an external mechanical system to generate and maintain fluid flow. It has potential use in a myriad of applications including computer cooling, aeronautics, automobiles, nuclear

power plants, solar energy, aeolian and geothermal equipment, as well as in the food, agriculture and pharmaceutical industry [70].

Numerical simulation studies of natural convection usually in closed cavities are relatively extensive when compared to experimental studies. They involve using the finite-volume method in solving Navier-Stokes equations of mass, momentum and energy balance and applying the Boussinesq's Approximation to couple the hydrodynamic and thermal fields. Early studies by Khanafer, 2003 [71] used aqueous copper nanofluids in a two-dimensional enclosure and Grashof number ranging from $10^3 - 10^5$. The nanofluid was treated as single-phase with different thermal conductivity and viscosity models applied. An increase in heat transfer rate was found for each Grashof number. A correlation of the Nusselt number along the hot vertical wall to volume concentration $0 \leq \phi \leq 0.1$ and Rayleigh number $10^4 \leq Ra \leq 10^5$ was also derived, which revealed an increasing Nusselt number with both quantities.

$$Nu = 0.5163(0.4436 + \phi^{1.0809})Gr^{0.3123}$$

Ternik and Rudolf [72] investigated natural convection of Au, Al_2O_3, Cu and TiO_2 aqueous nanofluids in the range $10^3 \leq Ra \leq 10^5$. For each type of nanofluid investigated, the average Nusselt number along with overall heat transfer enhancement increased with both Rayleigh number and volume concentration. Greater enhancement was found for lower Rayleigh numbers. Enhancement values as high as 33% for Ra = 10^5 and $\phi = 0.1$ were reported by Ternik and Rudolf [72].

A variation to the natural convection in a square enclosure was made by Oztop and Abu Nada [73] where a heater of variable height $0.1 \leq h \leq 0.75\ m$ is mounted on one of the walls of the enclosure. Calculations were done over $10^3 \leq Ra \leq 5 \times 10^5$ and like previous studies, the average Nusselt number increased with increasing volume concentration over the entire Rayleigh number range. Heat transfer also correlated with the heater height.

A similar study to the study by Khanafer *et al.* [71] was done by Santra *et al.*, 2008 [74] where natural convection of aqueous copper nanofluids in a square enclosure in the range $10^4 \leq Ra \leq 10^7$ and $0.05\% \leq \phi \leq 5\%$ was studied. Interestingly a *decrease* in heat transfer was observed over any given Ra number with increasing volume concentration. A decrease in average Nusselt number was as high as 38.3% for $\phi = 5\%$

and $Ra = 10^7$. Furthermore, Santra *et al*. [74] observed the average Nusselt number was independent of the volume concentration, $\phi > 3\%$ at $Ra = 10^4$. This particular result was corroborated to some extent by Abu-Nada *et al.* [75] who used horizontal concentric annuli instead of a square enclosure. They reported heat transfer enhancement for $Ra = 10^3$ and $Ra = 10^5$, but intermediate values showed a reduction in heat transfer. Similarly to Santra *et al*. [74] there was a negligible effect of volume concentration on heat transfer at $Ra = 10^4$ as reported by Abu-Nada *et al.* [75]. The disparity in results found between Santra *et al*. [74] and Khanafer *et al.*[71] suggests the model for thermal conductivity and viscosity used in the numerical analysis is crucial. The studies above have the limitation of using idealised models for thermal conductivity and viscosity which often differ significantly with actual nanofluid behaviour. There is a wide range of possible models to select from Ho *et al.* [76] and demonstrated that the choice of model significantly affects and sometimes lead to contradictory results. This finding is supported by the disparity in the results of Khanafer and Santra *et al*.

In each of the preceding studies, idealised theoretical models were used to define thermal conductivity and viscosity behaviour. This is problematic since the actual thermophysical behaviour of nanofluid varies significantly for different nanoparticles. The disparity in results found between Santra *et al*. [74] and Khanafer *et al*. [71] also suggests the results of numerical analysis is highly dependent on the model of thermal conductivity and viscosity employed. There is a large number of possible combinations of thermal conductivity and viscosity models that can be used in analysis and Ho *et al*. [76] demonstrated that for the same parameters, the choice of model can even lead to contradictory results. A recent study by Jahanshahi *et al*. [77] using experimentally thermal conductivity values as opposed to theoretical models, showed an increase in average Nusselt number with increasing particle concentration for Rayleigh number $10^3 - 10^5$ and volume concentration 0–4% of SiO_2-water nanofluid. However, the viscosity model used was theoretical and no determination of the deviation from actual viscosity was made. The numerical analysis in the present study is also supplemented by experimental characterisation of the thermo-physical properties of the MWCNT.

Among the small amount of literature available on natural convection, a notable experimental study was done by Putra *et al.*[78]. Using water-based alumina and copper oxide nanofluids inside a horizontal cylinder with differential end temperatures a

deterioration of heat transfer was observed. The experiment used volume concentration ranging from 1–4% and Rayleigh number $10^6 - 10^9$. Deterioration as high as 300% was measured for 4% CuO nanofluid at Ra number of 5×10^3. This deterioration in heat transfer with increasing particle concentration was corroborated by Wen and Ding [79] using TiO_2 nanofluids in a rectangular enclosure heated from below. The decrease in heat transfer was greater at low Rayleigh number. Ho *et al* [80] using Al_2O_3 in a vertical square enclosure with differential side wall temperature also observed 'degradation' in heat transfer for particle concentration greater than 2% over the entire range of Rayleigh numbers tested. However, they also observed an enhancement of up to 18% in heat transfer for particle concentration of 0.1%.

2.8 Conclusion

Chapter 2 covered a range of topics related to the use of nanofluids as heat transfer fluids. The two-step method of preparation, in conjunction with ultrasonication to improve nanofluid stability, was found to be most widely used in the literature. It has the advantage of being reliable and applicable over a wide range of temperatures and volume fraction. Several models and experimental results of thermal conductivity and viscosity of nanofluids have been reported. Despite the lack of uniformity in results, studies do show an enhancement in both thermal conductivity and viscosity with increasing particle concentration for a given range. However, there are numerous other factors affecting nanofluid behaviour which include nanoparticle shape, size and temperature of nanofluid. The development of a hybrid model working for different nanofluids is almost impossible. For practicality, many researchers have developed models restricted to a narrow range of nanofluid parameters.

Lastly, literature on natural convection in nanofluids were also reviewed which revealed significant contradictions in reported results. The studies on natural convection are largely numerical and the choice of thermal conductivity and viscosity model used in the simulation influenced the results obtained. Such discrepancies clearly illustrate the need for more nanofluid experimental studies in natural convection which is currently limited. The present study uses experimentally determined thermo-physical properties of water-based MWCNT nanofluids.

CHAPTER 3. THERMAL CONDUCTIVITY AND VISCOSITY MEASUREMENTS

3.1 Introduction

This chapter outlines the measurement used to determine the effective thermal conductivity and viscosity of samples of nanofluids with different particle concentration. The KD2 Pro based on the Transient Hot Wire (THW) method was used. A cylindrical cell with a mountable design for the thermal conductivity probe contains the sample fluid and the heating element. All the theories and assumptions applied in this chapter are based on information collected from the preceding literature studies.

3.2 Nanofluid preparation

A range of nanofluid concentrations was investigated and the preparation method was the widely used two-step method outlined in Chapter 2.1. Based on Assael *et al*. [39] studies on MWCNT nanofluids which yielded a maximum thermal conductivity enhancement of 38% for 0.6% volume concentration, the volume concentrations used in the present study range from 0–1%. Higher concentration nanofluids were more difficult to prepare using the present ultrasonication method and, therefore, show less stability. This is the approximate range of volume concentration expected to be used in real engineering applications. If the volume concentration was considerably higher, there would be other factors like increased abrasion and clogging of fluid pathways as well as increased sedimentation rate of nanoparticles which would require regular changing. All this would render the use of high-particle concentration nanofluids impractical. MWCNT used were sourced from MK Nano and have the following dimension range: inner diameter, 3–5 nm; outer diameter, 10–20 nm and lengths, 10–30 µm. The hydroxyl group was added to the MWCNTs surface by treatment with acid giving it greater dispersion stability and have nominal density 2.1 g/cm^3. To achieve a desired volume concentration ϕ, the required mass of particles m_p to be added to base fluid is calculated from:

$$\phi = \frac{(m_p/\rho_p)}{(\frac{m_p}{\rho_p} + \frac{m_f}{\rho_f})}$$

$$m_p = \frac{\phi \frac{\rho_p}{\rho_f} m_f}{1 - \phi}$$

A process of ultrasonication is employed to disperse the nanoparticles in water. Of the previously used dispersion techniques using surfactant, sodium dodecyl benzene sulfonate (SDBS) resulted in less stable nanofluids at high temperatures (Wen and Ding [38]) and so was not considered. According to Bandyopadhyaya *et al.* [81] surfactants like gum arabic (GA) was found to be better than other commonly used surfactants like sodium dodecyl sulphate (SDS) and cetyl trimethyl ammonium chloride (CTAC). Using Wet-TEM to scan aqueous solutions of MWCNT nanofluids, Garg *et al*. [82] found an optimum ultrasonication time of 40 minutes when using 130W, 20 kHz ultrasonication probe at maximum power on nanofluids with mass fraction of GA and MWCNT as 0.25% and 1%, respectively. Similarly, using mass of GA to m_p ratio of 1:4 and sonication time of 40 minutes, the nanofluids were sonicated using the Q700 sonicator provided by QSonica Company. It was operated at 700 W, 20 kHz and amplitude set to 75% of maximum. Sonication was done in a constant temperature bath maintained at a low temperature to prevent the nanofluid from evaporating. Evaporation would alter the volume fraction. Figure 3-1 shows the mass balance used to measure mass of particle to be added to base fluid and Table 3-1 shows the different sonication times for the range of nanofluid particle and surfactant concentration used.

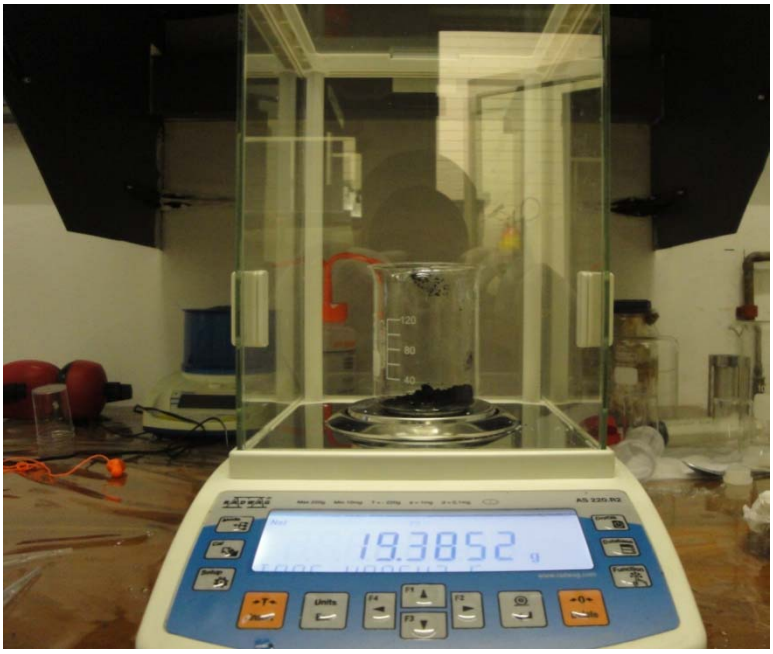

Figure 3-1: Mass balance for measuring masses

Table 3-1: Nanoparticle and surfactant concentration and sonication time

ϕ(%)	$m_p(g)$	Sonication time (min)
0.02	0.025	30
0.04	0.050	30
0.06	0.076	30
0.08	0.101	30
0.10	0.126	40
0.20	0.253	40
0.50	0.633	40
1.00	1.273	40

The sonicator used in the study is the Q700 sonicator from QSonica which operates at 700 W, 20 kHz with the amplitude set to 75% of maximum. The 20 kHz electric signal is used to vibrate a piezo-electric crystal attached to the probe. The resulting mechanical vibrations are amplified and transmitted down the probe to the tip dipped in the nanofluid sample. The high frequency vibration of the tip causes rapid formation and collapse of micro bubbles in the fluid. The bubbles collapse with significant energy generating shockwaves which provides a mixing force and a shear force enough to breakup any nanoparticle clusters present in the fluid. Figure 3-2 shows the sonication of a nanofluid sample in a temperature-controlled water bath.

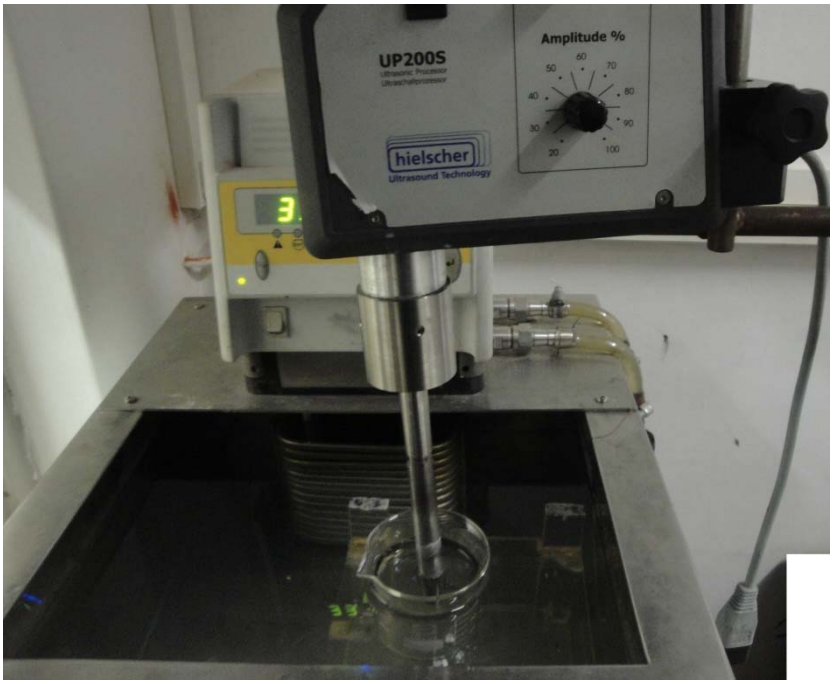

Figure 3-2: Sonication of nanofluids in temperature controlled water bath

A water bath set to 5 °C was used to maintain the solution at a low temperature. This is necessary, because the cavitation process generates a significant amount of heat and if temperature is left to rise, it will lead to evaporation of the base fluid. The resulting nanofluid samples showed visual stability for over three weeks after preparation and experimentation was completed. Figure 3-3 shows the progression of sedimentation in nanofluid samples left in quiescent states for periods of time ranging from before sonication to three weeks after sonication.

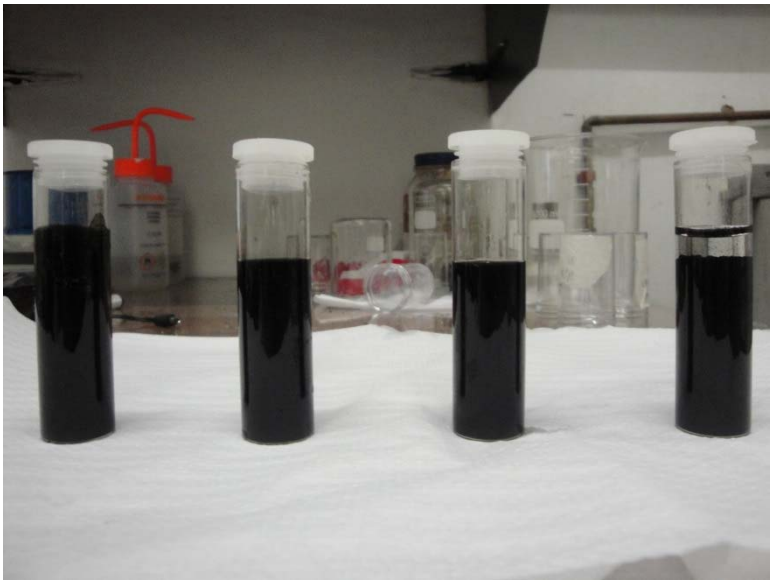

Figure 3-3: Nanofluid samples before (first from right) and after sonication.

Figure 3-4 shows the TEM image of MWCNT. The nanotube diameter and length were observed to be within the range: inner diameter, 3–5 nm; outer diameter, 10–20 nm and lengths, 10–30 μm as specified by the manufacturer.

Figure 3-4: TEM image of MWCNT nanofluid. Scale: 200 nm

3.3 Thermal conductivity measurement

The KD2 Pro from Decagon devices was used in measuring the thermal conductivity of the nanofluid samples which is based on the transient hot wire (THW) technique. A $\pm 5\%$ was quoted by Decagon devices. However, building the THW from the first principle is outside the scope of the present study. All measurements are carried out at 300 K, the bulk temperature of interest at which the numerical study is also carried out. This is well within the operating range of the device. Similarly to the sonication process, the temperature is maintained at a constant value using an insulated water bath. Vibrations from the pump and water circulation can induce convection currents in the fluid sample, therefore, the water bath was temporarily switched off before measurements were taken. The KD2 Pro sensor used was 60 mm long with 1.3 mm diameter. The measurement process of the KD2 Pro involves a 30 s temperature equilibration period followed by a heating period over half the read time. The read time was set to the minimum of 60 s at a low power mode. This was to ensure the sample fluid

was not heated excessively which would have resulted in the presence of convection currents. 15 minutes was allowed between readings to allow sufficient time for the fluid to cool. Calibration was done using de-ionised water at 300 K. Figure 3-5 shows the use of the KD2 Pro to measure a sample of nanofluid in a temperature-controlled water bath.

Figure 3-5: KD2 Pro with probe in nanofluid sample in water bath

Figure 3-6 shows results from experimental measurements compared to two models of thermal conductivity in carbon nanotubes, namely Deng and Zheng [33] and Nan et al. [83]. Both models take into account the non-spherical and non-straightness of the nanotubes. Appendix A gives the calculated thermal conductivity values using the different models.

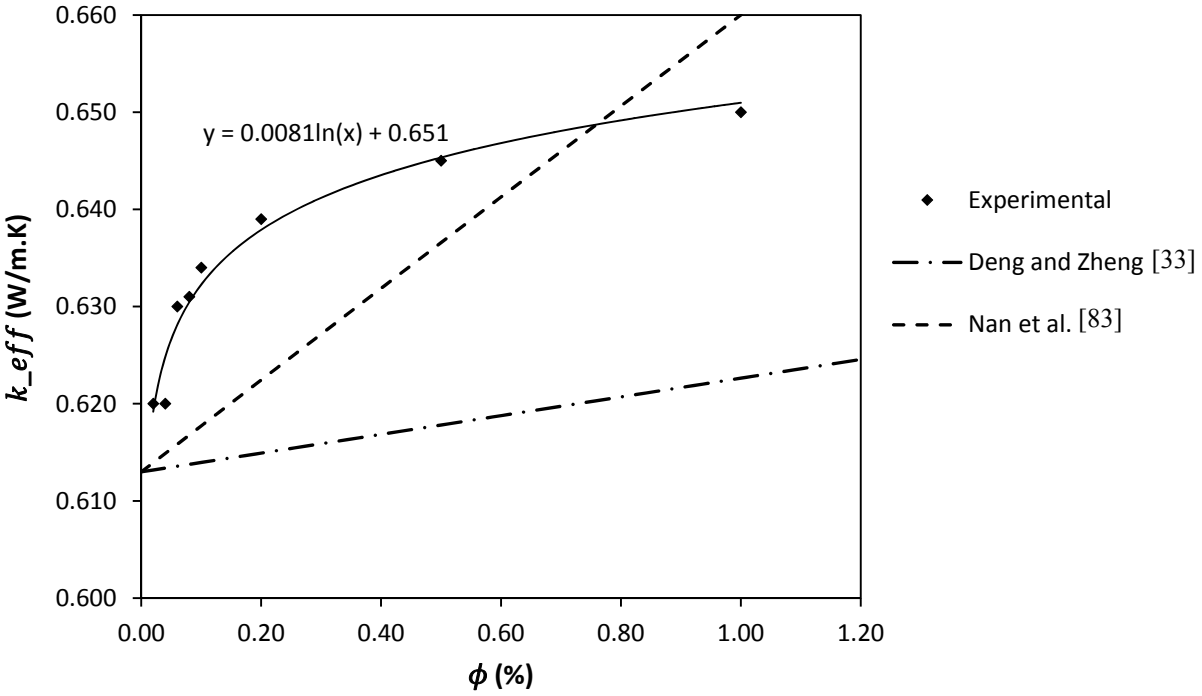

Figure 3-6: Experimental and theoretical values of thermal conductivity at varying ϕ

Both Xie *et al*. [84] and Meyer *et al*. [85] reported 7% and 8% enhancement in thermal conductivity respectively for water at volume fraction 1% compared to 6% measured in the present study. The theoretical models, however, both underestimate the thermal conductivities especially at low volume fractions. Nan *et al*. [83] is closest to experimental results with a maximum difference of 2.6% for the range tested. A significant limitation of both theoretical models is the omission of temperature effects. Since thermal conductivity is a thermo-physical property, temperature is important, especially for the Brownian motion mechanism.

3.4 Viscosity measurement

Viscosity measurement for nanofluid samples of volume fraction 0–1% was measured using the SV10 Sine-wave Vibro Viscometer. It consists of two thin-plate sensors caused to vibrate at a constant sine-wave vibration of resonance frequency 30 Hz and amplitude of $\approx 0.4\,mm$ in the sample fluid. The small amplitude is to avoid any alteration to the sample fluid. This vibration is driven by an electric current in turn generated by an accurate electromagnetic drive. The damping effect induced by the sample fluid is detected as a change in the electric signal needed to maintain the vibration at the same set frequency and amplitude of 30 Hz and $0.4\,mm$ respectively. Since the damping effect is due to the viscosity of the sample fluid, it can be related to the electric signal as follows:

$$F = F_0 sin\omega t$$

$$= m\frac{d^2x}{dt^2} + C\frac{dx}{dt} + Kx$$

The first, second and third term in equation 3.3 describe the inertial force of vibration, the viscous damping force and the correction force from internal springs respectively. The device is designed such that at resonance, the inertial force of vibration and correction force from the springs cancel. The general solution to equation 3.3 is of the form:

$$x(t) = A_p sin(\omega_n t + \theta)$$

$$A_p = \mathrm{F}_0/\omega_n C$$

The values A_p, F_o, ω_n *and* C are the amplitude, driving force, natural frequency of the system and coefficient of viscous damping respectively. The equation demonstrates that for a known amplitude and natural frequency, the driving force is proportional to the coefficient of viscous damping and therefore to viscosity. The device is calibrated using de-ionised water at 300 K and the values are programmed into the device. The SV10 also comes with a temperature probe and a water jacket that can be connected to a water bath. This is to ensure the viscosity values correspond to a specific temperature. As discussed in 2.5, viscosity is temperature dependent. Figure 3-7 shows the SV-10 Vibro Viscometer used in the study. The insulated pipes are inlets and outlets between the temperature-controlled water bath and the water jacket for the sample cup.

Figure 3-7: SV-10 Vibro Viscometer

Figure 3-8 shows results from experimental measurements compared to the widely-used Brinkman's model [43]. Results were also compared to Brenner and Condiff's model [44], which takes into account the non-spherical shape of the carbon nanotubes. Appendix A gives the calculated viscosity values using the different models.

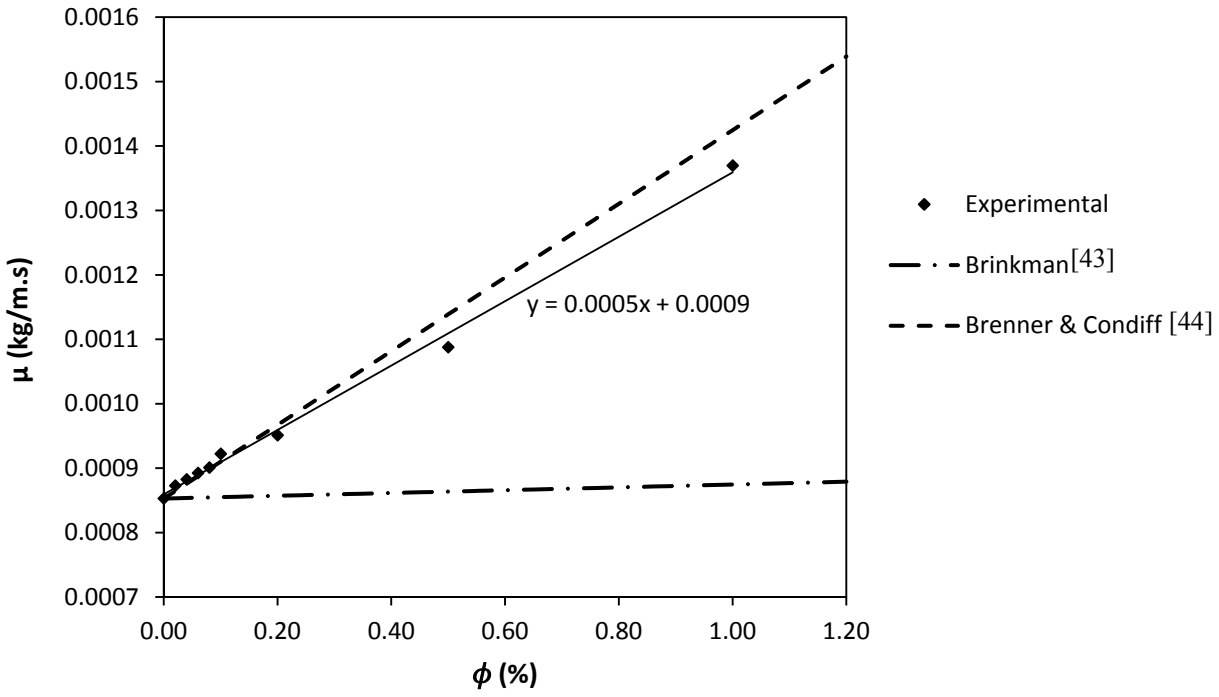

Figure 3-8: Experimental and theoretical values of viscosity at varying ϕ at 300K

It can also be seen that Brinkman's model [43]is unsuitable for carbon nanotubes while Brenner and Condiff's model [44]shows good correlation with a maximum 2.8% difference for the concentration range considered.

3.5 Conclusion

The nanofluid samples were prepared using the two-step method and ultrasonication. The nanofluid thermal conductivity data was measured using Decagon KD2 Pro thermal properties analyser for the volume fraction range of $0-1\%$. The SV10 Sine-wave Vibro Viscometer was used in measuring viscosity. All measurements were carried out at 27ºC and they maintained stability beyond experimentation time. Both thermal conductivity and viscosity were found to increase by increasing particle concentration. There was a poor correlation between present experimental data of thermal conductivity as well as viscosity, and the available models which they based on spherical particles in literature. However, Nan *et al*'s model [83] for thermal conductivity and Brenner and Condiff's model [44] for viscosity, take into account the non-spherical shape of nanotubes and showed less than 3.0 % difference with the corresponding experimental data .

CHAPTER 4. NUMERICAL ANALYSIS

4.1 Introduction

This chapter outlines that the CFD analyses were done using CD Adapco's Star CCM+ (v8.06). Experimental results of thermal conductivity and viscosity from chapter 3 were used as input function in the simulation of natural convection. This differs from previous studies which use existing models without justifying whether they correlate well with the nanofluid properties being studied. Based on experimental results, projections were made for higher particle concentrations of up to 8%.The validity of both the simulation and projections will be assessed in chapter 5 where the full experimental setup is used to study the heat transfer performance of nanofluids. Description of the mathematical model is followed by a mesh independence study. The CFD code was compared to the De Vahls benchmark results. Natural convection was investigated using temperature and velocity profiles along with isotherms and streamlines. Appendix C shows quantitative results in the form of various temperature and velocity colour contours obtained from CFD analysis carried out in this chapter.

4.2 Mathematical formulation

A 2D square enclosure is considered with length L and differentially heated side walls of temperature T_H and T_C. The top and bottom walls are considered to be well insulated and therefore adiabatic. The nanofluid is treated as single-phase, Newtonian and incompressible and the flow generated is laminar. Furthermore, viscous dissipation in the energy equation is considered negligible. The hydrodynamic and thermal fields are related using Boussinesq's approximation which requires density of the fluid to vary. Otherwise, the averages of other thermo-physical properties are assumed constant in the enclosure and are given in Figure 4-1 below.

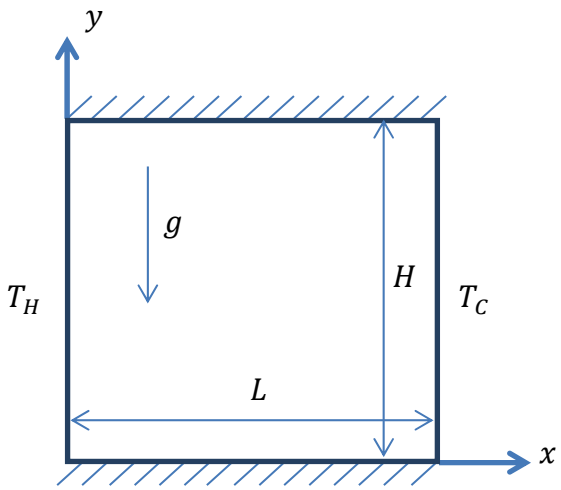

Figure 4-1: Physical model for problem and coordinate system

Table 4-1: Initial thermo-physical values

Property	$\rho\ (kg/m^3)$	$k\ (W/mK)$	$c_p(J/KgK)$	$\beta\ (1/K)$
Water	997.1	0.613	4179	0.00021
MWCNT	2100	20	470	0.000007

Applying Navier Stokes' equations to the model and using the subscripts n for nanofluid terms, the following equations apply [72]:

Continuity: $\boldsymbol{\nabla} \cdot v = 0$

Momentum: $\rho \frac{D\boldsymbol{V}}{Dt} = -\nabla \boldsymbol{P} + \boldsymbol{\nabla} \cdot (\mu \boldsymbol{\nabla u}) + (\rho\beta)_n \, \boldsymbol{g}\,(T - T_c)$

Energy: $\frac{DT}{Dt} = \boldsymbol{\nabla} \cdot \left(\frac{k}{(\rho c_p)_n} \boldsymbol{\nabla} T \right)$

The thermo-physical properties used in the equations above vary with volume concentration as follows:

Density: $\rho_n = (1-\phi)\rho_f + \phi\rho_p$

Specific heat: $(\rho c_p)_n = (1-\phi)(\rho c_p)_f + \phi(\rho c_p)_p$

Thermal coefficient: $(\rho\beta)_n = (1-\phi)(\rho\beta)_f + \phi(\rho\beta)_p$

Buoyancy source term $\boldsymbol{f} = \rho\, \boldsymbol{g}\, \beta\, (T_{ref} - T)$

The following boundary conditions follow from the formulation above:

Adiabatic top and bottom wall:	$\frac{\partial T}{\partial y} = 0$	$0 \le x \le L$ and $0 \le y \le H$
Constant temperature sidewall:	$T(0,y) = T_H;$ $T(L,y) = T_C;$	$x = 0;\ x = L;$
No-slip boundary condition:	$u = v = 0$	$x = 0\ and\ 0 \le y \le H$ $x = L\ and\ 0 \le y \le H$ $y = 0\ and\ 0 \le x \le L$ $y = H\ and\ 0 \le x \le L$

The effect of varying particle concentration on heat transfer rate is evaluated by calculating the local and average Nusselt number along the hot wall of the square enclosure which is given by:

$$Nu_H = -\frac{k_n}{k_f}\frac{\partial T(y)}{\partial x}\bigg|_{x=0}$$

$$\overline{Nu} = \frac{1}{H}\int_0^H Nu_H\, dy$$

Heat transfer rates at each particle concentration are also compared at different Rayleigh number Ra given by:

$$Ra = \frac{\rho_n(\rho c_p)_n g\beta_n(T_H - T_C)L^3}{\mu_n k_n}$$

4.3 Mesh independence study and validation

Both mesh generation and simulation was done using CD Adapco's Star-CCM+ Code (v 8.06). Since the domain of analysis is relatively simple, the need for compromising between computational cost and fidelity of results that one usually encounters when performing CFD calculations is not present. Mesh refinement was carried out until there was no significant change in Nusselt number obtained for each mesh. At this point the solution can be considered to be independent of the meshing applied to the domain. From the various meshing types available, a square grid was applied to a 2D model. Although refinement could have been restricted to the boundaries, as mentioned earlier, computational cost was not an important factor. Results for maximum and average Nusselt number, along the hot wall for water-filled square cavity at $Ra = 10^6$, are given in Table 4-2 below for different mesh sizes.

Table 4-2: Nusselt number values with decreasing mesh sizes

Mesh size, $x^* = y^*$	Nu_{avg}	Nu_{max}
80 x 80	9.400	20.752
100 x 100	9.335	20.336
120 x 120	9.302	20.090
160 x 160	9.265	19.792
200 x 200	9.248	19.673
220 x 220	9.243	19.635
240 x 240	9.239	19.604
260 x 260	9.236	19.577
280 x 280	9.234	19.558

Figure 4-2 shows the graph of average Nusselt number of the hot temperature wall for water-filled square cavity at $Ra = 10^6$. Convergence was achieved at $x^* = y^* = 280$ based on the error criterion of $\left|Nu_{avg}^{i} - Nu_{avg}^{i+1}\right| \leq 0.000001$.

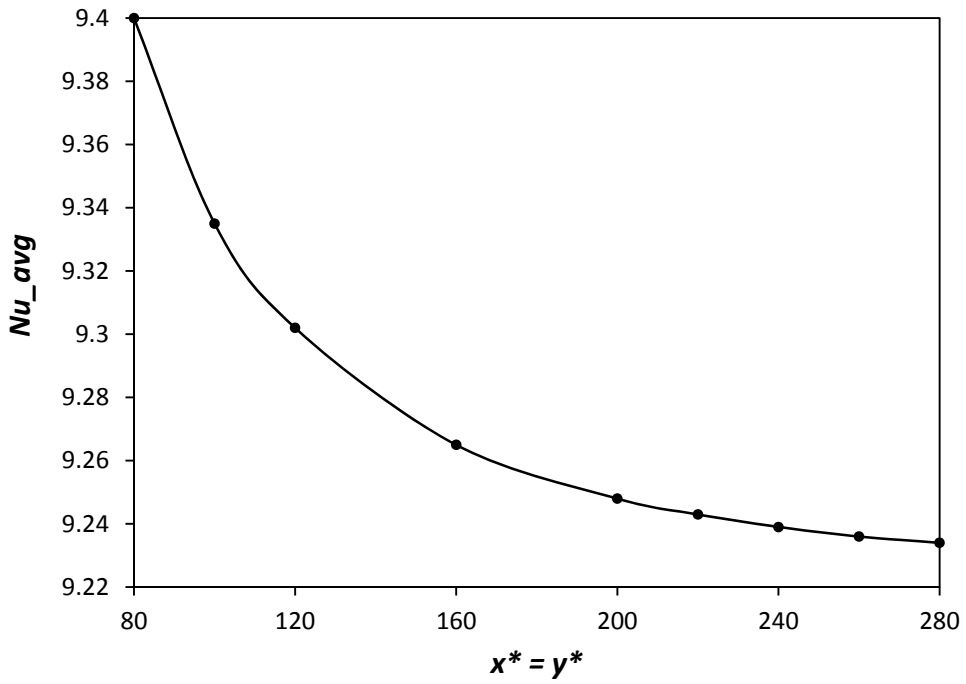

Figure 4-2: Convergence of Nu_{avg} with increasing mesh refinement (x* = y*)

An estimate of numerical uncertainty involved with using mesh size $x^* = y^* = 280$ is obtained by applying Richardson's extrapolation technique to table 4-2 (Roache [86] and Ternik and Rudolf [72]).

$$Nu' = Nu_1 - (Nu_2 - Nu_1)/(r^p - 1)$$

where Nu_1 is the solution based on the finest grid and Nu_2 on the next coarser grid. r is the ratio of successive mesh sizes, $r = 1.08$ and p, the order of convergence is calculated as:

$$p = \frac{ln\left(\frac{Nu_3 - Nu_2}{Nu_2 - Nu_1}\right)}{ln\ 2} \approx 0.5850$$

$$Nu' = 9.234 - (9.236 - 9.234)/(1.08^{0.5850} - 1) = 9.191$$

The difference between the Nu value based on the finest mesh and the extrapolated value Nu' is 0.47% which is sufficiently low for one to proceed with the mesh size $x^* = y^* = 280$.

To validate the simulation parameter, a numerical analysis was done for an air-filled square enclosure at Ra number $10^4 - 10^6$ and $Pr = 0.71$. Results were compared to benchmark results from previous research on the same problem statement by De Vahl Davis [87] and Turan *et al*. [88].

Table 4-3: Comparison of Nusselt number with current and previous studies

Ra		Current Study	(De Vahl Davis, 1983)	(Turan *et al.* 2010)
10^3	Nu_{avg}	1.118	1.118	1.118
	Nu_{max}	1.502	1.506	1.506
10^4	Nu_{avg}	2.252	2.243	2.245
	Nu_{max}	3.539	3.528	3.531
10^5	Nu_{avg}	4.519	4.519	4.520
	Nu_{max}	7.725	7.717	7.717
10^6	Nu_{avg}	8.830	8.799	8.823
	Nu_{max}	17.650	17.925	17.530

Table 4-3 shows good agreement between the three studies compared over the entire Ra number range. The maximum deviation calculated between the current study and De Vahl Davis is 1.6%, which occurs at $Ra = 10^6$ for Nu_{avg}. The maximum deviation between the current study and Turan *et al.* is 0.67%, which occurs at $Ra = 10^6$ for Nu_{max}, where both deviations are within acceptable limits. Better agreement was achieved between the current study and Turan *et al.*, 2010.

Figure 4-3 illustrates the variation of isotherms and streamline fields for natural convection of air in a square cavity for $Ra = 10^3 - 10^6$ and $Pr = 0.71$. They show the increasing circulation strength with increasing Ra number. This is to be expected as increasing Ra corresponds to increase in buoyancy. Figure 4-3 shows good correlations with previous results [72][87], [88] and further confirms the validity of the numerical process to be used in the following sections.

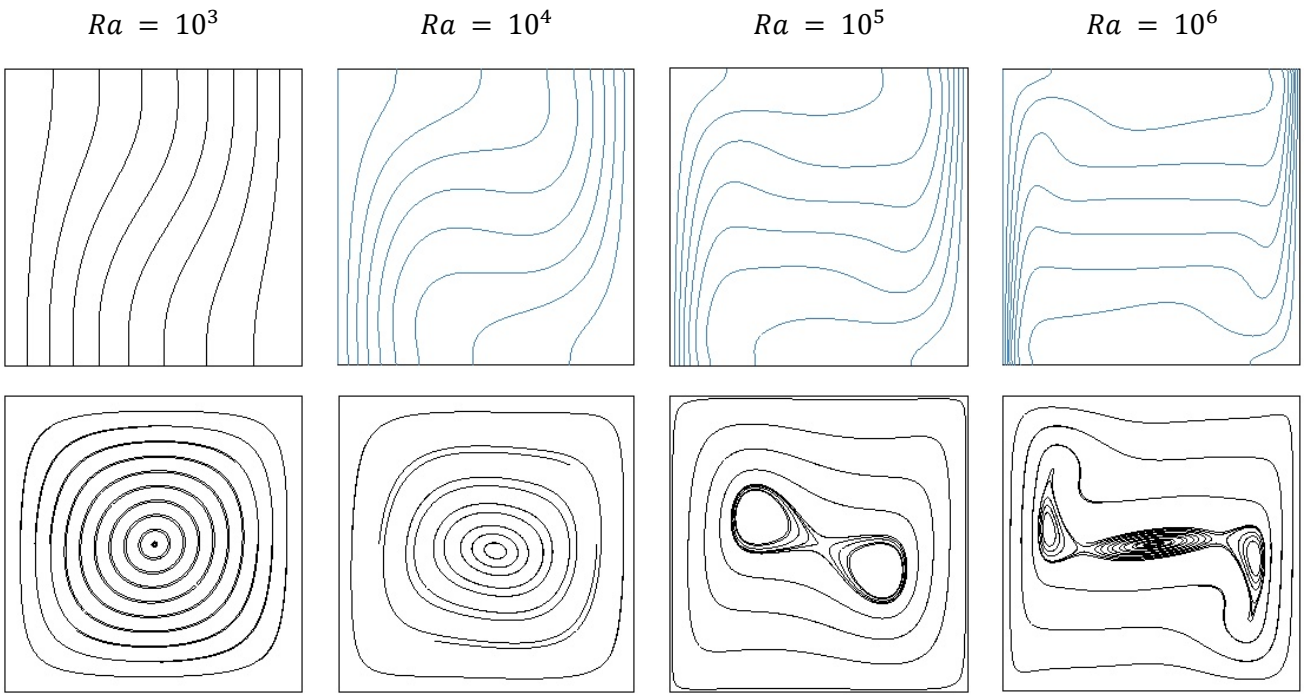

Figure 4-3: Isotherms (top) and streamline (bottom) contours for air in square cavity for *Ra* = 10^3–10^6

4.4 Results and discussion

Water-based carbon nanofluids were considered in this study. Water is evaluated at $Pr = 5.83$ corresponding to temperature 300 K. Using the numerical process in chapter 4 a study was carried out on carbon nanofluids for volume concentrations ranging from 0–1% at reference temperature 300 K and for Rayleigh number $10^4 - 10^6$based on experimental values measured in chapter 3 and the theoretical model which matches best with measured values. The carbon nanotubes are of inner diameter, 3–5 nm; outer diameter, 10–20 nm and lengths, 10–30 μm. The thermo-physical properties of the base fluid and nanoparticles were given in Table 4-1 (Kim *et al*. [89]).

Table 4-4: Theoretical thermal conductivity and viscosity models

Thermal conductivity	Dynamic viscosity
$k_{eff} = 0.0081 \ln \phi + 0.651$	$\mu_{eff} = 0.0005\phi + 0.0009$

In this study, the Nusselt number is used to characterise the efficiency of the different concentrations of nanofluids. The Nusselt number is highly dependent on the temperature and velocity distribution in the enclosure, therefore, analysis should start with a study of the flow structure.

4.5 Temperature distribution variation with ϕ

In Figures 4-4 to 4-7, the temperature distribution is taken at the axial midline of the cavity with normal vector $[x, y, z] = [0, 0, 1]$ for non-dimensionalised temperature $T^* = \frac{T - T_c}{T_h - T_c}$.

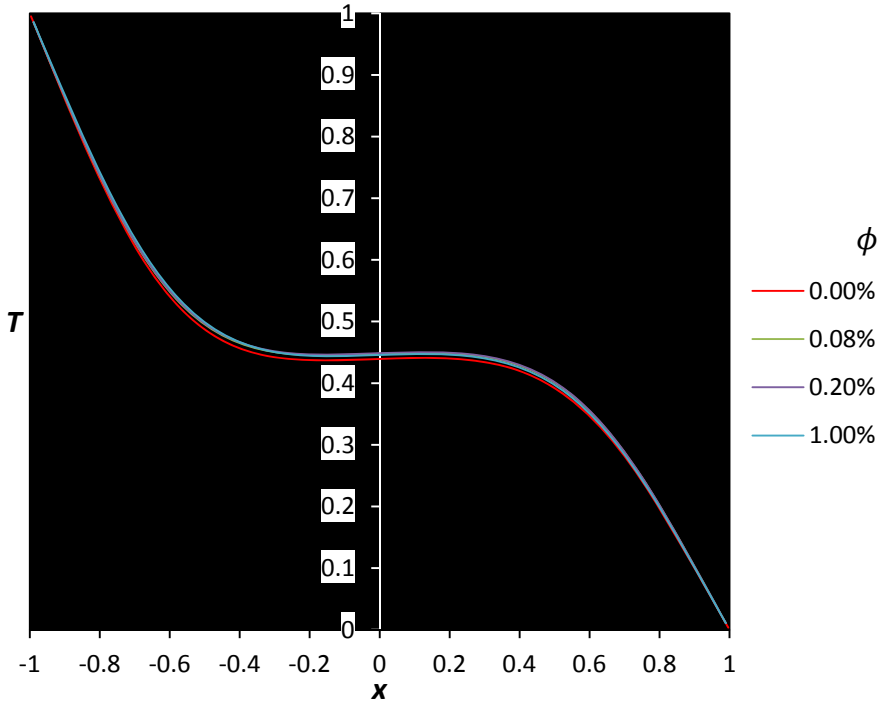

Figure 4-4: Temperature variation along axial midline x = [-1, 1] for different volume concentration (ϕ) at $Ra = 10^4$

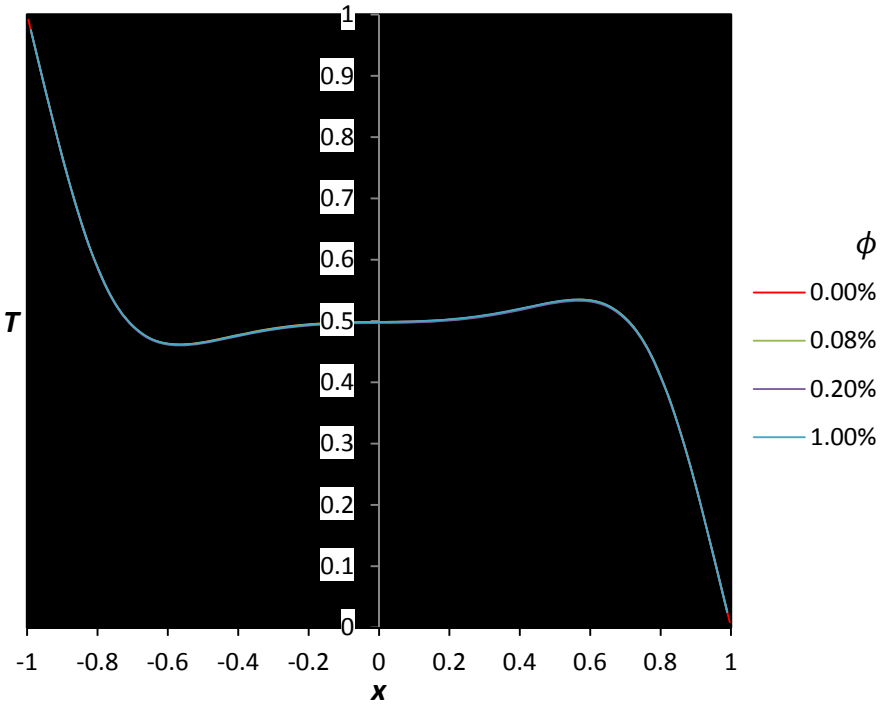

Figure 4-5: Temperature variation along axial midline x = [-1, 1] for different volume concentration (ϕ)at $Ra = 10^6$

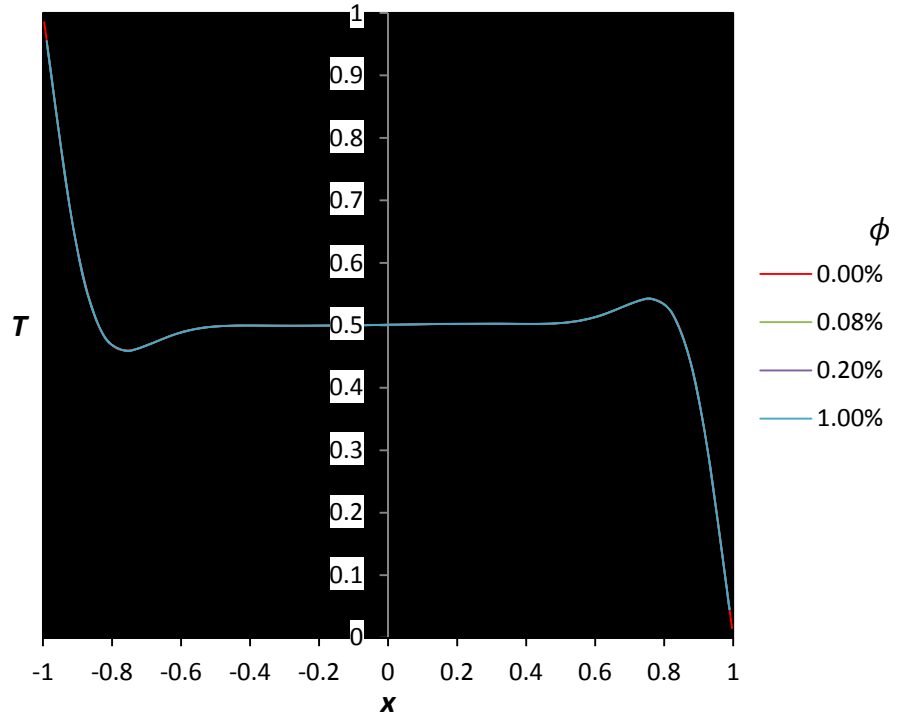

Figure 4-6: Temperature variation along axial midline x = [-1, 1] for different volume concentration (ϕ) at $Ra = 10^8$

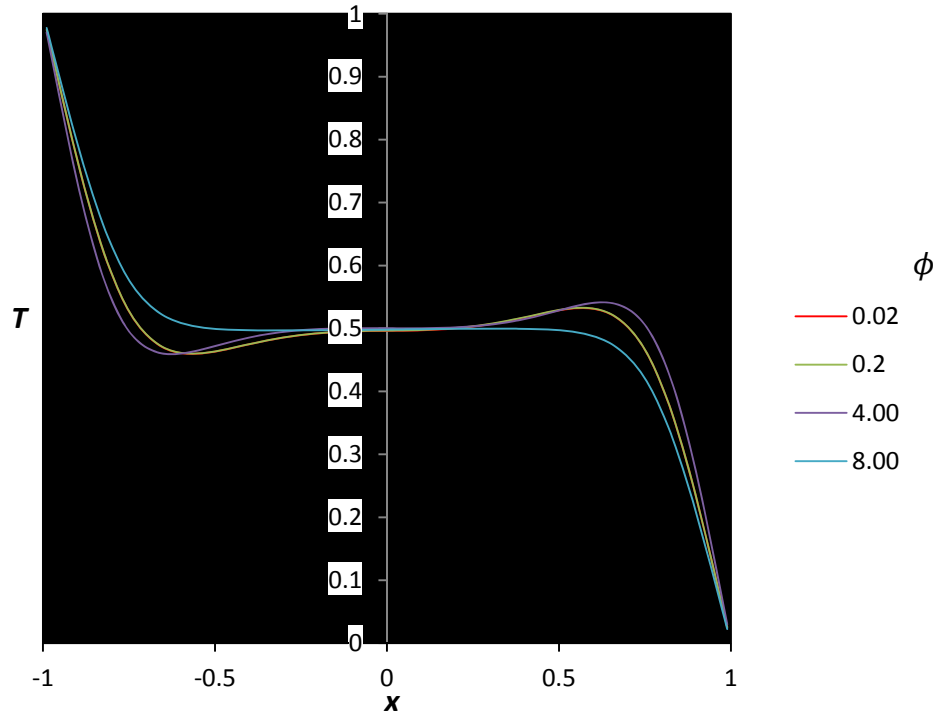

Figure 4-7 Temperature variation along axial midline x = [-1, 1] predicted for different volume concentration (ϕ)at $Ra = 10^6$

A region around the core of the cavity exists where temperature is uniform and at approximately the average of the two wall temperatures of 300 K. It can be seen that as the Rayleigh number increases, the region increases in size. Another view is that for a given ϕ, increasing Ra corresponds with increasing non-linearity of the temperature profiles. This is due to the increased buoyancy effect while viscous forces remain fairly constant, in turn increasing the strength of the convective currents. It was observed in chapter 3 that both thermal conductivity and viscosity increase with ϕ. However, for the particle concentration range under consideration, there is *no* significant effect of changing ϕ on the temperature profiles. This can be attributed to the increases in thermal conductivity and viscosity, both of which have opposite effects on convective heat transfer being equally matched, which illustrates the core of the present study. The change in buoyancy forces and the viscous forces are virtually cancelled out as ϕ increases, therefore, registering any significant change in the temperature profile. However, using the theoretical model to test for higher concentrations, it can be seen from figure 4-4 that as ϕ increases, the size of the central region with uniform temperature decreases. This is expected because with an increasing thermal conduction, the conduction rate through the fluid is increased, resulting in increased penetration of heat to the core region. Viscosity could also contribute to the decreasing size of the central region because by definition, increasing viscosity will result in decreasing velocity of the fluid. Therefore, the rate at which convection current removes heat from the central region is expected to reduce. As a result, the region decreases in size as the ϕ increases. The thermal boundary increases instead.

4.6 Y-velocity distribution variation with ϕ

In Figures 4-8 to 4-11, the velocity distribution in the y-direction is taken at the axial midline of the cavity with normal vector $[x, y, z] = [0, 1, 0]$.

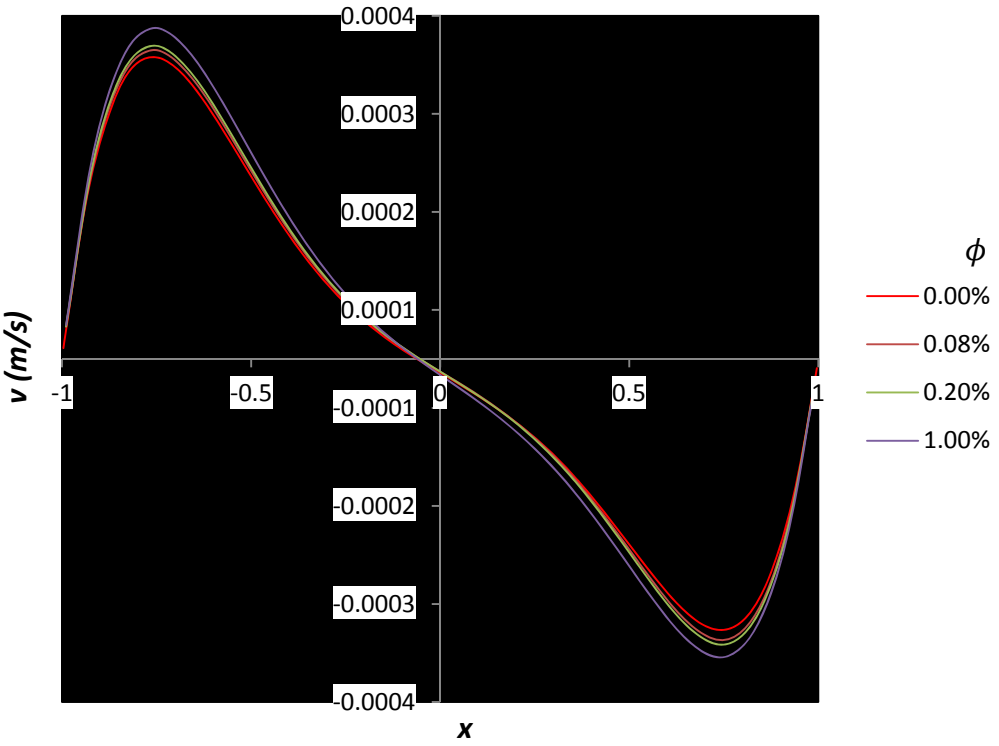

Figure 4-8: Y-velocity variation along axial midline x = [-1, 1] for different volume concentration (ϕ)at $Ra = 10^4$

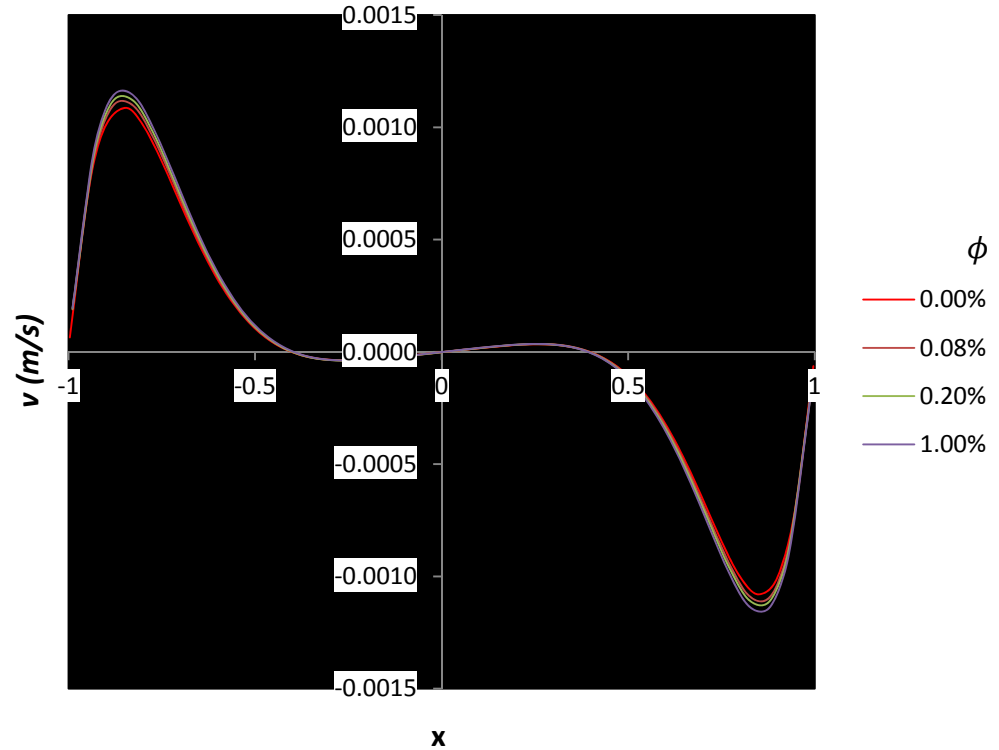

Figure 4-9: Y-velocity variation along axial midline x = [-1, 1] for different volume concentration (ϕ)at $Ra = 10^6$

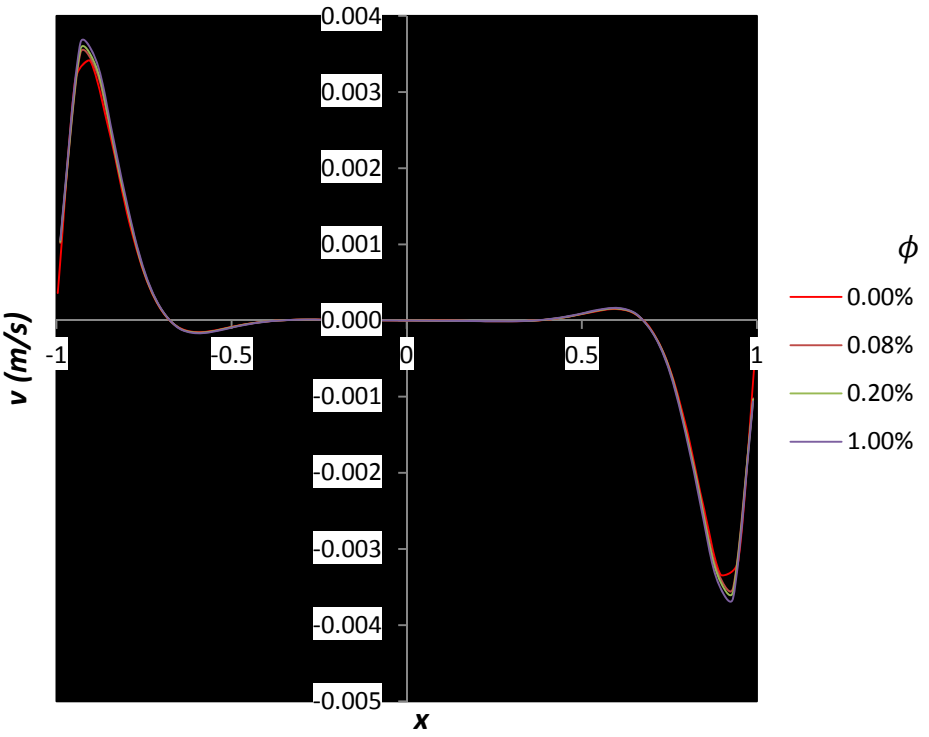

Figure 4-10: Y-velocity variation along axial midline x = [-1, 1] for different volume concentration (ϕ)at $Ra = 10^8$

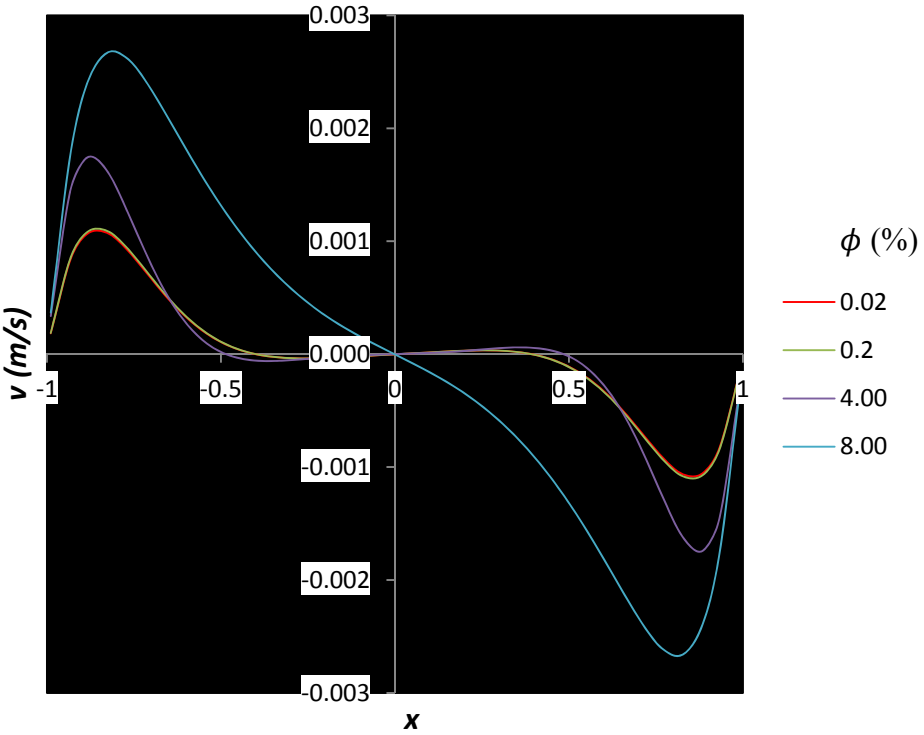

Figure 4-11: Y-velocity variation along axial midline x = [-1, 1] projected for different volume concentration (ϕ) at $Ra = 10^6$

From figures 4-8 to 4-11, the maximum velocity at each value of Ra increases with increasing ϕ.This is also supported by the theoretical model used for higher ϕ values. Similarly to the temperature profiles, the size of the central region with uniform velocity increases with increasing Ra number. In addition, the absolute maximum velocity increases with increasing Ra number. This is attributed to the increased buoyancy effect. For a given ϕ value, increasing Ra strengthens the buoyancy effects while viscous effects remain fairly constant thereby increasing the overall convective heat transfer.

However, for the range considered, variation with ϕ is minimal and this is due to the same effect explained in sub-chapter 4.5 for the temperature profiles. Thermal conductivity and viscosity have a counteracting effect on convective heat transfer and here the central problem is again illustrated: which of the two properties is dominant? Increase in maximum velocity with ϕ values indicates the increase in thermal conductivity (which strengthens the buoyancy effect) slightly outbalances the increase in viscosity (which decreases the overall buoyancy effect). Although increasing ϕ is expected to cause the fluid to become more viscous and reduce the velocities, the increase in thermal conductivity counters this effect by increasing convection. As mentioned in 4.5, there is increased penetration of heat in the fluid with increasing, therefore, the central region of uniform velocity decreases with increasing ϕ. The effects described are more clearly seen in Figure 4-11, which shows velocity distribution based on the theoretical model and is similar to figures 4-8 to 4-10. They all show that maximum velocity is measured near the walls. Figure 4-11 also shows that velocity increases significantly with concentration.

4.7 Isotherm and streamline variation with ϕ

Figures 4-12 1nd 4-13 show the variation in isotherms and streamlines with particle concentration. Similarly to the temperature and velocity profiles, for the range of ϕ values under consideration, there is no significant change in the isotherms and streamline patterns at a given Ra number as illustrated in figure 4-9. This is true for other Ra numbers using experimental results.

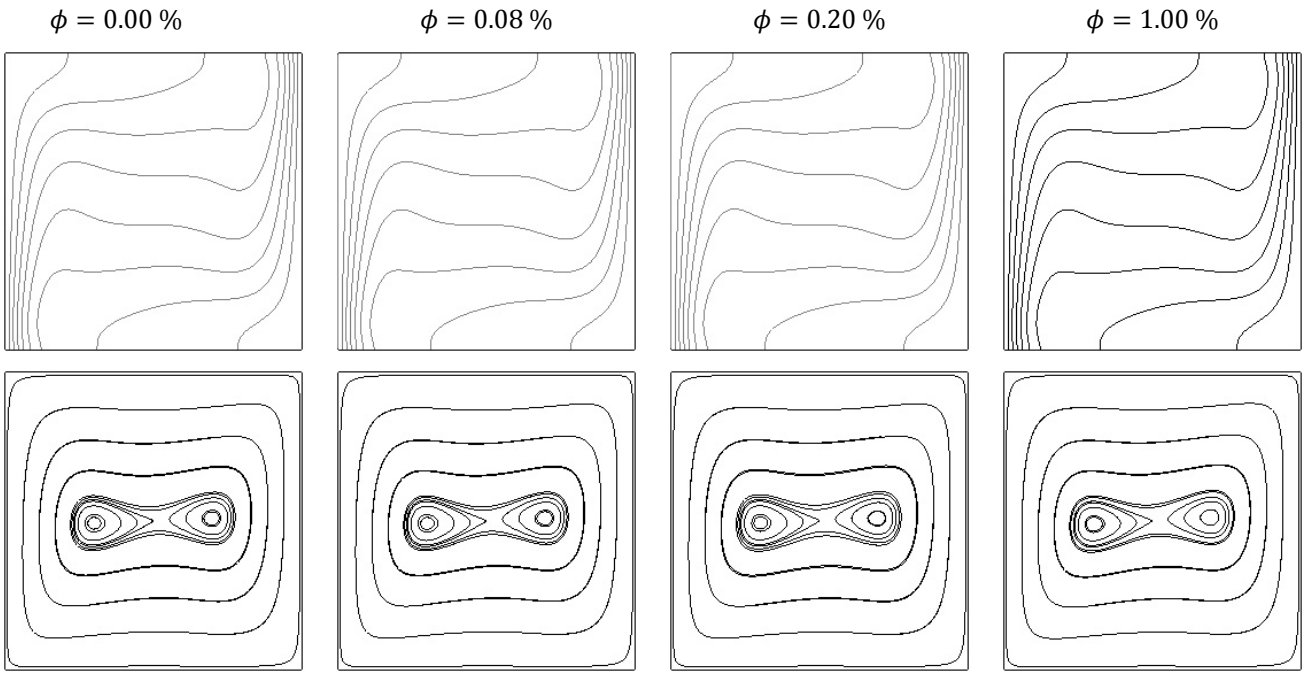

Figure 4-12: Isotherm (top) and streamline (bottom) variation with volume concentration(ϕ) for $Ra = 10^6$

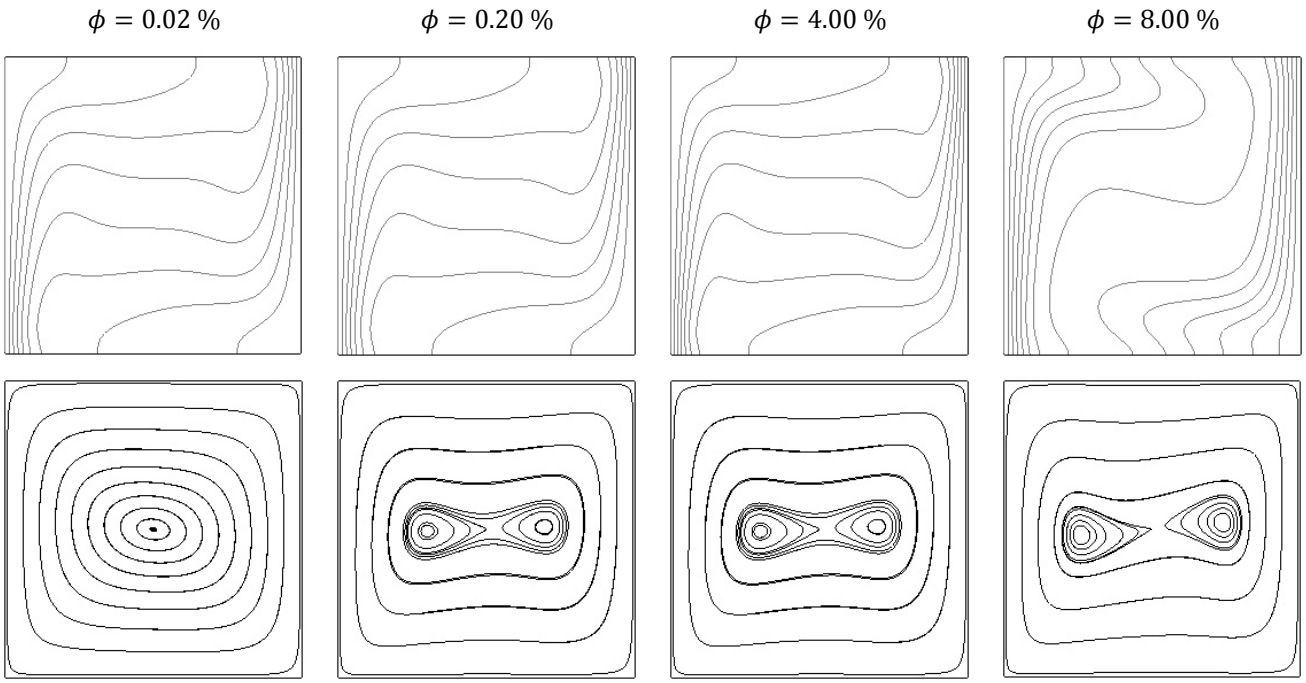

Figure 4-13: Projected isotherm (top) and streamline (bottom) variation with volume concentration(ϕ)for $Ra = 10^6$

For higher particle concentrations, a variation in the isotherms and streamline as determined from the theoretical model becomes more evident. Both the thermal and velocity boundary layers near the wall increase with ϕ. This is more clearly indicated by the start of a straightening of the isotherm lines in figure 4-12 and 4-13. Additionally, the

two central vortices of the streamlines begin to merge into a single vortex as ϕ increases. The increase in ϕ increases the viscosity of the nanofluid thereby causing a reduction in fluid velocity and consequently in buoyancy forces as well. However, there's an increase in thermal conductivity with ϕ which leads to increase in heat penetration through the fluid, thereby thickening the thermal boundary layer.

4.8 Isotherm and streamline variation with Ra

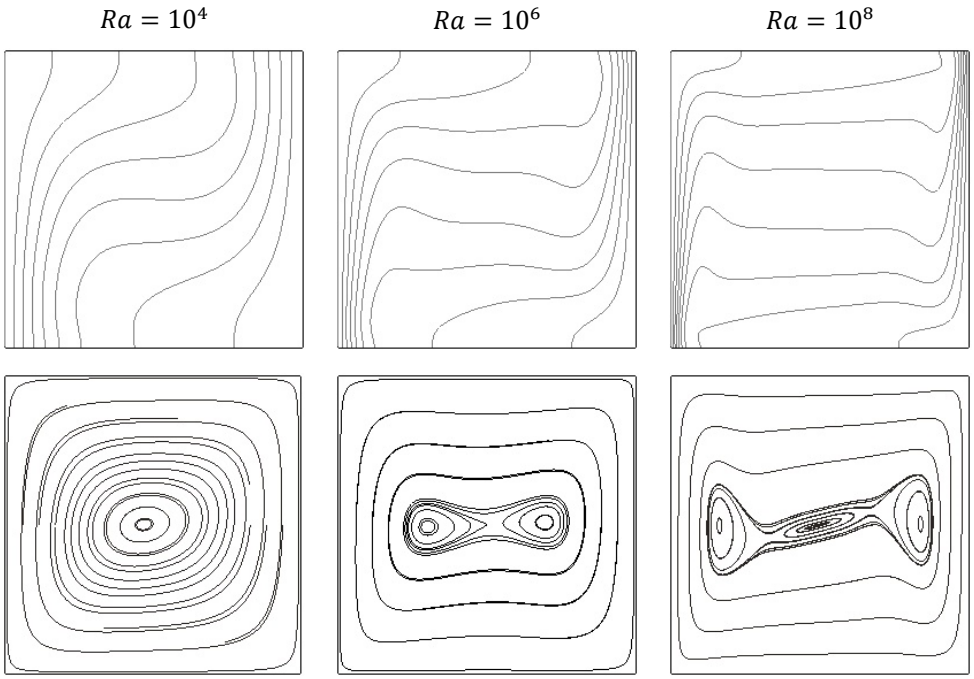

Figure 4-14: Isotherm (top) and streamline (bottom) variation with Rayleigh number for volume concentration ϕ ≥1.00 %

Figure 4-14 shows that the strength of convective flow increases with increasing Ra. As mentioned in sub chapter 4.1 and 4.2, an increase in Ra corresponds with an increase in the buoyancy effect while viscous effects remain fairly constant. The isotherms illustrate the decrease in the thickness of the thermal boundary layer with increasing Ra. Similarly, the streamlines show the decrease in the thickness of velocity boundary layer near the wall while the central region of uniform temperature and velocity increases in size. From the formulation of the Nusselt number, the thickening of the thermal boundary ∂x results in an increase in the calculated Nusselt number.

$$Nu_h = -\frac{k_n}{k_f}\frac{\partial T(y)}{\partial x}\Big|_{x=0}$$

4.9 Variation of Nusselt number with ϕ and Ra

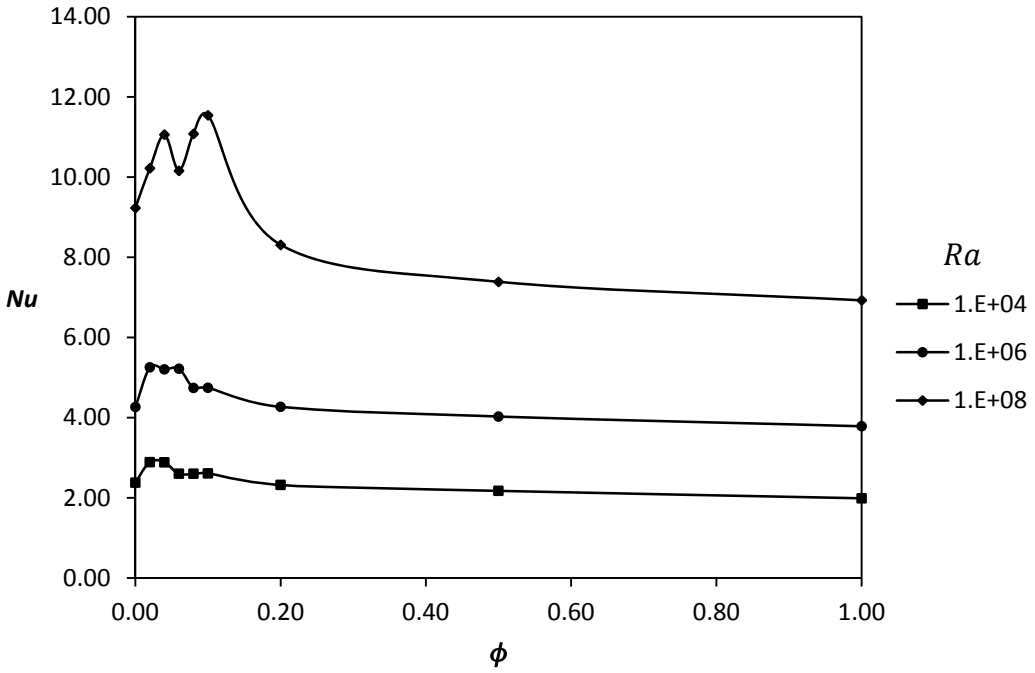

Figure 4-15: Variation of average Nusselt number on the hot wall with volume concentration(ϕ)at different Rayleigh numbers

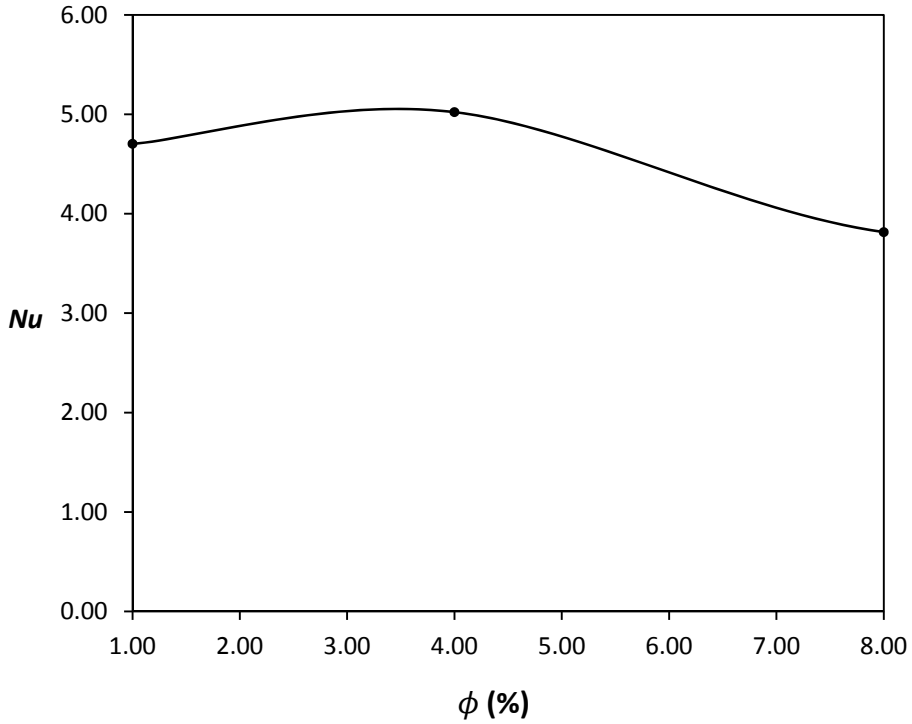

Figure 4-16: Projected variation of average Nusselt number on the hot wall forϕ ≥1.00 % and $Ra = 10^6$

In Figure 4-15 the Nusselt number increases with concentration up to a maximum beyond which the Nusselt number declines rapidly to a value below the Nusselt number

of base fluid. The enhancement in the Nusselt number is the largest (22%) for $Ra = 10^8$ at 0.14% volume fraction. The ratio of the Nusselt number maxima to the reference$(N_{\phi=0})$ also increases with the increasing Ra number. This could be explained by the relatively low viscosity at low particle concentration while the thermal conductivity effect dominates resulting in an overall enhancement in heat transfer. The decrease in Nu value for $\boldsymbol{\phi} = 0.08$ at $Ra = 1 \times 10^8$ was found to be anomalous and can be attributed to the experimental error involved in obtaining thermal conductivity and viscosity values.

When considering much higher concentration values using the theoretical model, Nu number fluctuates significantly. For example, in figure 4-16, the Nusselt number decreases for $4 \leq \phi \leq 8\%$, but increases for $2 \leq \phi \leq 4\%$. The fluctuation in figure 4-16 also indicates a far more complex correlation exists between thermal conductivity and ϕ as well as between viscosity and ϕ. An increase is observed in the Nusselt number with an increasing Ra number. This is as a result of the overall increase in buoyancy effect mentioned in 5.1. At high Ra number, the increased buoyancy effect shows heat transfer by convective flow is increased.

4.10 Conclusion

Simplified thermal conductivity and viscosity models that fit experimental results (obtained in chapter 3) were used in the numerical study for natural convection in cavity flow filled in by nanofluids. Based on a 2D mathematical formulation, a mesh independence study was carried out which achieved convergence at cell number $x^* = y^* = 280$. Temperature and velocity profile, as well as isotherms and streamlines, indicate an increase in both thermal conductivity and viscosity effects on the heat transfer performance. However, these effects are counteracting and the variation in overall heat transfer performance was shown using the variation in the Nusselt number with nanofluid concentration. For the range of particle concentration tested, an increase was observed up to 0.14% particle concentration where it reaches a maximum of 22% enhancement in the Nusselt number for $Ra = 10^8$. Enhancement in the Nusselt number was less at lower Ra numbers and occurred at lower particle concentrations. Beyond the maximum, heat transfer performance deteriorated. The existence of an optimum Nusselt number suggests the possibility of the use of nanofluids to improve heat transfer applications. Results from the validity of the numerical analysis and the projections made

will be assessed in chapter 5 where a full experimental setup is used to study natural convection in nanofluids.

CHAPTER 5. EXPERIMENTAL STUDY

5.1 Introduction

Chapter 5 presents that the experimental studies were done to determine the heat transfer performance of different concentration aqueous MWCNT nanofluids as characterised by Nusselt number and compared to the CFD analysis. The experimental setup and experimental procedure are explained. The experimental results confirm the validity of the simulation results and the projections made in chapter 4.

5.2 Experimental setup

The test section shown in Figure 5-1 consists of a cubic enclosure fabricated from polycarbonate and the side walls replaced with a tube-in-shell heat exchanger made of copper. The heat exchangers act as the constant hot and cold temperature walls T_h and T_c respectively. Each heat exchanger has an inlet and outlet to allow for circulation of water – the internal heat transfer fluid for the heat exchanger and completely separate from the test sample inside the cavity. A drainage plug leading to an outlet pipe is fitted to the bottom wall of the cavity to allow for easy removal of the test sample. The test section was then placed in an insulation box with 40 mm thick Styrofoam walls on all six sides and supported by a wooden frame as shown in figure 5-2.

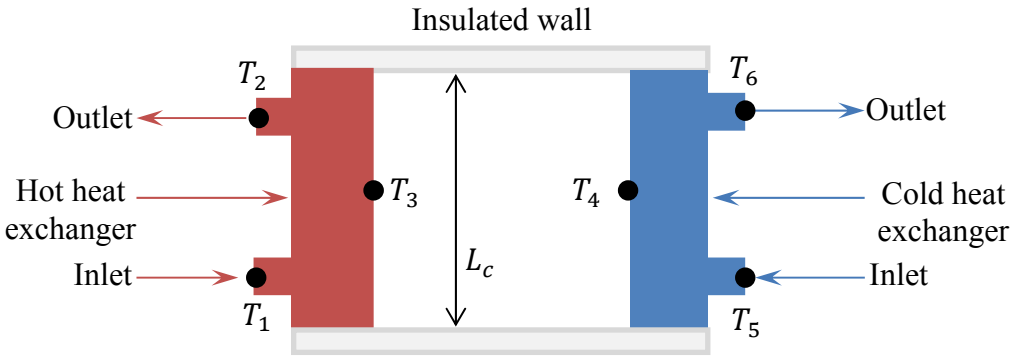

Figure 5-1: Cavity assembly and thermocouple locations for temperature measurements

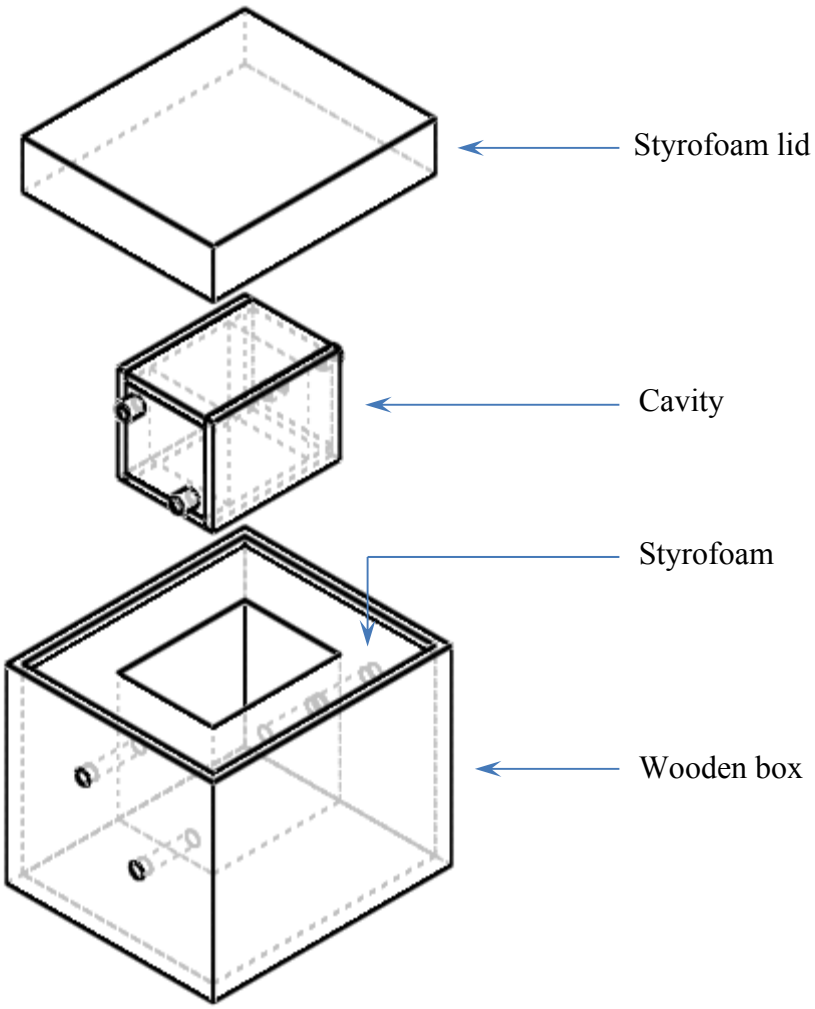

Figure 5-2: Test section and insulation box assembly

The experimental setup shown in Figure 5-3 shows the flow system used to generate and maintain the wall temperatures of the cavity. Each heat exchangers' inlet and outlet were connected to the computer controlled, constant temperature bath supplied by Polyscience with temperature range -40° to +200°C and stability within 0.005°C. Ball valves were fitted to the inlet side of the heat exchanger to regulate the flow. An ultrasonic flow meter, also on the inlet side, accurately measures the volume flow rate to within $\pm$ 0.5% of actual value. All pipes and ducts were sufficiently insulated to minimise heat loss. To measure temperature at desired locations (T_1 to T_6) on the test section, 1.2 mm Type J thermocouples were used. Temperature readings at any given location were given by thermocouple pairs soldered into the wall of the heat exchangers and average temperature readings were taken. Soldering ensured isothermal boundary conditions at the junctions and provided physical stability against any fluid movement in the cavity.

All leads from the thermocouples and the flow meter were labelled and connected to the data acquisition (DAQ) system supplied by National Instruments and programmed with Lab VIEW software to a sample rate of two measurements per second for two hour durations. Readings were taken immediately from the start of experimental runs and recorded in real time to monitor the transient state of the system and ensure that steady-state conditions have been reached. Readings were displayed on a computer interfaced to the DAQ.

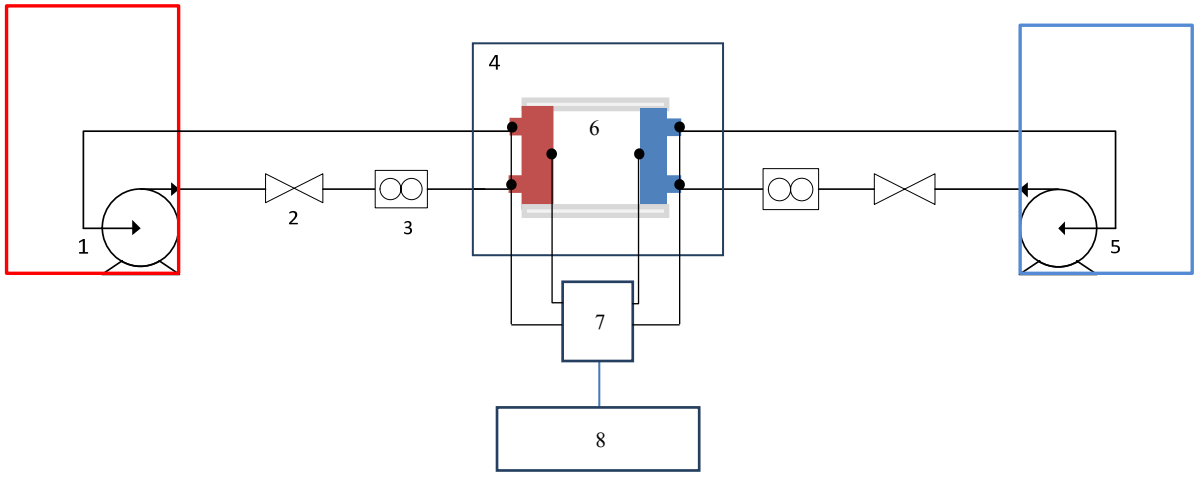

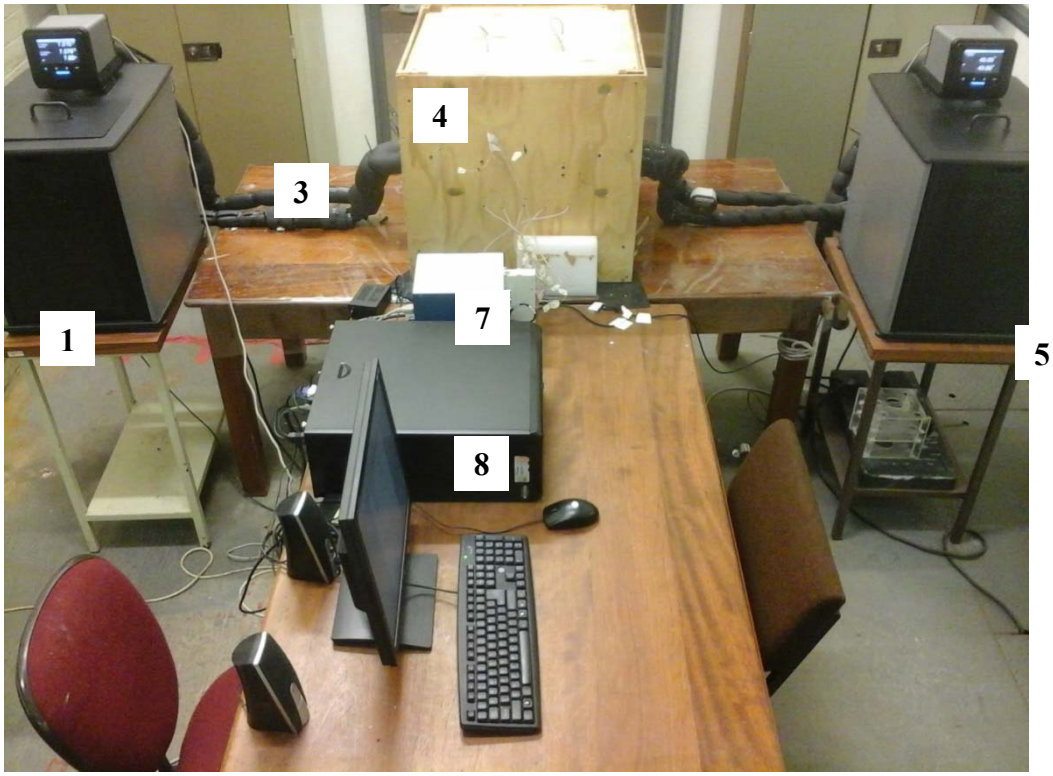

Figure 5-3: Experimental setup - 1: Hot side water bath + pump; 2: Valve (not visible in photo); 3: Flow meter; 4: Insulation box; 5: Cold side water bath + pump; 6: test section (not visible in the photo); 7: DAQ; 8: Computer

5.3 Experiment procedure

For each test run the cavity was thoroughly cleaned with distilled water and allowed to dry before filling the cavity with the test sample. Great care was taken to gently fill the cavity and prevent gas bubbles forming. Constant temperature baths were used to set and maintain the wall temperatures. The parameter $\Delta T = T_h - T_c$ was defined. The range of ΔT values used in the test runs was 10–30°C, which corresponds to Ra number between 2.1×10^8 and 6×10^8. ΔT should neither be too small to ensure that significant convective flow is generated, nor too large to prevent the development of turbulent conditions in the cavity. The Rayleigh number Ra, used in the experiment was adjusted by varying ΔT. For the given dimensions of the cavity and the thermo-physical properties of the test sample, the mean temperature T_m and Rayleigh number Ra were calculated as follows:

$$T_m = (T_h + T_c)/2 = 300$$

$$Ra = \frac{\rho_n (\rho c_p)_n g \beta_n (T_h - T_c) L^3}{\mu_n k_n}$$

The experimental data were reduced to the non-dimensional heat transfer coefficient: Nusselt number Nu, using the parameters in Table 5-1 and the following calculations: Appendix A gives the values of parameters used in the experiment.

Table 5-1: Experimental worksheet

Parameter	Description
ϕ	Volume fraction
k_n	Thermal conductivity of nanofluid
v	Flow rate
$\dot{m}$	Mass flow rate
T_h	Hot wall temperature
T_c	Cold wall temperature
T_1	Hot heat exchanger inlet temperature
T_2	Hot heat exchanger outlet temperature
T_3	Hot wall temperature
T_4	Cold wall temperature
T_5	Cold heat exchanger inlet temperature
T_6	Cold heat exchanger outlet temperature
ΔT	Temperature difference: $T_h - T_c$
$\Delta T'$	Temperature difference: $T_1 - T_2$
q	Heat flux
h	Heat transfer coefficient

Mass flow rate $\dot{m}_1$ and $\dot{m}_2$ in kg/s to the hot and cold heat exchanger respectively was calculated using the flow rate, v_1 and v_2 measured by the calibrated flow meters using:

$$\dot{m}_\iota = \rho_i v_i$$

Using the temperature difference $\Delta T'_i$ between the inlet and the outlet water to the heat exchangers, the heat flux in W/m^2 on the two heat exchangers was given by:

$$q_\iota = \frac{\dot{m}_\iota c_p \, \Delta T'_\iota}{L^2}$$

Finally, the heat transfer coefficient for the hot surface in $W/m^2.C$ and the associated Nusselt number were then given by:

$$h = \frac{q_i}{T_3 - T_4}$$

$$Nu = \frac{hL_c}{k_n}$$

5.4 Results and discussion

A good starting point for experimentation is distilled water or with $\phi = 0.0\%$ as the test fluid. This provided a good overview of the system performance of the system. The time change of temperatures $T_1 - T_6$ is shown in Figure 5-4. Steady-state conditions were reached after 4 800 s and after a smooth transient period indicated by the smooth graphs. The smooth graphs also indicate that the flow regime was laminar. Similar smooth temperatures were reported by Ho *et al*. [80], Wen & Ding [79] and Putra *et al*. [78] among others. Although great care was taken to isolate the setup and limit all disturbances, irregularity in graphs of Figures 5-6 and 5-7 for T_6 readings were attributed to vibrations from occasional disturbances from the environment. The delay in reaching steady-state conditions was similar for different nanofluid concentrations and can be attributed to the large difference between the initial and final (steady) state of the experimental setup. Allowing for signal noise, a constant steady state temperature is reached which indicates that effects from nanofluid stratification of concentration layer and/or sedimentation was negligible and therefore the nanofluid can be considered homogeneous.

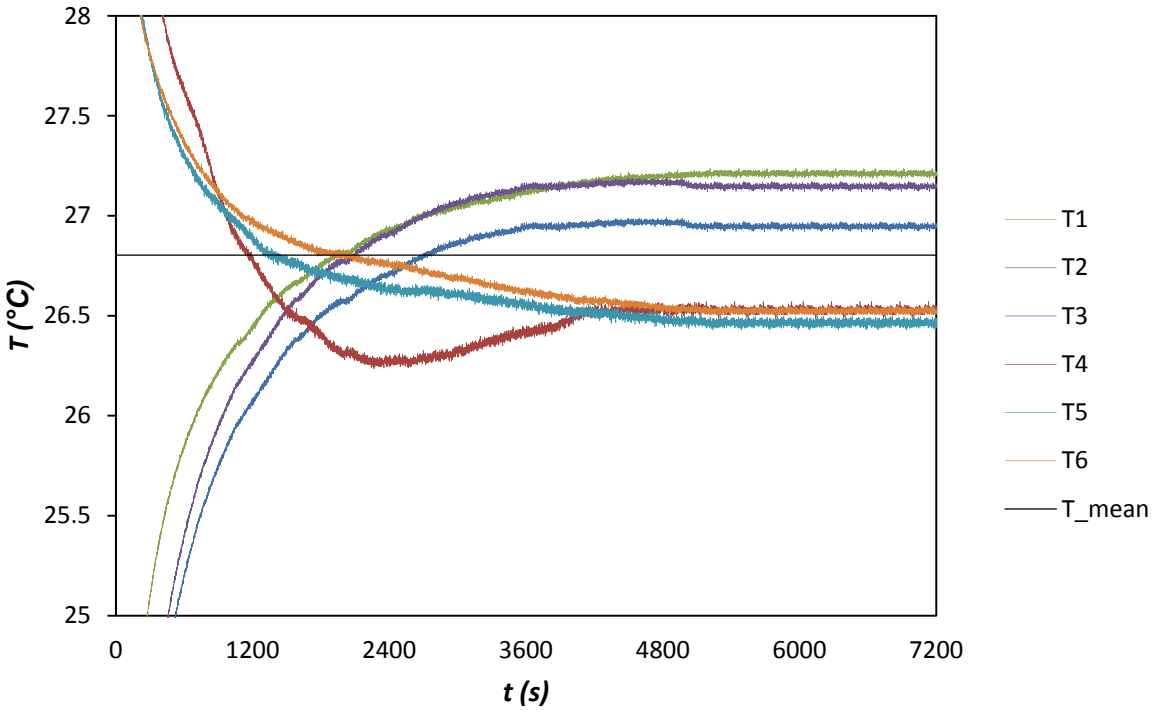

Figure 5-4: Temperature variation of thermocouples T_1 to T_6 with time (t) for ϕ = 0.0% and $Ra = 10^8$

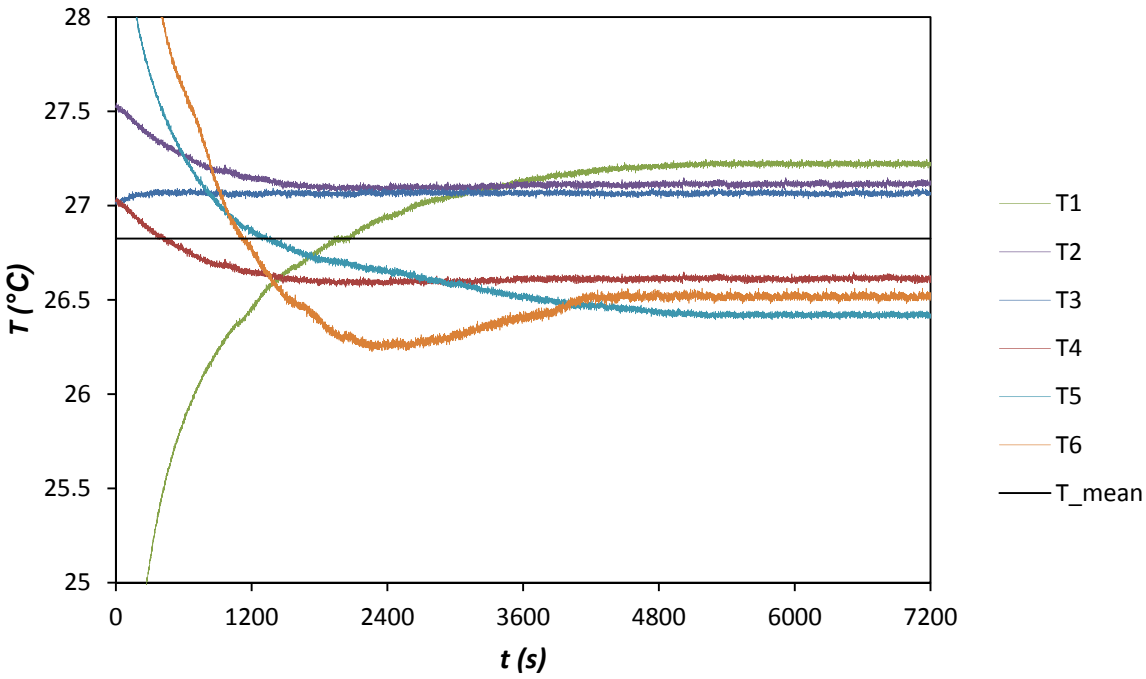

Figure 5-5: Temperature variation of thermocouples T_1 to T_6 with time (t) for ϕ = 0.1% and $Ra = 10^8$

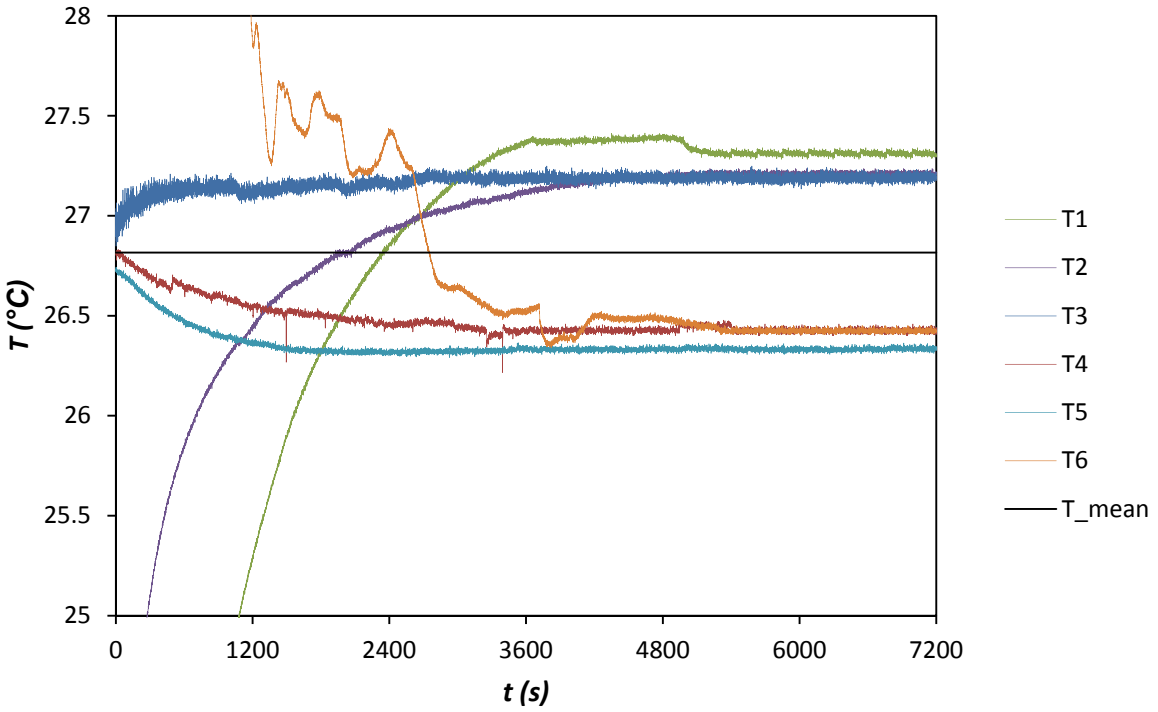

Figure 5-6: Temperature variation of thermocouples T_1 to T_6 with time (t) for ϕ = 0.5% and $Ra = 10^8$

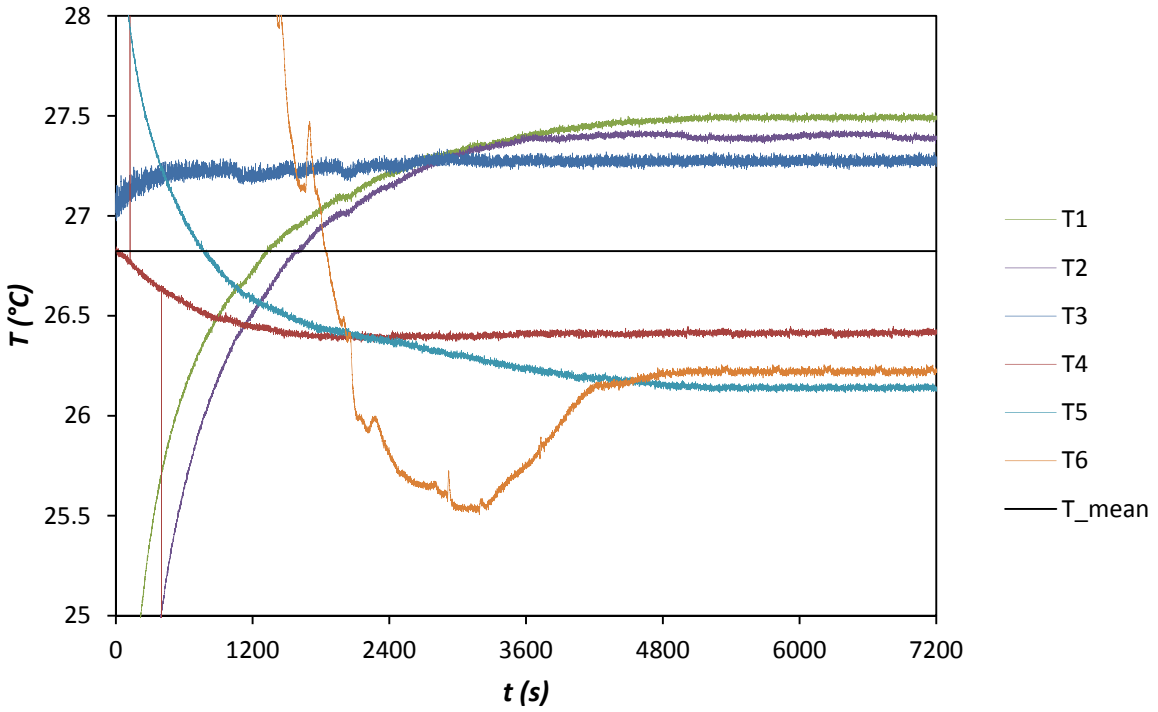

Figure 5-7: Temperature variation of thermocouples T_1 to T_6 with time (t) for ϕ =1.0% and $Ra = 10^8$

Considering graphs 5-4 to 5-7, the steady state gap between temperature readings from the hot side wall and the cold side wall widens clearly. The mean temperature ofT_1 to T_6 however stays the same at $\approx 26.8\,°C$. An uncharacteristic increase in noise levels in T_3 readings for concentrations 0.5 and 1.0% can be observed in figure 5-6 and 5-7 while all other temperature readings maintain the same noise levels. This can be explained by the increased local interactions between nanoparticles and the thermocouple junctions due to increased particle concentration.

For convection experiments between 2 walls, it's important to ensure heat loss to the environment is minimised. This means the heat lost by the external circulating fluid at the hot wall should ideally balance out the heat gained by the external circulating fluid at the cold wall. To check the heat balance, the heat flux difference $\Delta q = q_h - q_c$ between the hot and cold wall respectively were calculated for the concentrations tested. Figure 5-8 represents the heat balance between the hot and cold wall.

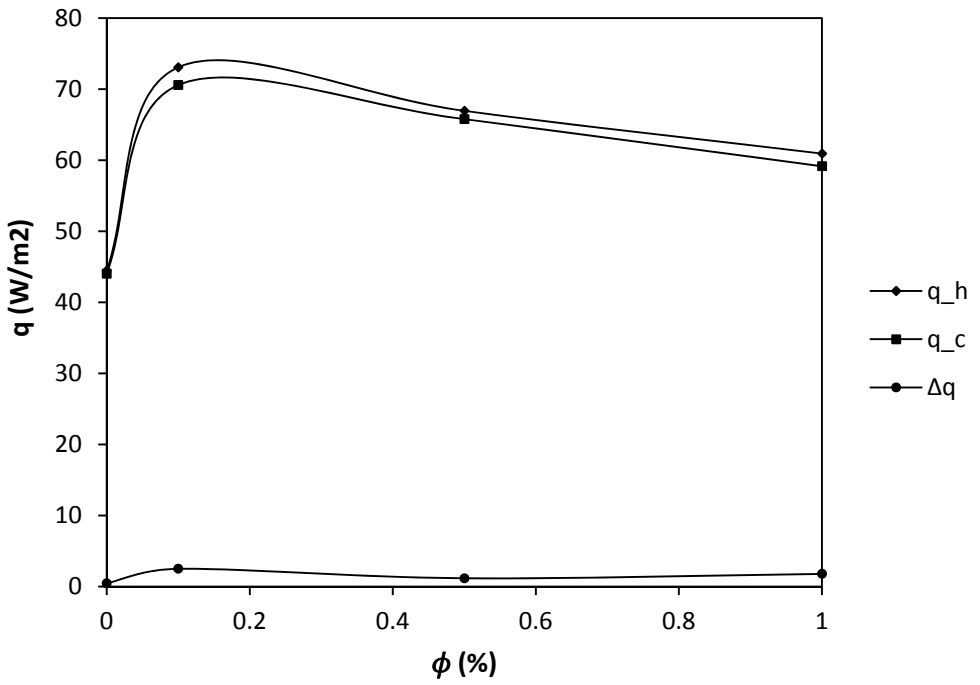

Figure 5-8: Heat transfer variation at hot wall q_H and cold wall q_C with volume concentration (ϕ)

Figure 5-8 shows there is an average Δq value of $1.2\,W/m^2$. In ideal conditions,Δq should be zero but due to unavoidable heat loss through the insulation, Δq is always non-zero. However, from Figure 5-8 Δq approaches zero at $\phi = 0$ %. It was also expected that the maximum Δq value will occur at the concentration of maximum heat fluxes

$q_h$andq_c. In this case it occurred at $\phi = 0.1\%$ for $\Delta q = 2.0\ W/m^2$. The value of Δq is a good measure of experimental error and with reference toq_h, the average and maximum error in heat flux measurements were 2.4 % and 3.4%.

Using steady-state results for q_h the average heat transfer coefficient for natural convection and Nusselt number can be calculated at the hot wall the nominal Rayleigh number of $Ra = 10^8$ and are shown in Figure 5-9.

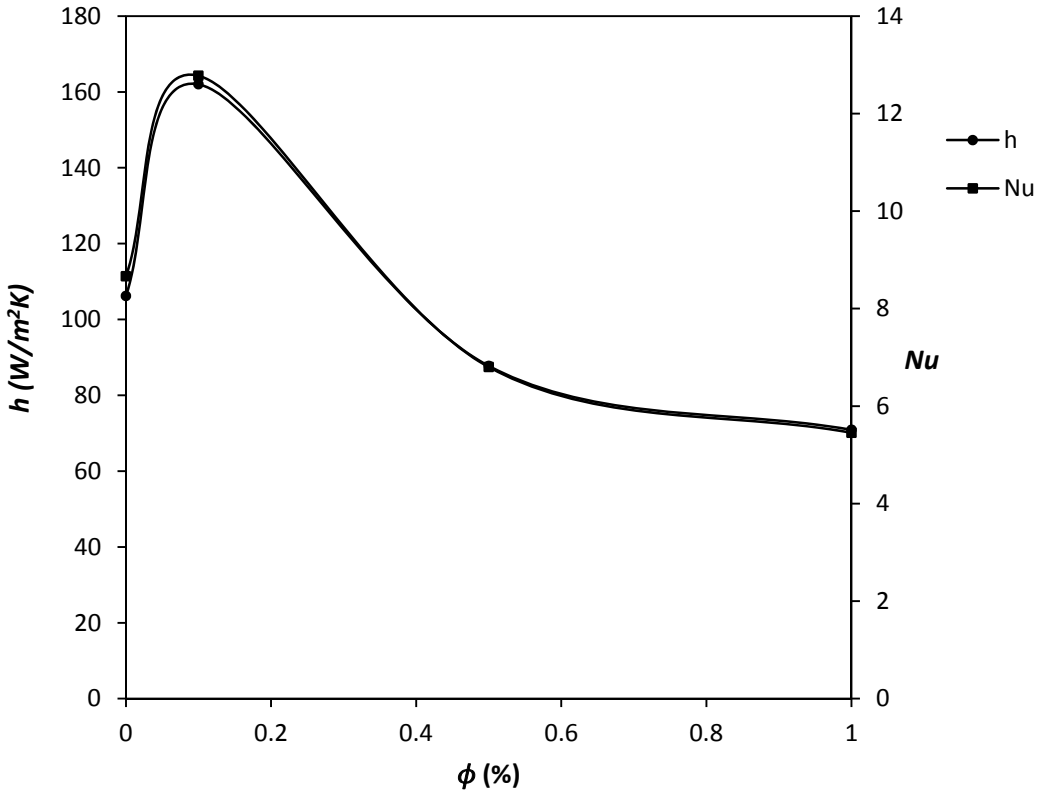

Figure 5-9: Nusselt number variation with volume concentration (ϕ)

Figure 5-9 shows the existence of an optimum particle volume concentration besides which the heat transfer performance deteriorates. There's an initial rapid increase in heat transfer performance between 0 and 0.1 before a steep drop occurs for concentrations between 0.1 and 0.5 %. The rate of decrease in Nusselt number is gradual for concentrations greater than 0.5%. Graphs of Nusselt number were obtained by Abu Nada [90] and Oueslati *et al.*[91] who both studied natural convection of aqueous aluminium oxide nanofluids in square cavity using numerical analysis had maximums. The fluctuations in the Nusselt number reveal the counteracting effects of thermal conductivity and viscosity involved in natural convection in a nanofluid medium. For the relatively high Rayleigh number of $Ra = 10^8$, the convective forces are more dominant

than conductive forces in the heat transfer. The presence of nanoparticles serves to increase the viscosity of the nanofluid which in turn reduces the convective currents near the hot wall. The reduction in convective currents increases the thermal boundary at the hot wall and reduces its temperature gradient thereby causing a decrease in the Nusselt number This effect is less significant for lower particle concentrations of nanofluid and the enhancement in thermal conductivity brought about by the presence of the nanoparticles causes an overall enhancement in the Nusselt number. However, as the particle concentration is elevated, there is a significant reduction in the convective currents due to increased viscosity and this is sufficient to lower the Nusselt number.

Comparison of experimental results with results from numerical analysis in figure 4-15 shown here in figure 5-10 shows an agreement in the overall shape of the Nusselt number graph whereby there's a rapid initial increase and decrease in both graphs before there's a settling to a slightly diminishing value. The maximum enhancement in Nusselt number in the experimental study occurs at 0.1 % and was found to be 42% which is almost double the 22 % obtained from the numerical analysis of chapter 4.

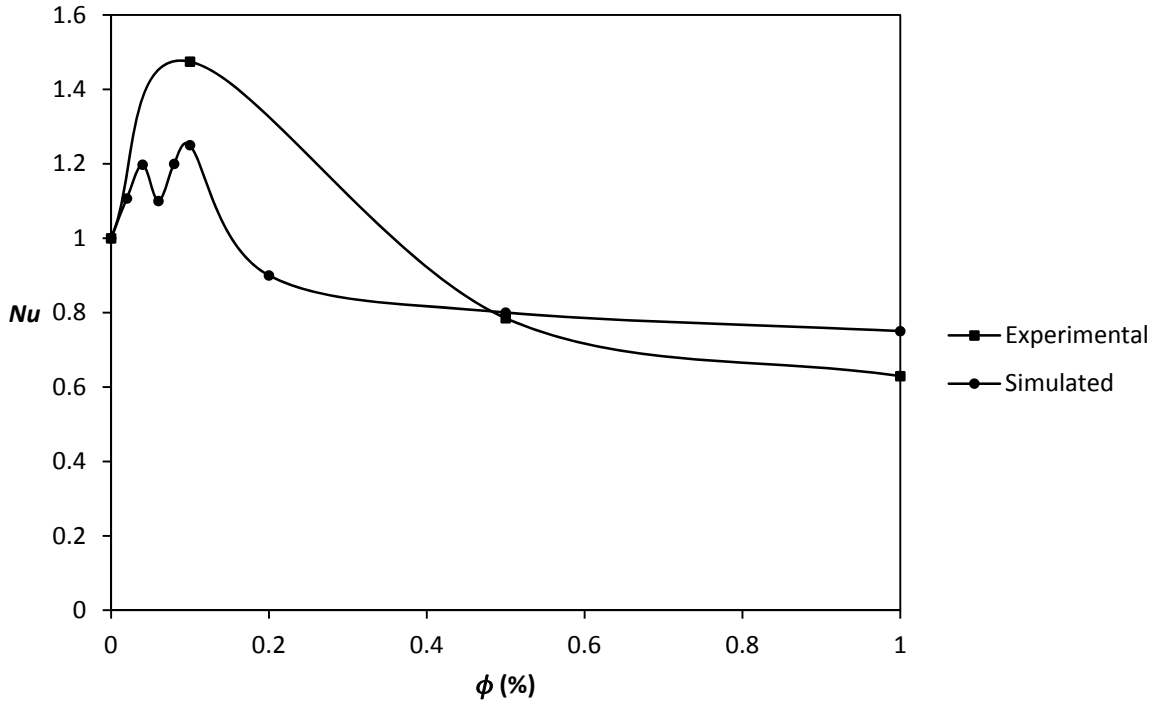

Figure 5-10: Comparison between normalised Nusselt number results from experimental and simulation study for $Ra=10^8$

Figure 5-10 also shows that the shape of the Nusselt number graph from numerical results varies from the experimental results. The prominent double peak in the Nusselt

number graph obtained from numerical results between 0 and 0.1% were non-existent in experimental results. This can be attributed to the assumptions implicit in the numerical analysis. An important example is that thermo-physical properties assigned to the nanofluid constant throughout the analysis. For the general Nusselt number equation: $Nu = cRa^n$ where c and n are empirical constants specific to a nanofluid type, the heat transfer performance of nanofluids is determined by the combined effect of relative changes in the thermophysical properties in relation to the base fluid. However, only the relative change in thermal conductivity was beneficial to the heat transfer performance of the nanofluid. Relative changes in viscosity, specific heat, thermal coefficient and density as a result of increased particle concentration in nanofluids all brought about detrimental effects to the heat transfer performance.

5.5 Conclusion

Investigation into cavity flow natural convection of MWCNT-water nanofluids has done experimentally and numerically. The investigation was carried out for particles volume concentrations of 0 to 1% and Ra number between 2.1×10^8 and 6×10^8. The heat transfer performance was characterised by Nusselt number. Experimental results on natural convection yielded a maximum enhancement in Nusselt number of 42 % at volume concentration of 0.1%. It then deteriorates between 0.1 and 1% volume concentration. Nusselt number graphs obtained from numerical and experimental studies were very similar, however, the enhancement values differed by about 20%. Results from the numerical study underestimated level of the enhancement and this can be attributed by the lake of important effects of Brownian motion and Thermophoresis in the CFD software (the available CFD software packages are not designed for nanoscale heat transfer). Both effects are alsodifficult to systematically define in numerical analysis or quantifying experimentally. Nevertheless, results from both experimental and numerical studies indicate the strong possibility of the use of nanofluids to enhance the performance of various heat transfer applications. The similar shapes of the Nusselt number graph also show that the projections can be a useful indication of nanofluid behaviour at higher concentration. However, higher concentration are difficult to prepare with the traditional ultrasonication method and as shown in figure 4-16, there is an eventual deterioration in heat transfer performance at higher concentrations. Error analyses show the maximum error in the Nusselt number was 7.4%, which is due to measurement and propagated errors.

CHAPTER 6. CONCLUSION

The heat transfer performance of MWCNT nanofluids in a square enclosure has been studied for the range of particle volume concentrations $0 \leq \phi \leq 1.0\,\%$ using experimentally determined values of thermal conductivity and viscosity. The analysis of higher volume fractions of $\phi \geq 1.0\,\%$was done using theoretical models of thermal conductivity and viscosity that best fit experimental results. The heat transfer performance was characterised by the Nusselt number and this parameter was calculated for Rayleigh numbers between$10^4 - 10^8$ with base fluid at Prandtl number of 5.83.

CD Adapco's Star-CCM+ Code (v 8.06) was used to carry out the numerical study. The grid independence study done before analysis of the nanofluids yielded a less than 0.47% discretisation error and results of simulation of convection in air-filled enclosure matched benchmark results from De Vahl [87] to within 1.6 %. The first result of this study is to find poor correlation between experimental properties and theoretical models based on spherical nanoparticles when applied to MWCNT nanofluids. This can be attributed mainly to the non-spherical nature of carbon-nanotubes while most theoretical models are based on spherical nanoparticles. However, the model proposed by Nan *et al*. [34] for thermal conductivity and the model used by Brenner & Condiff for viscosity [44] which incorporates the aspect ratio and anisotropic properties of non-spherical nanoparticles in their formulation showed good correlation with observed experimental values.

From the analysis of heat transfer in a square enclosure filled with different particle concentration of nanofluids, the second result of the study was the increase in heat transfer performance as characterised by the Nusselt number with increasing the Ra number. Between $Ra = 10^4$ and$Ra = 10^8$, there was a 130% increase in the average Nusselt number.

The third result of the study relates the effect of varying particle concentration on the heat transfer performance characterised by the Nusselt number. Here the counter-acting effects of increasing thermal conductivity and increasing viscosity was shown. The combined effect of both increasing thermal conductivity and increasing viscosity due to increasing particle concentration had an enhancement effect on the heat transfer performance below 0.1%. Between 0.2 and 1% there was no significant change in Nusselt number with increasing particle concentration for the range of experimental

particle concentrations considered, however, a decline in heat transfer performance can be observed especially for higher Rayleigh numbers. It is this area of study where there are many conflicting results in the literature. Further analysis of higher particle concentrations revealed a general decline in heat transfer performance with increasing particle concentration albeit with significant fluctuations. These fluctuations were attributed to the nonlinear behaviour of the thermal conductivity and viscosity models with counteracting effects on the average Nusselt number at the particle concentration range studied. The studies that show some increase in heat transfer performance with increasing particle concentration may be limited to the nanoparticles used or the concentration range considered.

Lastly, it was found that after an initial enhancement in heat transfer performance in nanofluids characterised by Nusselt number, there's gradual decline for the particle concentration range tested. The experimental results indicated the existence of an optimum particle concentration at which heat transfer in MWCNT nanofluids is maximised. In the present work a maximum enhancement of 42% occurs at about 0.1% particle volume concentration, but further experimental work to locate the value more precisely is required. The difference in the graphs of Nusselt number variation with particle concentration between the numerical and experimental studies shows the limitation of analysing nanofluids by theoretical and numerical means. This limitation stems from the difficulty in defining the totality of the very complex nanofluid behaviour. Experimental studies are therefore crucial in understanding nanofluids thermal-fluid behaviour.

It can be concluded that nanofluids as heat transfer fluid have demonstrated significant enhancement in heat transfer performance to be considered seriously. However, the range of concentration at which heat transfer performance is maximised is very narrow and would require tight control mechanisms to maintain.

This study is part of a larger on-going study that seeks to determine the efficacy of nanofluids as heat transfer fluids and for which nanoparticle types and associated concentration heat transfer is maximised. Further work in this regard can study convection in a wider range of nanofluids and determine the particle concentrations for which increase in heat transfer performance offsets the increase in pumping power.

REFERENCES

[1] M. J. Assael, C. F. Chen, I. Metaxa, and W. A. Wakeham, “Thermal conductivity of suspensions of carbon nanotubes in water,” *Int. J. Thermophys.*, vol. 25, no. 4, pp. 971–985, 2004.

[2] J. C. Maxwell, (1882). "An Elementary Treatise on Electricity". 2nd ed. Oxford : Clarendon Press. pp14.

[3] S. U. S. Choi, “Enhancing thermal conductivity of fluids with nanoparticles,” in *Proceedings of the 1995 ASME International Mechanical Engineering Congress and Exposition*, 1995, vol. 231, pp. 99–105.

[4] S. K. Das, S. U. S. Choi, and H. E. Patel, “Heat Transfer in Nanofluids — A Review Heat Transfer in Nanofluids —,” no. January 2013, pp. 37–41, 2007.

[5] H. Akoh, Y. Tsukasaki, S. Yatsuya, and A. Tasaki, “Magnetic properties of ferromagnetic ultrafine particles prepared by vacuum evaporation on running oil substrate,” *Journal of Crystal Growth*, vol. 45. pp. 495–500, 1978.

[6] J. A. Eastman, U. S. Choi, S. Li, L. J. Thompson, and S. Lee, “Enhanced Thermal Conductivity through the Development of Nanofluids,” *MRS Proceedings*, vol. 457. pp. 3 – 11, 1997.

[7] T. X. Phuoc, Y. Soong, and M. K. Chyu, “Synthesis of Ag-deionized water nanofluids using multi-beam laser ablation in liquids,” *Opt. Lasers Eng.*, vol. 45, pp. 1099–1106, 2007.

[8] A. K. Singh and V. S. Raykar, “Microwave synthesis of silver nanofluids with polyvinylpyrrolidone (PVP) and their transport properties,” *Colloid Polym. Sci.*, vol. 286, pp. 1667–1673, 2008.

[9] C.-H. L. C.-H. Lo and T.-T. Tsung, “High Thermal Conductivity Nanofluid Fabrication by Continuously Controlled Submerged Arc Nano Synthesis System (CC-SANSS),” *2006 Sixth IEEE Conf. Nanotechnol.*, vol. 2, 2006.

[10] S. Witharana, C. Hodges, D. Xu, X. Lai, and Y. Ding, "Aggregation and settling in aqueous polydisperse alumina nanoparticle suspensions," *J. Nanoparticle Res.*, vol. 14, no. 5, p. 851, Apr. 2012.

[11] C. H. Lo, T. T. Tsung, L. C. Chen, C. H. Su, and H. M. Lin, "Fabrication of copper oxide nanofluid using submerged arc nanoparticle synthesis system (SANSS)," *J. Nanoparticle Res.*, vol. 7, pp. 313–320, 2005.

[12] W. Yu and H. Xie, "A review on nanofluids: Preparation, stability mechanisms, and applications," *Journal of Nanomaterials*, vol. 2012. 2012.

[13] S. Lee, S. U.-S. Choi, S. Li, and J. A. Eastman, "Measuring Thermal Conductivity of Fluids Containing Oxide Nanoparticles," *Journal of Heat Transfer*, vol. 121. p. 280, 1999.

[14] X. Wang, X. Xu, and S. U. S. Choi, "Thermal Conductivity of Nanoparticle – Fluid Mixture," *J. Thermophys. Heat Transf.*, vol. 13, no. 4, 1999.

[15] W. Xian-ju and L. I. Xin-fang, "Influence of pH on Nanofluids Viscosity and Thermal Conductivity," *Chinese Phys. Lett.*, vol. 056601, no. 5, 2009.

[16] X. Wang and A. S. Mujumdar, "Heat transfer characteristics of nanofluids: a review," *Int. J. Therm. Sci.*, vol. 46, pp. 1–19, 2007.

[17] S. K. Das, N. Putra, P. Thiesen, and W. Roetzel, "Temperature Dependence of Thermal Conductivity Enhancement for Nanofluids," *Journal of Heat Transfer*, vol. 125, no. 4. p. 567, 2003.

[18] A. Ghadimi, R. Saidur, and H. S. C. Metselaar, "A review of nanofluid stability properties and characterization in stationary conditions," *Int. J. Heat Mass Transf.*, vol. 54, no. 17–18, pp. 4051–4068, 2011.

[19] Y. Hwang, J. K. Lee, C. H. Lee, Y. M. Jung, S. I. Cheong, C. G. Lee, B. C. Ku, and S. P. Jang, "Stability and thermal conductivity characteristics of nanofluids," *Thermochim. Acta*, vol. 455, pp. 70–74, 2007.

[20] X. Wei and L. Wang, "Synthesis and thermal conductivity of microfluidic copper nanofluids," *Particuology*, vol. 8, pp. 262–271, 2010.

[21] J. Hong, S. H. Kim, and D. Kim, "Effect of laser irradiation on thermal conductivity of ZnO nanofluids," *J. Phys. Conf. Ser.*, vol. 59, pp. 301–304, Apr. 2007.

[22] R. Hamilton and O. Crosser, "Thermal conductivity of heterogeneous two-component systems," *Ind. Eng. Chem. …*, vol. 1, pp. 187–191, 1962.

[23] C. G. Granqvist and O. Hunderi, "Conductivity of inhomogeneous materials: Effective-medium theory with dipole-dipole interaction," *Phys. Rev. B*, vol. 18, pp. 1554–1561, 1978.

[24] D. P. H. Hasselman and L. F. Johnson, "Effective Thermal Conductivity of Composites with Interfacial Thermal Barrier Resistance," *Journal of Composite Materials*, vol. 21. pp. 508–515, 1987.

[25] Q. Xue, "Effective-medium theory for two-phase random composite with an interfacial shell," *J. Mater. Sci. Technol.*, vol. 16(4), pp. 367–369, 2000.

[26] S. U. S. Choi, Z. G. Zhang, W. Yu, F. E. Lockwood, and E. A. Grulke, "Anomalous thermal conductivity enhancement in nanotube suspensions," *Appl. Phys. Lett.*, vol. 79, no. 14, p. 2252, 2001.

[27] M. J. Biercuk, M. C. Llaguno, M. Radosavljevic, J. K. Hyun, A. T. Johnson, and J. E. Fischer, "Carbon nanotube composites for thermal management," *Appl. Phys. Lett.*, vol. 80, pp. 2767–2769, 2002.

[28] H. S. Aybar, M. Sharifpur, M. R. Azizian, M. Mehrabi, and J. P. Meyer, "Nanofluids A Review of Thermal Conductivity Models for Nanofluids," *Heat Transf. Eng.*, vol. 36, no. 13, 2015.

[29] P. Keblinski, S. R. Phillpot, S. U. S. Choi, and J. A. Eastman, "Mechanisms of heat flow in suspensions of nano-sized particles (nanofluids)," *Int. J. Heat Mass Transf.*, vol. 45, pp. 855–863, 2001.

[30] J. A. Eastman, S. R. Phillpot, S. U. S. Choi, and P. Keblinski, "Thermal Transport In Nanofluids," *Annu. Rev. Mater. Res.*, vol. 34, pp. 219–246, 2004.

[31] C.-W. Nan, R. Birringer, D. R. Clarke, and H. Gleiter, "Effective thermal conductivity of particulate composites with interfacial thermal resistance," *J. Appl. Phys.*, vol. 81, pp. 6692–6699, 1997.

[32] W. Evans, R. Prasher, J. Fish, P. Meakin, P. Phelan, and P. Keblinski, "Effect of aggregation and interfacial thermal resistance on thermal conductivity of nanocomposites and colloidal nanofluids," *Int. J. Heat Mass Transf.*, vol. 51, pp. 1431–1438, 2008.

[33] B. Lamas, B. Abreu, A. Fonseca, N. Martins, and M. Oliveira, "Critical analysis of the thermal conductivity models for CNT based nanofluids," *Int. J. Therm. Sci.*, vol. 78, pp. 65–76, 2014.

[34] Q. Z. Xue, "Model for the effective thermal conductivity of carbon nanotube composites," *Nanotechnology*, vol. 17. pp. 1655–1660, 2006.

[35] `W. Yu and S. U. S. Choi, "The role of interfacial layers in the enhanced thermal conductivity of nanofluids: A renovated Maxwell model," *J. Nanoparticle Res.*, vol. 5, pp. 167–171, 2003.

[36] P. Bhattacharya, S. K. Saha, A. Yadav, P. E. Phelan, and R. S. Prasher, "Brownian dynamics simulation to determine the effective thermal conductivity of nanofluids," *J. Appl. Phys.*, vol. 95, pp. 6492–6494, 2004.

[37] C. Cremers and H. Fine, "Thermal conductivity," in *Proceedings of Twenty-First International Conference on Thermal Conductivity*, 1990, p. 29.

[38] D. Wen and Y. Ding, "Effective thermal conductivity of aqueous suspensions of carbon nanotubes (carbon nanotube nanofluids)," *J. Thermophys. Heat Transf.*, vol. 18, pp. 481–485, 2004.

[39] M. J. Assael, C. F. Chen, I. Metaxa, and W. A. Wakeham, "Thermal conductivity of suspensions of carbon nanotubes in water," *Int. J. Thermophys.*, vol. 25, pp. 971–985, 2004.

[40] L. S. Sundar, M. K. Singh, E. V. Ramana, B. Singh, J. Grácio, and A. C. M. Sousa, "Enhanced thermal conductivity and viscosity of nanodiamond-nickel nanocomposite nanofluids.," *Sci. Rep.*, vol. 4, p. 4039, 2014.

[41] S. K. Das, N. Putra, P. Thiesen, and W. Roetzel, "Temperature Dependence of Thermal Conductivity Enhancement for Nanofluids," *J. Heat Transfer*, vol. 125, no. 4, p. 567, 2003.

[42] R. S. Vajjha and D. K. Das, "Experimental determination of thermal conductivity of three nanofluids and development of new correlations," *Int. J. Heat Mass Transf.*, vol. 52, no. 21–22, pp. 4675–4682, Oct. 2009.

[43] H. C. Brinkman, "The viscosity of concentrated suspensions and solutions," *J. Chem. Phys.*, vol. 20, no. 4, 1952.

[44] H. Brenner and D. W. Condiff, "Transport mechanics in systems of orientable particles. IV. convective transport," *Journal of Colloid and Interface Science*, vol. 47. pp. 199–264, 1974.

[45] G. K. Batchelor, "Brownian diffusion of particles with hydrodynamic interaction," *J. Fluids Mech.*, vol. 74, pp. 1–29, 1976.

[46] I. M. Krieger and T. J. Dougherty, "A Mechanism for Non□Newtonian Flow in Suspensions of Rigid Spheres," *J. Rheol. (N. Y. N. Y).*, vol. 3, no. 1, 1959.

[47] H. Chen, Y. Ding, and C. Tan, "Rheological behaviour of nanofluids," *New J. Phys.*, vol. 9, 2007.

[48] M. Kole and T. K. Dey, "Investigation of thermal conductivity, viscosity, and electrical conductivity of graphene based nanofluids," *J. Appl. Phys.*, vol. 113, no. 8, p. 084307, 2013.

[49] R. Prasher, P. E. Phelan, and P. Bhattacharya, "Effect of aggregation kinetics on the thermal conductivity of nanoscale colloidal solutions (nanofluid)," *Nano Lett.*, vol. 6, pp. 1529–1534, 2006.

[50] J. H. Lee, K. S. Hwang, S. P. Jang, B. H. Lee, J. H. Kim, S. U. S. Choi, C. J. Choi, K. Sik, S. Pil, B. Ho, J. Ho, and C. Jin, "Effective viscosities and thermal conductivities of aqueous

nanofluids containing low volume concentrations of Al2O3 nanoparticles," *Int. J. Heat Mass Transf.*, vol. 51, pp. 2651–2656, 2008.

[51] C. T. Nguyen, F. Desgranges, N. Galanis, G. Roy, T. Maré, S. Boucher, and H. Angue Mintsa, "Viscosity data for Al2O3-water nanofluid-hysteresis: is heat transfer enhancement using nanofluids reliable?," *Int. J. Therm. Sci.*, vol. 47, pp. 103–111, 2008.

[52] S. M. S. Murshed, K. C. Leong, and C. Yang, "Investigations of thermal conductivity and viscosity of nanofluids," *Int. J. Therm. Sci.*, vol. 47, pp. 560–568, 2008.

[53] K. B. Anoop, S. Kabelac, T. Sundararajan, and S. K. Das, "Rheological and flow characteristics of nanofluids: Influence of electroviscous effects and particle agglomeration," *J. Appl. Phys.*, vol. 106, 2009.

[54] M. S. Liu, M. C. C. Lin, I. Te Huang, and C. C. Wang, "Enhancement of thermal conductivity with CuO for nanofluids," *Chem. Eng. Technol.*, vol. 29, pp. 72–77, 2006.

[55] M. J. Pastoriza-Gallego, C. Casanova, J. L. Legido, and M. M. Piñeiro, "CuO in water nanofluid: Influence of particle size and polydispersity on volumetric behaviour and viscosity," *Fluid Phase Equilib.*, vol. 300, pp. 188–196, 2011.

[56] P. K. Namburu, D. P. Kulkarni, D. Misra, and D. K. Das, "Viscosity of copper oxide nanoparticles dispersed in ethylene glycol and water mixture," *Exp. Therm. Fluid Sci.*, vol. 32, pp. 397–402, 2007.

[57] L. Chen, H. Xie, Y. Li, and W. Yu, "Nanofluids containing carbon nanotubes treated by mechanochemical reaction," *Thermochim. Acta*, vol. 477, pp. 21–24, 2008.

[58] T. X. Phuoc, M. Massoudi, and R. Chen, "Viscosity and thermal conductivity of nano fluids containing multi-walled carbon nanotubes stabilized by chitosan," *Int. J. Therm. Sci.*, vol. 50, no. 1, pp. 12–18, 2011.

[59] Y. Yang, Z. G. Zhang, E. A. Grulke, W. B. Anderson, and G. Wu, "Heat transfer properties of nanoparticle-in-fluid dispersions (nanofluids) in laminar flow," *Int. J. Heat Mass Transf.*, vol. 48, pp. 1107–1116, 2005.

[60] S. Bobbo, L. Fedele, A. Benetti, L. Colla, M. Fabrizio, C. Pagura, and S. Barison, "Viscosity of water based SWCNH and TiO2 nanofluids," *Exp. Therm. Fluid Sci.*, vol. 36, pp. 65–71, 2012.

[61] H. Xie, L. Chen, and Q. Wu, "Measurements of the viscosity of suspensions (nanofluids) containing nanosized Al2O3 particles," *High Temp. High Press.*, vol. 37, no. 127–135, 2008.

[62] V. Sridhara and L. N. Satapathy, "Al2O3-based nanofluids: a review.," *Nanoscale Res. Lett.*, vol. 6, no. 1, p. 456, Jan. 2011.

[63] R. Prasher, D. Song, J. Wang, P. Phelan, R. Prasher, D. Song, J. Wang, and P. Phelan, "Measurements of nanofluid viscosity and its implications for thermal applications," *Appl. Phys. Lett.*, vol. 133108, no. 2006, 2006.

[64] Y. Ding, H. Alias, D. Wen, and R. A. Williams, "Heat transfer of aqueous suspensions of carbon nanotubes (CNT nanofluids)," *Int. J. Heat Mass Transf.*, vol. 49, no. 1–2, pp. 240–250, Jan. 2006.

[65] G. H. Ko, K. Heo, K. Lee, D. S. Kim, C. Kim, Y. Sohn, and M. Choi, "An experimental study on the pressure drop of nanofluids containing carbon nanotubes in a horizontal tube," *Int. J. Heat Mass Transf.*, vol. 50, pp. 4749–4753, 2007.

[66] A. Indhuja, K. S. Suganthi, S. Manikandan, and K. S. Rajan, "Journal of the Taiwan Institute of Chemical Engineers Viscosity and thermal conductivity of dispersions of gum arabic capped MWCNT in water : Influence of MWCNT concentration and temperature," *J. Taiwan Inst. Chem. Eng.*, vol. 44, no. 3, pp. 474–479, 2013.

[67] Y. He, Y. Jin, H. Chen, Y. Ding, D. Cang, and H. Lu, "Heat transfer and flow behaviour of aqueous suspensions of TiO2 nanoparticles (nanofluids) flowing upward through a vertical pipe," *Int. J. Heat Mass Transf.*, vol. 50, pp. 2272–2281, 2007.

[68] W.-Q. Lu and Q.-M. Fan, "Study for the particle's scale effect on some thermophysical properties of nanofluids by a simplified molecular dynamics method," *Eng. Anal. Bound. Elem.*, vol. 32, no. 4, pp. 282–289, Apr. 2008.

[69] K. B. Anoop, T. Sundararajan, and S. K. Das, "Effect of particle size on the convective heat transfer in nanofluid in the developing region," *Int. J. Heat Mass Transf.*, vol. 52, pp. 2189–2195, 2009.

[70] a. Baïri, E. Zarco-Pernia, and J. M. García De María, "A review on natural convection in enclosures for engineering applications. the particular case of the parallelogrammic diode cavity," *Appl. Therm. Eng.*, vol. 63, no. 1, pp. 304–322, 2014.

[71] K. Khanafer, K. Vafai, and M. Lightstone, "Buoyancy-driven heat transfer enhancement in a two-dimensional enclosure utilizing nanofluids," *Int. J. Heat Mass Transf.*, vol. 46, no. 19, pp. 3639–3653, Sep. 2003.

[72] P. Ternik and R. Rudolf, "Heat transfer enhancement for natural convection flow of water-based nanofluids in a square enclosure," *Int. J. Simul. Model.*, vol. 11, no. 1, pp. 29–39, Mar. 2012.

[73] H. F. Oztop and E. Abu-Nada, "Numerical study of natural convection in partially heated rectangular enclosures filled with nanofluids," *Int. J. Heat Fluid Flow*, vol. 29, no. 5, pp. 1326–1336, Oct. 2008.

[74] A. K. Santra, S. Sen, and N. Chakraborty, "Study of heat transfer augmentation in a differentially heated square cavity using copper–water nanofluid," *Int. J. Therm. Sci.*, vol. 47, no. 9, pp. 1113–1122, Sep. 2008.

[75] E. Abu-Nada, Z. Masoud, and a. Hijazi, "Natural convection heat transfer enhancement in horizontal concentric annuli using nanofluids," *Int. Commun. Heat Mass Transf.*, vol. 35, no. 5, pp. 657–665, May 2008.

[76] C. J. Ho, M. W. Chen, and Z. W. Li, "Numerical simulation of natural convection of nanofluid in a square enclosure: Effects due to uncertainties of viscosity and thermal conductivity," *Int. J. Heat Mass Transf.*, vol. 51, no. 17–18, pp. 4506–4516, Aug. 2008.

[77] M. Jahanshahi, S. F. Hosseinizadeh, M. Alipanah, a. Dehghani, and G. R. Vakilinejad, "Numerical simulation of free convection based on experimental measured conductivity in a square cavity using Water/SiO2 nanofluid," *Int. Commun. Heat Mass Transf.*, vol. 37, no. 6, pp. 687–694, Jul. 2010.

[78] N. Putra, W. Roetzel, and S. K. Das, "Natural convection of nano-fluids," *Heat Mass Transf.*, vol. 39, no. 8–9, pp. 775–784, Dec. 2002.

[79] D. Wen and Y. Ding, "Formulation of nanofluids for natural convective heat transfer applications," *Int. J. Heat Fluid Flow*, vol. 26, no. 6, pp. 855–864, Dec. 2005.

[80] C. J. Ho, W. K. Liu, Y. S. Chang, and C. C. Lin, "Natural convection heat transfer of alumina-water nanofluid in vertical square enclosures: An experimental study," *Int. J. Therm. Sci.*, vol. 49, no. 8, pp. 1345–1353, Aug. 2010.

[81] R. Bandyopadhyaya, E. Nativ-Roth, O. Regev, and R. Yerushalmi-Rozen, "Stabilization of Individual Carbon Nanotubes in Aqueous Solutions," *Nano Lett.*, vol. 2, pp. 25–28, 2002.

[82] P. Garg, J. L. Alvarado, C. Marsh, T. A. Carlson, and D. A. Kessler, "An experimental study on the effect of ultrasonication on viscosity and heat transfer performance of multi-wall carbon nanotube-based aqueous nanofluids," *Int. J. Heat Mass Transf.*, vol. 52, no. 21–22, pp. 5090–5101, 2009.

[83] C. W. Nan, Z. Shi, and Y. Lin, "A simple model for thermal conductivity of carbon nanotube-based composites," *Chemical Physics Letters*, vol. 375. pp. 666–669, 2003.

[84] H. Xie, H. Lee, W. Youn, and M. Choi, "Nanofluids containing multiwalled carbon nanotubes and their enhanced thermal conductivities," *J. Appl. Phys.*, vol. 94, no. 8, 2003.

[85] J. P. Meyer, T. J. Mckrell, and K. Grote, "The influence of multi-walled carbon nanotubes on single- phase heat transfer and pressure drop characteristics in the transitional flow regime of smooth tubes," *Int. J. Heat Mass Transf.*, vol. 58, no. 1–2, pp. 597–609, 2013.

[86] P. J. Roache, "Quantification Of Uncertainty In Computational Fluid Dynamics," *Annual Review of Fluid Mechanics*, vol. 29. pp. 123–160, 1997.

[87] G. De Vahl Davis, "Natural convection of air in a square cavity: a bench mark numerical solution," *Int. J. Numer. Methods Fluids*, vol. 3, pp. 249–264, 1983.

[88] O. Turan, N. Chakraborty, and R. J. Poole, "Laminar natural convection of Bingham fluids in a square enclosure with differentially heated side walls," *J. Nonnewton. Fluid Mech.*, vol. 165, no. 15–16, pp. 901–913, Aug. 2010.

[89] P. Kim, L. Shi, A. Majumdar, and P. L. Mceuen, "Mesoscopic thermal transport and energy dissipation in carbon nanotubes," *Phys. B Condens. Matter*, vol. 323, no. 1–4, pp. 67–70, 2002.

[90] E. Abu-Nada, Z. Masoud, H. F. Oztop, and A. Campo, "Effect of nanofluid variable properties on natural convection in enclosures," *Int. J. Therm. Sci.*, vol. 49, no. 3, pp. 479–491, Mar. 2010.

[91] F. S. Oueslati and R. Bennacer, "Heterogeneous nanofluids: natural convection heat transfer enhancement.," *Nanoscale Res. Lett.*, vol. 6, no. 1, p. 222, Jan. 2011.

APPENDIX A. CALCULATED VALUES AND MODELS USED

Appendix A gives experimental results and calculated values from the models used in chapters 4 and 5

Table A-1: Thermo-physical properties

ϕ (%)	$m_p\ (g)$	$m_{GA}\ (g)$	$\rho_n\left(\frac{kg}{m^3}\right)$	$c_{p_n}\ (\frac{\mathrm{J}}{\mathrm{kg\ ^\circ C}})$	$\beta_n\left(\frac{1}{T}\right)$
0.00	0	0	996.557	4179.000	0.000275
0.02	0.025205041	0.012602521	996.778	4177.437	0.000274887
0.04	0.050420168	0.025210084	996.998	4175.875	0.000274774
0.06	0.075645387	0.025210084	997.219	4174.314	0.000274661
0.08	0.100880705	0.025220176	997.440	4172.753	0.000274549
0.10	0.126126126	0.031531532	997.660	4171.193	0.000274436
0.20	0.25250501	0.063126253	998.764	4163.403	0.000273873
0.50	0.633165829	0.158291457	1002.074	4140.136	0.000272192
1.00	1.272727273	0.318181818	1007.591	4101.698	0.000269414

Table A-2: Thermal conductivity models considered

k_I: Maxwell

$$k_f\left[\frac{2+2k^*+2\phi(k^*-1)}{2+2k^*-\phi(k^*-1)}\right]$$

k_II:

$$k_f\left[1+\frac{n(k^*-1)\phi}{(k^*+n-1)-(k^*-1)\phi}\right]$$

k_III: Deng and Zheng [33]

$$k_f\left[1+\frac{\eta\phi/3}{\frac{k_f}{\eta k_{33}^{ce}}+H(\eta p)}\right]$$

$$k_{33}^{ce}=k_{33}^{c}/(1+2R_K k_{33}^{c}/L)$$

$$H(p)=\frac{1}{p^2-1}\left[\frac{p}{\sqrt{(p^2-1)}}\ln\left(p+\sqrt{(p^2-1)}\right)-1\right]$$

$$\eta=L^{ce}/L$$

$$p=L/a=$$

k_IV: Nan *et al.*[34]

$$\frac{k_{eff}}{k_f}=\frac{3+\phi(\beta_x+\beta_z)}{3-\phi(\beta_x)}$$

$$\beta_x=\frac{2(k_{11}^{c}-k_b)}{k_{11}^{c}+k_b};\qquad \beta_x=\frac{k_{33}^{c}}{k_b}-1$$

$$k_{11}^{c}=\frac{k_p}{1+\frac{2a_k k_p}{d\,k_f}};\qquad k_{33}^{c}=\frac{k_p}{1+\frac{2a_k k_p}{L\,k_f}}$$

$$a_k=R_k k_f=8(10^{-8})\frac{m^2K}{W}k_f$$

Table A-3: Theoretical K values in ($W \cdot m^{-1} \cdot K^{-1}$)

ϕ (%)	k_I	k_II	k_III	k_IV	$k_{readings}$
0.00	0.613	0.613	0.613	0.613	0.613
0.02	0.613172978	0.6168774	0.613192769	0.613946485	0.620
0.04	0.613345989	0.6207548	0.613385538	0.61489272	0.620
0.06	0.613519033	0.6246322	0.613578307	0.615838706	0.630
0.08	0.613692109	0.6285096	0.613771077	0.616784441	0.631
0.10	0.613865218	0.632387	0.613963846	0.617729927	0.634
0.20	0.61473125	0.651774	0.614927691	0.622453614	0.639
0.50	0.617334246	0.709935	0.617819228	0.636587361	0.645
1.00	0.62168897	0.80687	0.622638457	0.660019956	0.650
4	0.648255609	1.38848	0.651553828	0.797449086	
8	0.684889416	2.16396	0.690107656	0.972641366	

Table A-4: Viscosity models considered

μ_n_I: Brinkman [43]	μ_n_II: Brenner and Condiff [44]
$\mu_n = \mu_f/(1-\phi)^{2.5}$	$\mu = \mu_o(1 + \eta\phi)$ $\eta = \frac{0.312r}{\ln(2r) - 1.5} + 2 - \frac{0.5}{\ln(2r) - 1.5} - \frac{1.872}{r}$

Table A-5: Theoretical and experimental Viscosity values in kg/m. s

ϕ (%)	μ_{n_I}	μ_{n_II}	$\mu_{reading}$	$\mu_{corrected}$
0.00	0.000853	0.000853	0.86	0.000853
0.02	0.00085425	0.000864436	0.87	0.000873
0.04	0.000855508	0.000875873	0.88	0.000883
0.06	0.000856774	0.000887309	0.89	0.000892
0.08	0.000858049	0.000898746	0.90	0.000901
0.10	0.000859332	0.000910182	0.92	0.000922
0.20	0.000865873	0.000967364	0.95	0.000951
0.50	0.000886757	0.001138911	1.09	0.001088
1.00	0.000925761	0.001424821	1.38	0.001370
4	0.001269946	0.003140285		
8	0.002022634	0.005427569		

Table A-6: Experimental thermo-physical calculations

ϕ	k_n (W·m^{-1}·K^{-1})	$\rho_n\left(\frac{kg}{m^3}\right)$	c_{p_n} ($\frac{\text{J}}{\text{kg °C}}$)	$\beta_n\left(\frac{1}{T}\right)$	μ_calc ($\frac{kg}{m}$	ρv_{hot}	ρv_{cold}	$\dot{m}_1\ (kg)$	$\dot{m}_2\ (kg)$
0	0.613	996.56	4179.00	0.000275	0.000853	4.07E-07	4.37E-07	0.000406	0.000435
0.1	0.634	997.66	4171.19	0.000274	0.000922	4.07E-07	4.37E-07	0.000406	0.000435
0.5	0.645	1002.07	4140.13	0.000272	0.001088	4.07E-07	4.37E-07	0.000406	0.000435
1	0.650	1007.59	4101.69	0.000269	0.001370	4.07E-07	4.37E-07	0.000406	0.000435

Table A-7: Averaged temperature readings

ϕ	T_1	T_2	T_3	T_4	T_5	T_6	ΔT	$\Delta T_h'$	$\Delta T_c'$
0	27.21178	27.14618	26.94618	26.52743	26.46421	26.52473	0.418751	0.065599	0.060519
0.1	27.22178	27.1138	27.06468	26.61366	26.41973	26.51693	0.451019	0.107977	0.097203
0.5	27.31143	27.21178	27.18949	26.42661	26.33357	26.42484	0.762883	0.099652	0.091271
1	27.49178	27.40022	27.27334	26.4138	26.13973	26.22258	0.859533	0.091558	0.082851

Table A-8: Heat transfer calculations

ϕ	$q_h\left(\frac{\mathrm{W}}{\mathrm{m}^2}\right)$	$q_c\left(\frac{\mathrm{W}}{\mathrm{m}^2}\right)$	$q_{balance}\left(\frac{\mathrm{W}}{\mathrm{m}^2}\right)$	$h_h\left(\frac{\mathrm{W}}{\mathrm{m}^2\mathrm{K}}\right)$	Nu_h
0	44.47616	44.01561325	0.460542234	106.2115	8.663254
0.1	73.07164	70.56416357	2.50747553	162.0145	12.77717
0.5	66.93533	65.7644371	1.170897166	87.73999	6.801549
1	60.92769	59.14345271	1.784232377	70.88463	5.452664

APPENDIX B. ERROR CALCULATIONS

Measurements taken from thermocouples used in Chapter 5 were averaged and shown in Table A-7 using:

$$\bar{t} = \frac{1}{n}\sum_{1}^{n} t_i$$

Where n is the number of readings of individual temperature readings t_i taken in the last 1200s of experimental runs when steady-state conditions have been reached. The standard deviation σ at each thermocouple is given by equation below and results are in table B-1 below.

$$\bar{t} = \sqrt{\frac{\sum_1^n (t_i - \bar{t})^2}{n-1}}$$

Table B-1: Standard deviations of thermocouple readings T_1 to T_6

ϕ	σ_1	σ_2	σ_3	σ_4	σ_5	σ_6
0	0.007792	0.007452	0.007452	0.011111	0.011690	0.008311
0.1	0.007792	0.008748	0.008120	0.008913	0.008311	0.011111
0.5	0.008875	0.007792	0.015687	0.009084	0.008503	0.008574
1	0.007792	0.010812	0.014497	0.008748	0.008311	0.010620

The standard deviation of mean σ_m is given by equation below and results are in Table B-2:

$$\sigma_{m_i} = \frac{\sigma_i}{\sqrt{n}}$$

Table B-2: Standard error in the mean of thermocouple readings T_1 to T_6

ϕ	σ_{m_1}	σ_{m_2}	σ_{m_3}	σ_{m_4}	σ_{m_5}	σ_{m_6}
0	0.000159	0.000152	0.000152	0.000227	0.000239	0.000170
0.1	0.000159	0.000179	0.000166	0.000182	0.000170	0.000227
0.5	0.000181	0.000159	0.000320	0.000185	0.000174	0.000175
1	0.000159	0.000221	0.000296	0.000179	0.000170	0.000217

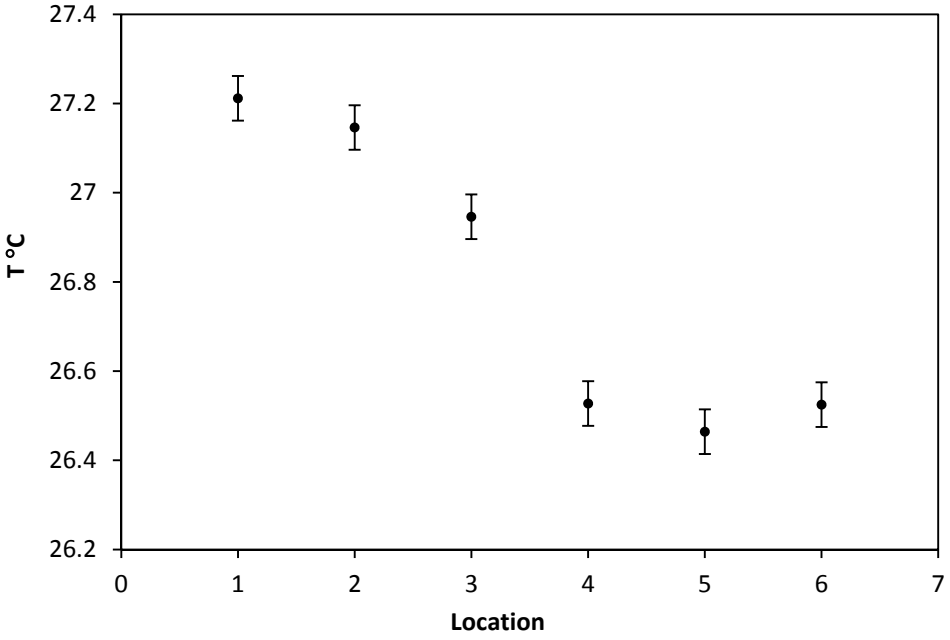

Figure B - 1: Error in temperature measurement at thermocouples T1 – T6

Table B-3: Independent reading errors in apparatus used

Error	Description	Value
δm	Mass	$\pm 0.0001\ g$
δV	Volume	$\pm 1\ ml$
δL	Length	$\pm 0.01\ mm$
δv	Volume flow rate	$\pm 0.75\%$
δT	Temperature	$\pm 0.1\ °C$
δk	Thermal conductivity	5%
δc_p	Specific heat	5%
$\delta \mu$	Viscosity	1%

The larger of the two types of errors (the standard error and the reading error), was used in propagated error calculations. Parameters in the equation below are described in Table 5-1

$$\frac{\delta \rho}{\rho} = \sqrt{\left(\frac{\delta m}{m}\right)^2 + \left(\frac{\delta V}{V}\right)^2}$$

$$\frac{\delta m_p}{m_p} = \sqrt{\left(\frac{\delta \rho_p}{\rho_p}\right)^2 + \left(\frac{\delta \rho_f}{\rho_f}\right)^2 + \left(\frac{\delta m}{m}\right)^2}$$

$$\frac{\delta \dot{m}}{\dot{m}} = \sqrt{\left(\frac{\delta \rho}{\rho}\right)^2 + \left(\frac{\delta v}{v}\right)^2}$$

$$\delta \Delta T' = \sqrt{(\delta T_1)^2 + (\delta T_2)^2}$$

$$\frac{\delta q}{q} = \sqrt{\left(\frac{\delta \dot{m}}{\dot{m}}\right)^2 + \left(\frac{\delta c_p}{c_p}\right)^2 + \left(\frac{\delta \Delta T'}{\Delta T'}\right)^2 + 2\left(\frac{\delta L}{L}\right)^2}$$

$$\frac{\delta h}{h} = \sqrt{\left(\frac{\delta q}{q}\right)^2 + \left(\frac{\delta \Delta T'}{\Delta T'}\right)^2}$$

$$\frac{\delta Nu}{Nu} = \sqrt{\left(\frac{\delta h}{h}\right)^2 + \left(\frac{\delta L}{L}\right)^2 + \left(\frac{\delta k}{k}\right)^2}$$

Table B-4: Maximum calculated propagated error

Error	Description	Value
$\delta\rho/\rho$	Density	0.017
$\delta m_p/m_p$	Nanoparticle mass	0.6
$\delta\dot{m}/\dot{m}$	Mass flow rate	0.018
$\delta\Delta T'/\Delta T'$	Temperature difference	0.005
$\delta q/q$	Heat flux	0.054
$\delta h/h$	Heat transfer coefficient	0.054
$\delta Nu/Nu$	Nusselt number	0.074

Maximum error in calculated Nusselt number due to propagated error was therefore ≈ 7.4 %

APPENDIX C. TEMPERATURE AND VELOCITY COLOUR CONTOURS

Appendix C shows the various temperature and velocity colour contours obtained from CFD analysis carried out in chapter 4. They supplement the isotherms and streamlines generated and presented in chapter 4 by showing quantitatively the effect of changing particle concentration and Rayleigh number on natural convection in the square enclosure. Figures C-1 to C-8 are colour contours for Air at Prandtl number 0.71 used to compare the code with benchmark results from De Vahl Davis [87].

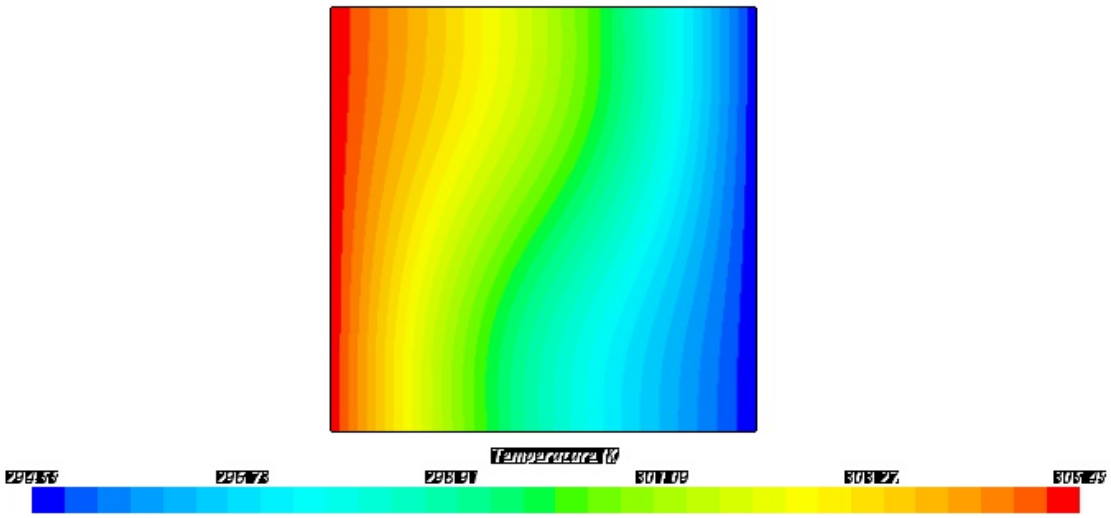

Figure C - 1: Air temperature colour contours $Ra = 10^3$

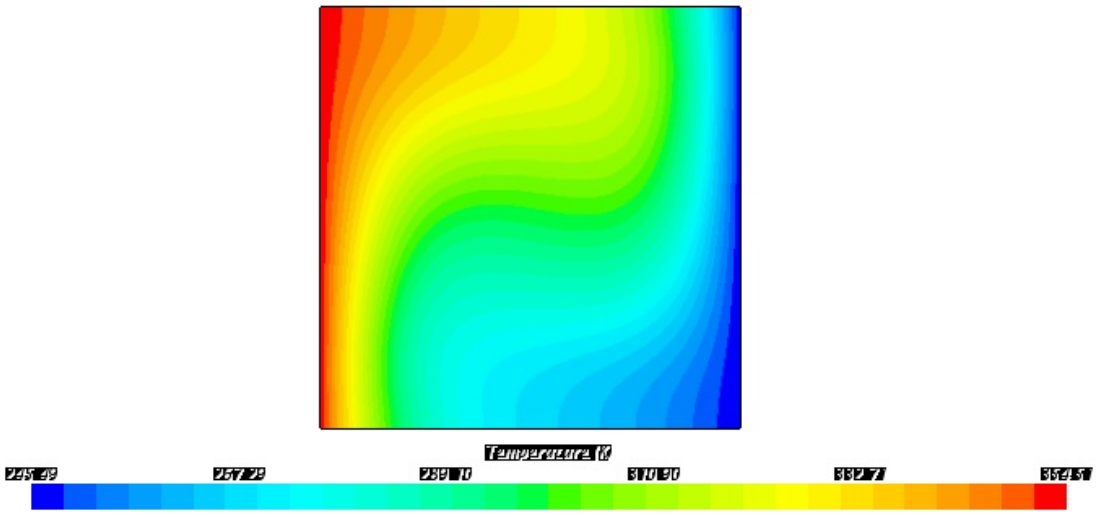

Figure C - 2: Air temperature colour contours $Ra = 10^4$

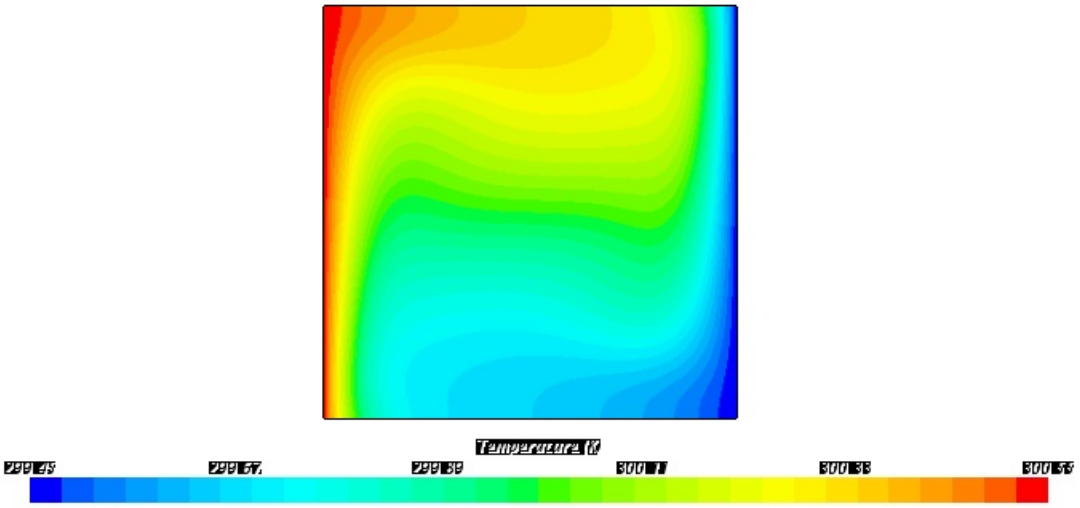

Figure C - 3: Air Temperature colour contours *Ra* = 10^5

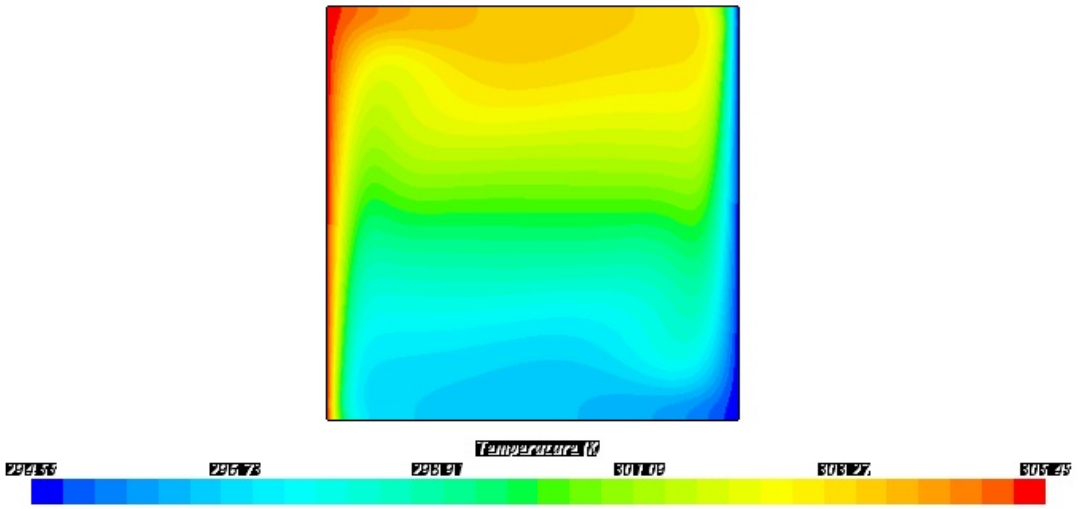

Figure C - 4: Air temperature colour contours *Ra* = 10^6

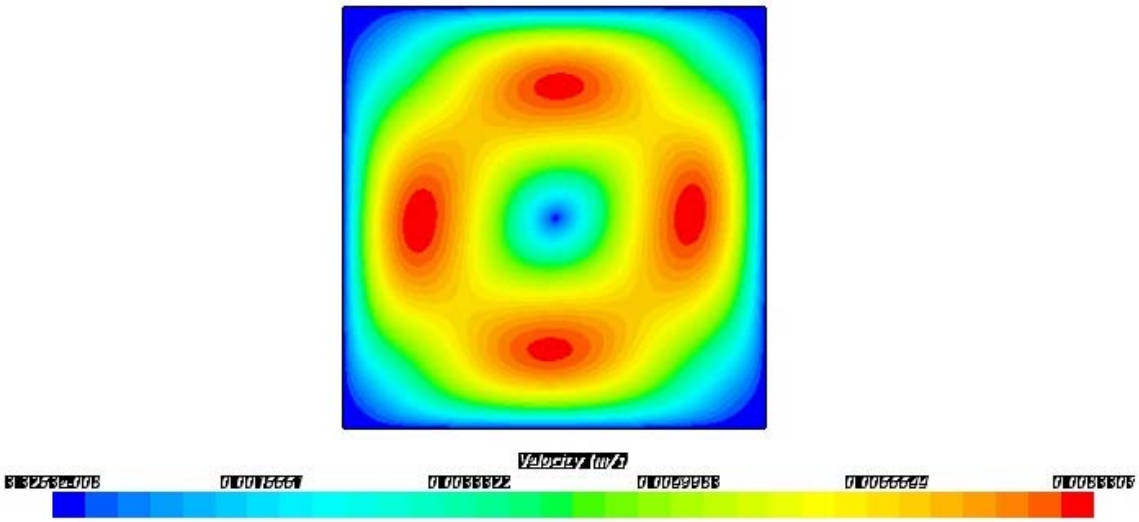

Figure C - 5: Air velocity colour contours *Ra* = 10^3

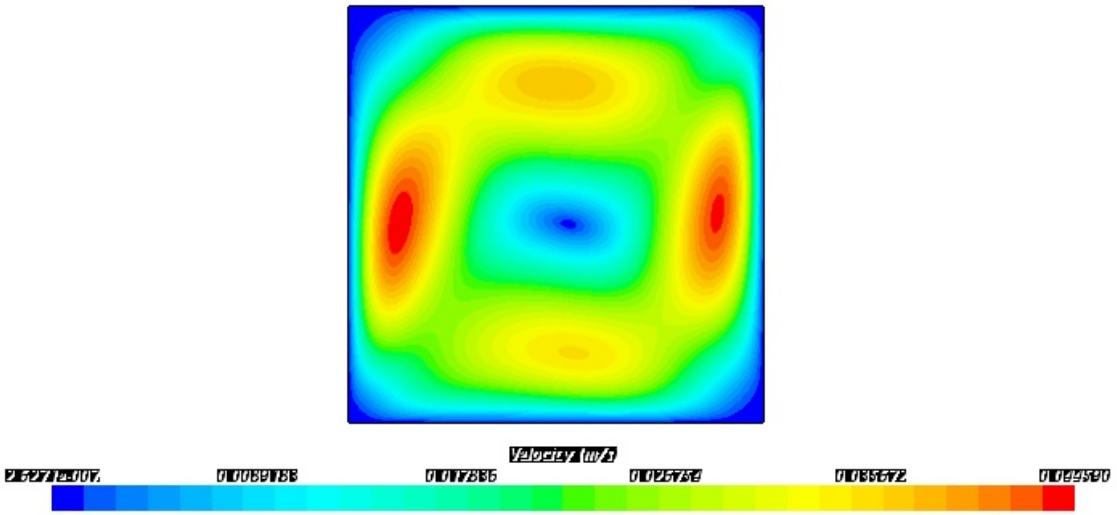

Figure C - 6: Air velocity colour contours *Ra* = 10^4

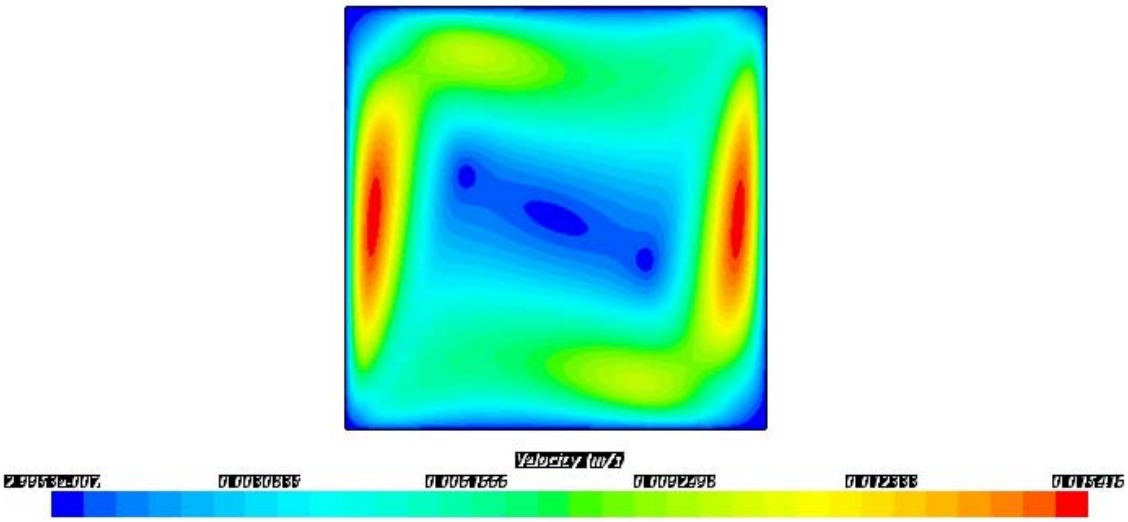

Figure C - 7: Air velocity colour contours *Ra* = 10^6

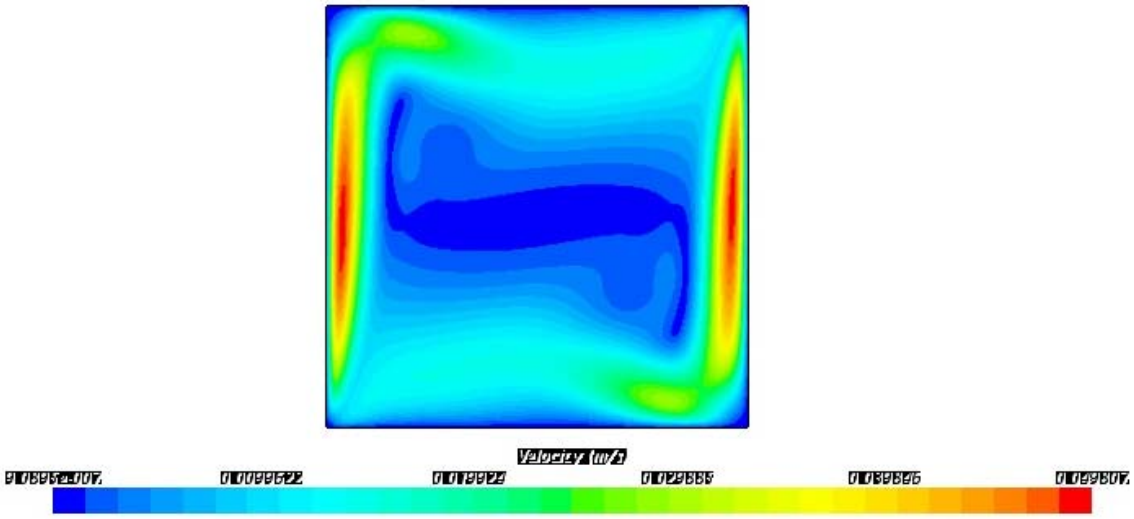

Figure C - 8: Air velocity colour contours *Ra* = 10^6

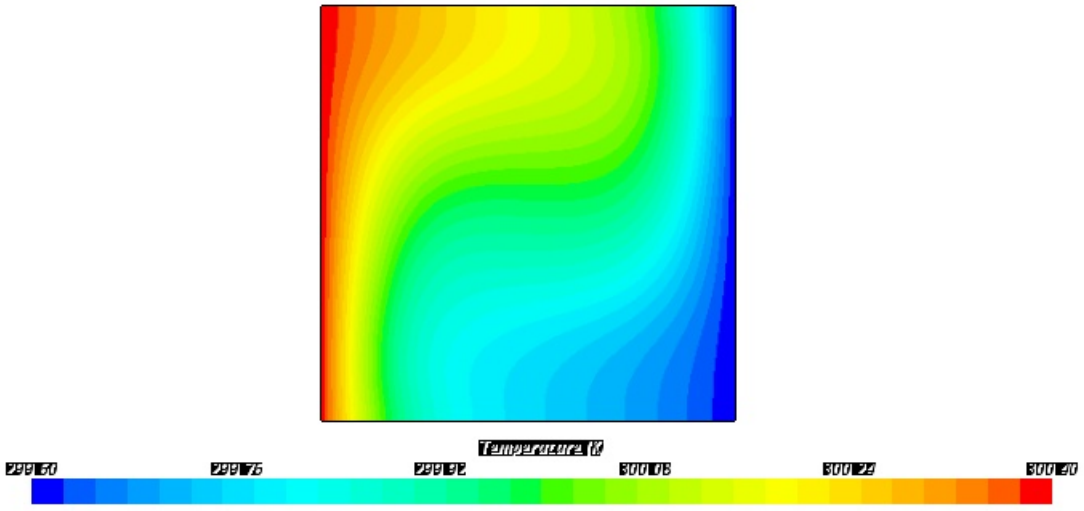

Figure C - 9: Nanofluid temperature colour contours *Ra* = 10^4

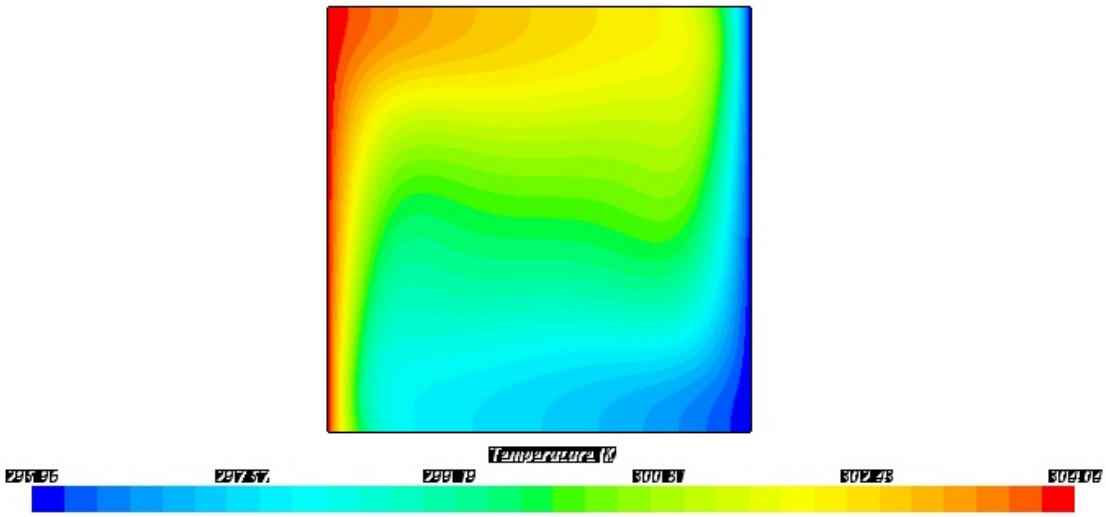

Figure C - 10: Nanofluid temperature colour contours *Ra* = 10^6

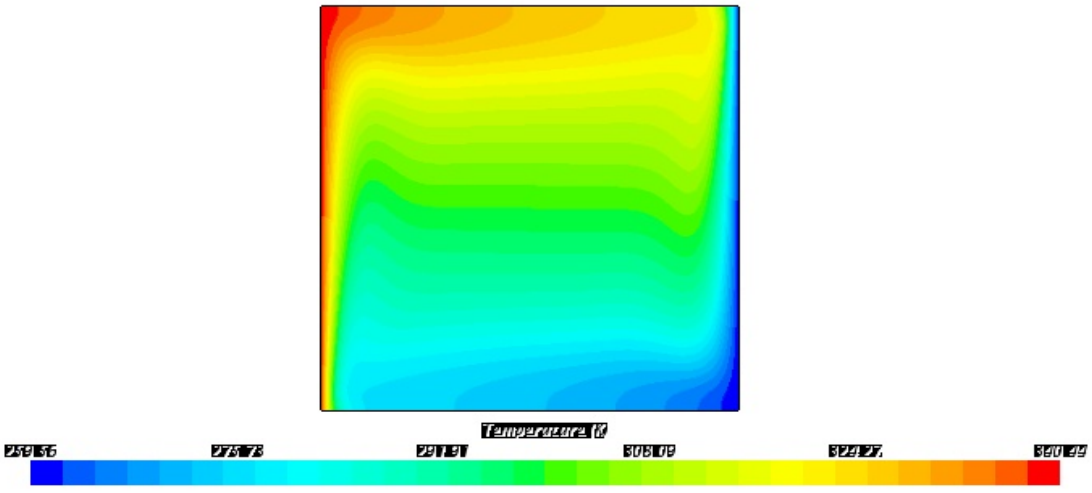

Figure C - 11: Nanofluid temperature colour contours *Ra* = 10^8

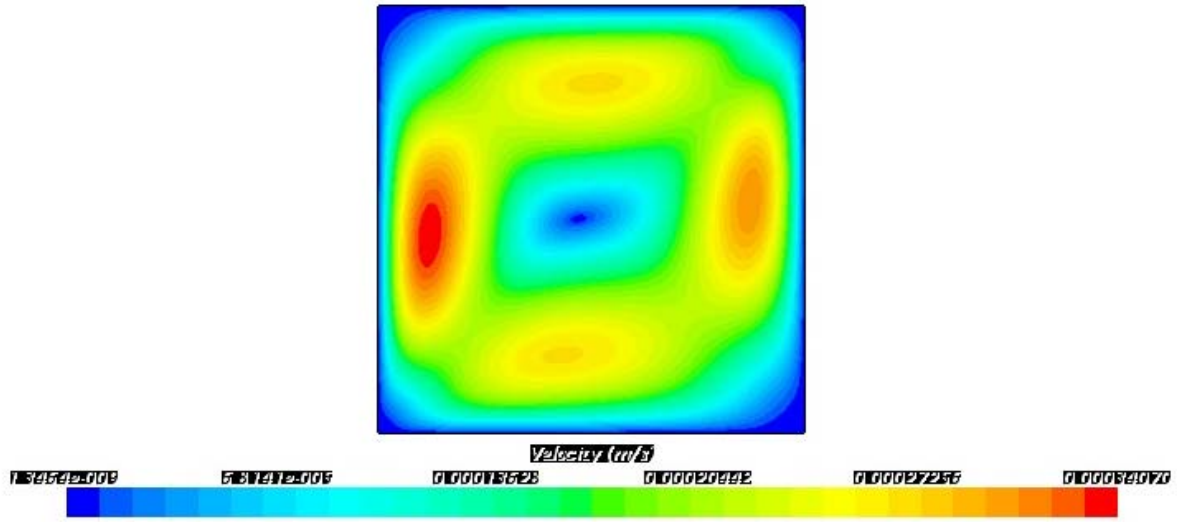

Figure C - 12: Nanofluid velocity colour contours *Ra* = 10^4

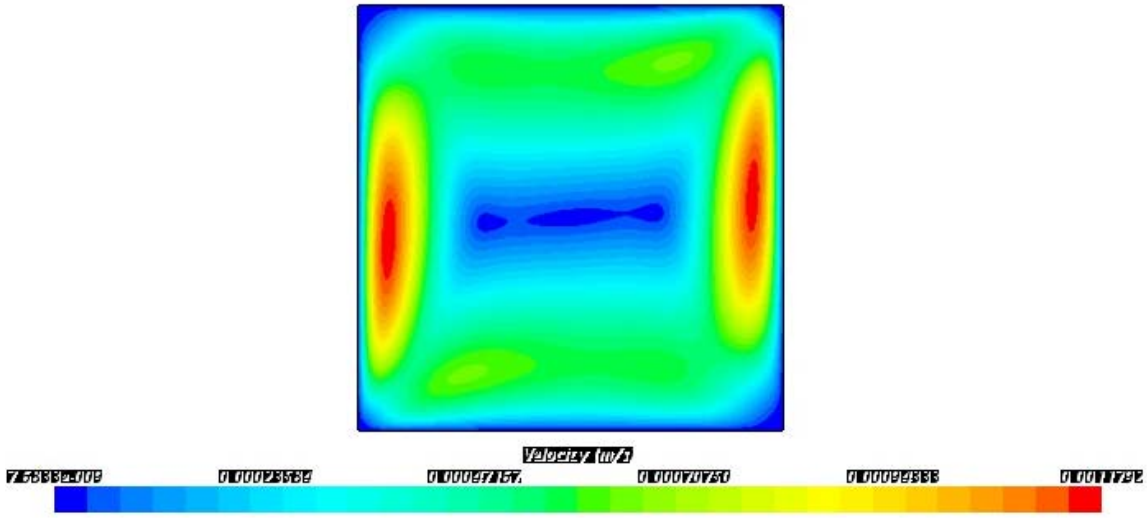

Figure C - 13: Nanofluid velocity colour contours *Ra* = 10^6

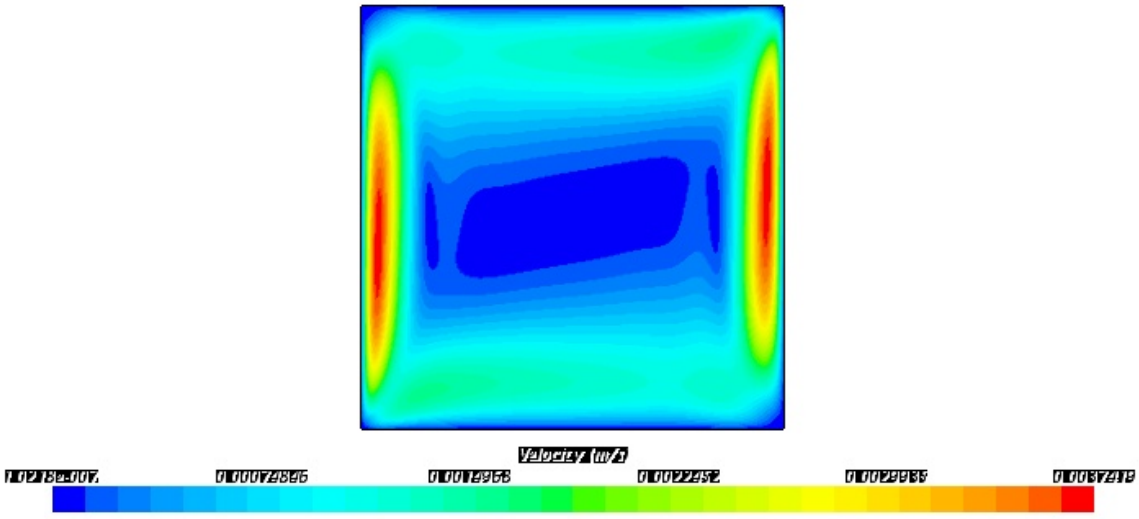

Figure C - 14: Nanofluid velocity colour contours *Ra* = 10^8

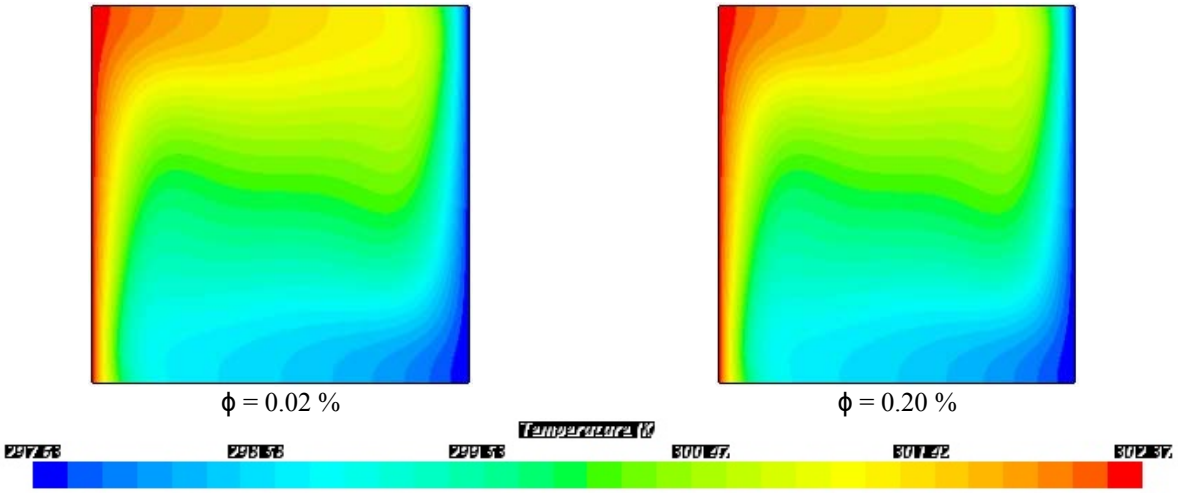

Figure C - 15: Nanofluid temperature colour contours for ϕ = 0.02% and 0.20%

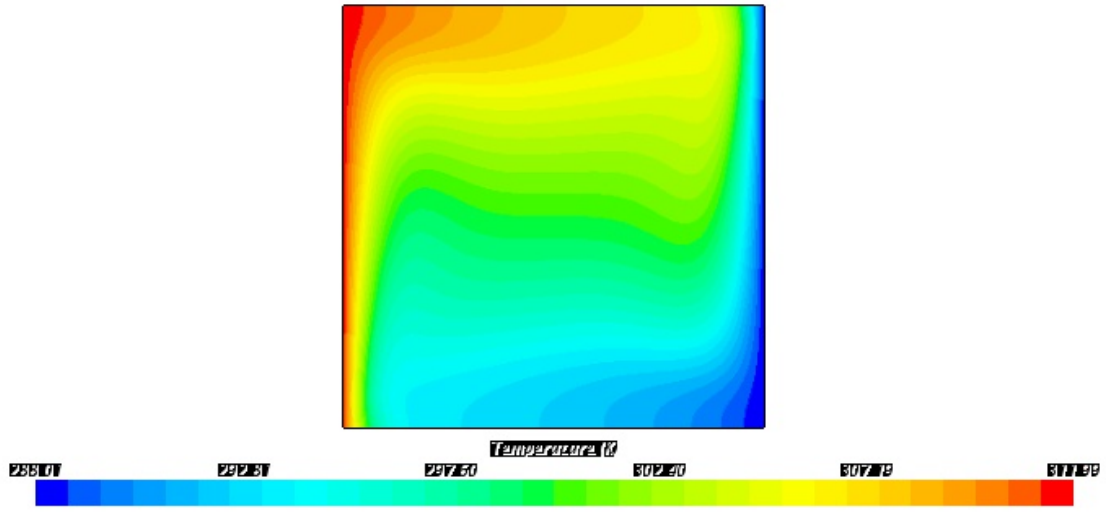

Figure C - 16: Nanofluid temperature colour contours ϕ = 4.00%

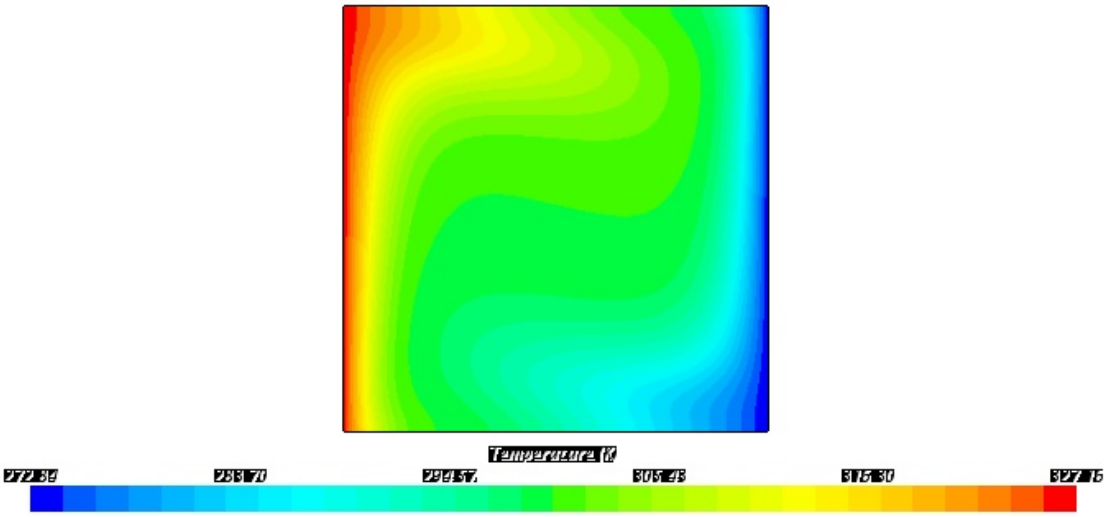

Figure C - 17: Nanofluid temperature colour contours ϕ = 8.00%

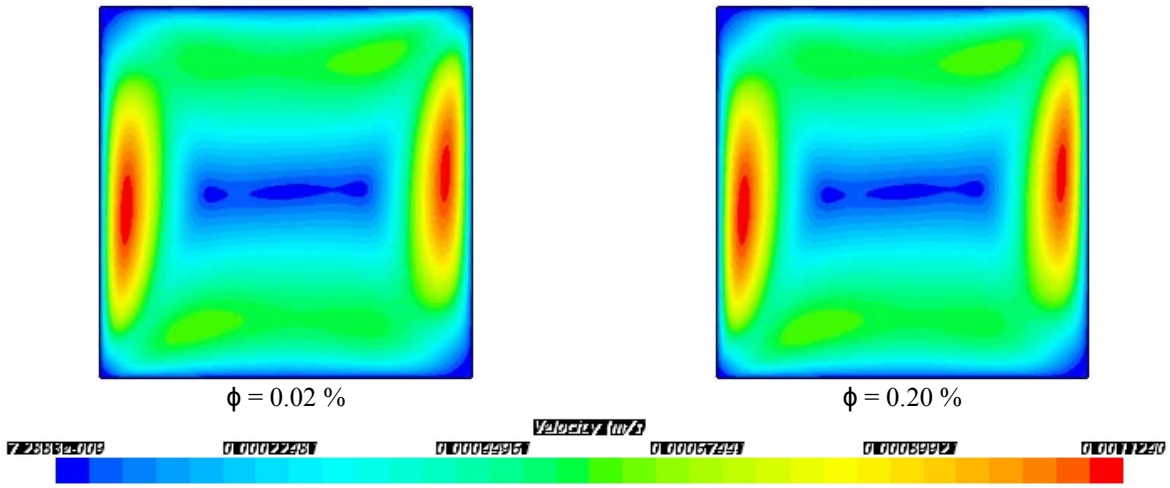

Figure C - 18: Nanofluid Velocity Colour Contours for ϕ = 0.02 % and 0.20 %

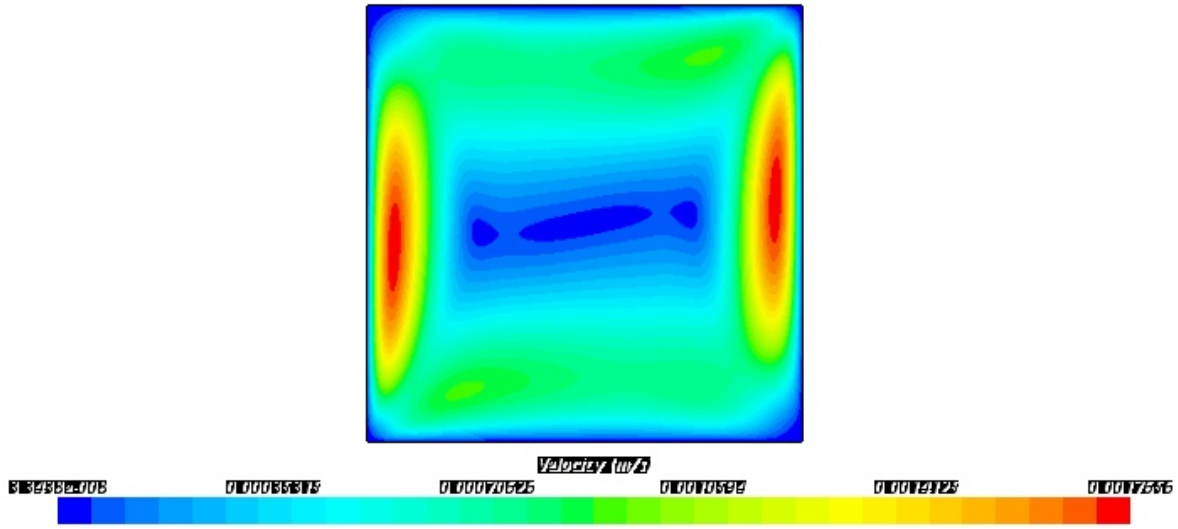

Figure C - 19: Nanofluid Velocity Colour Contours ϕ = 4.00 %

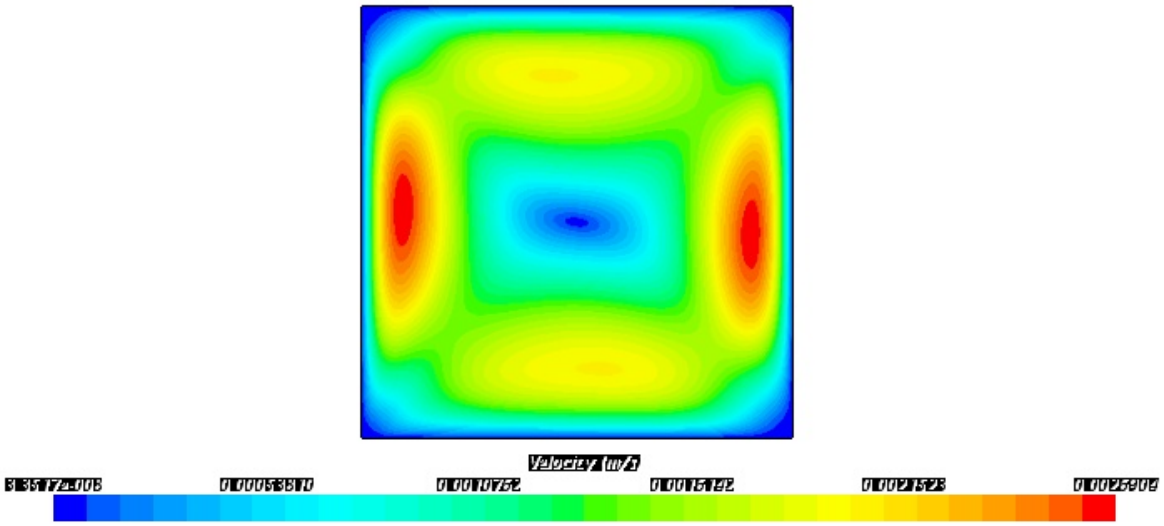

Figure C - 20: Nanofluid Velocity Colour Contours ϕ = 8.00 %